IN-SILICO SCREENING AND *IN-VITRO* VALIDATION OF PROTEIN INHIBITORS WITH PHARMACOLOGICAL ACTIVITY AGAINST *PLASMODIUM* MALARIA

Harrison Onyango Okello

A Research Thesis Submitted to the School of Natural Sciences in Partial Fulfillment of the Requirements for the Award of Degree of Masters of Science in Bioinformatics of Masinde Muliro University of Science and Technology

PLAGIARISM STATEMENT

STUDENT DECLARATION

1. I hereby declare that I know that the incorporation of material from other works or a paraphrase of such material without acknowledgment will be treated as plagiarism according to the Rules and Regulations of Masinde Muliro University of Science and Technology.
2. I understand that this thesis must be my own work.
3. I know that plagiarism is academic dishonesty and wrong and that if I commit any act of plagiarism, my thesis can be assigned a fail grade ("F").
4. I further understand that I may be suspended or expelled from the university for academic dishonesty.

Name: **Harrison Onyango Okello** Signature: ……..

Reg. No: **SBF/G/01-70241/2021** Date: ……..

SUPERVISOR(S) DECLARATION

I/We hereby approve the examination of this thesis. The thesis has been subjected to a plagiarism test, and its similarity index is not above 20%.

1. Name: **Dr. Okoth Patrick** Signature: ……. Date: ……..
2. Name**: Prof. Muoma John** Signature: ……. Date: ……..

DECLARATION

This thesis is my original work prepared with no other than the indicated sources and support and has not been presented elsewhere for a degree or any other award.

Signature: …… Date: ……

Name: Harrison Onyango Okello Reg. No.: SBF/G/01-70241/2021

CERTIFICATION

We, the undersigned, certify that we have read and hereby recommend for acceptance of Masinde Muliro University of Science and Technology a thesis entitled ***"In-Silico Screening and In-Vitro Validation of Protein Inhibitors with Pharmacological Activity against Plasmodium Malaria"***.

SUPERVISORS

Signature: ……. Date: ……..

Dr. OKOTH Patrick, PhD

Department of Biological Sciences

Masinde Muliro University of Science and Technology

Signature: ……. Date: ……..

Prof. MUOMA John, PhD

Department of Biological Sciences

Masinde Muliro University of Science and Technology

COPYRIGHT

DEDICATION

I dedicate this thesis to Annabel Dianah, my wife and partner upon life's way, son, Xolani S. Onyango, and daughter, Jahzara M. Onyango for their unwavering love, support, and prayers.

ACKNOWLEDGEMENT

I am forever grateful to God Almighty for good health, wisdom, and understanding that I needed to write this thesis. Overwhelming gratitude goes to my supervisors Dr. Patrick Okoth and Prof. John Muoma for their technical advice, top-notch guidance, and input during the preparation of this thesis. Special thanks go to Dr. Grace Gitau for identifying my strengths and directing me towards the right scholarly path. I also express my appreciation to my parents, Mr. William O. Okello and Mrs. Jane M. Okello for their consistent support and encouragement during the entire process of writing this work. To the entire Masinde Muliro University of Science and Technology fraternity, may God's favor be upon your lives for your cooperation and our frequent encounters that widened my knowledge base and shaped the idea that this thesis is founded on.

ABSTRACT

The World Health Organization (WHO) documents malaria as one of the leading causes of high morbidity and mortality worldwide. The disease affects millions and kills thousands of people annually. Efforts to reduce the global burden of malaria have prompted WHO to recommend prevention strategies like using anti-malarial drugs and malaria vaccines. However, these strategies have been ineffective because of anti-malarial drug resistance and the inefficacy of malaria vaccines. The current recommended drug combination is Artemisinin-based Combination Therapy (ACT). However, the extended ACTs clearance times, linked to the emergence of artemisinin monotherapy resistance recorded most recently in Africa and the Great Mekong region, pose a danger to its efficacy. Similarly, the RTS,S/AS01 (Mosquirix) vaccine's modest effectiveness against malaria at 36% among kids aged 5 to 17 months who need four doses, fails to aid malaria eradication. To address the limitations of current anti-malarial therapies and vaccines, this study aimed to: (1) identify novel PfHsp90 and PfCSP inhibitors with pharmacological activity against *Plasmodium* malaria through hierarchical virtual screening (HVS) using geldanamycin and monoclonal antibody L9 as reference ligands, respectively; (2) assess the stability of protein-inhibitor complexes via molecular dynamics simulations (MDS); and (3) validate the inhibitory efficacy of selected compounds through *in vitro* assays. Since *P. falciparum* heat shock protein 90 (PfHsp90) and *P. falciparum* circumsporozoite surface protein (PfCSP) are well-characterized malaria drugs and vaccines targets, respectively, this study sought to use them in discovering better efficacious malaria drug and vaccine candidates. Geldanamycin (GDM), a potent Hsp90 inhibitor with well-characterized binding to ATP-binding domain, was used to identify PfHsp90 inhibitors by screening it against the ZINC20 database via the ZINCPHARMER web server. This virtual screening process resulted in 17 hits. Monoclonal antibody (mAb) L9, with its high-affinity binding to the central NANP repeat region, was used to identify PfCSP inhibitors, yielding 23 hits. These ZINCPHARMER hits were subjected to drug-likeness and pharmacokinetics properties analysis in the SwissADME web server, and 18 (9 for PfHsp90 and 9 for PfCSP) of them satisfied the requirements. The 18 ZINC compounds were docked with PfHsp90 and PfCSP using the PyRx software to understand their interactions. From the molecular docking results, ZINC09060002 (-8.2 kcal/mol), ZINC72133064 (-7.8 kcal/mol), ZINC72163401 (-7.7 kcal/mol), ZINC72358537 (-8.1 kcal/mol), and ZINC72358557 (-7.6 kcal/mol) had better binding affinities to PfHsp90 than GDM (-7.5 kcal/mol). Similarly, ZINC25374360 (-8.1 kcal/mol), ZINC40144754 (-8.3 kcal/mol), and ZINC71996727 (-8.9 kcal/mol) bound strongly to PfCSP with binding affinities of less than -8.0 kcal/mol. The stability of these molecularly docked protein-inhibitor complexes was assessed through MDS using GROMACS 2022. The PfHsp90 inhibitors (ZINC72163401, ZINC72358537, and ZINC72358557) and PfCSP inhibitors (ZINC25374360 and ZINC71996727) formed stable complexes with their respective target proteins. These five compounds were subjected to *in vitro* validation using the Sybr Green I fluorescence assay. Cultured *P. falciparum* parasites were exposed to serial dilutions of each inhibitor, and parasite viability was quantified based on DNA-binding fluorescence intensity. IC_{50} values were calculated to determine the inhibitory potency of each compound. They showed promising inhibition of parasite growth with IC_{50} values ranging between 5 – 150 ng/mL. In this regard, the three PfHsp90 inhibitors are anti-malarial candidates while the two PfCSP inhibitors are potential vaccine adjuvants that might increase the efficacy of the existing Mosquirix vaccine. However, further structural optimization studies and clinical (*in vivo*) tests are necessary to ascertain the antimalarial activity of these compounds in humans.

Table of Contents

LIST OF TABLES

LIST OF FIGURES

LIST OF PLATES

ABBREVIATIONS AND ACRONYMS

ACT	Artemisinin-based Combination Therapy
ATP	Adenosine Triphosphate
CD4	Cluster of Differentiation 4
CD8	Cluster of Differentiation 8
CD40L	Cluster of Differentiation 40 Ligand
CDC	Center for Disease Control and Prevention
CRR	Central Repeat Region
CSP	Circumsporozoite Surface Protein
CTD	C-Terminal Domain
DNA	Deoxyribonucleic Acid
DOX	Doxycycline
DP	Degree of Polymerization
DPNA	Aspartic Acid, Proline, Asparagine, Alanine
EC	Endothelial Cells
EEF	Exoerythrocytic Form
Fb	Fibroblasts
GDM	Geldanamycin
HLA-DR	Human Leukocyte Antigens DR isotype
Hop	Heat Shock Protein 90-Heat Shock Protein 70 Organizing Protein
HSPC2	Heat Shock Protein C2
HSPG	Hepatic Heparan Sulfate Proteoglycans
Hsp	Heat Shock Protein
HTS	High Throughput Screening

IC_{50}	Half Maximal Inhibitory Concentration
IFN	Interferons
IL-2	Interleukin 2
ITC	Isothermal titration calorimetry
KCs	Kupffer cells
kDa	Kilodalton
LDH	Lactate Dehydrogenase (LDH)
LSECs	Liver Sinusoidal Endothelial Cells
MD	Middle Domain
MDS	Molecular Dynamics Simulation
mAb	Monoclonal Antibody
MSP9	Merozoite Surface Protein-9
NANP	Asparagine, Alanine, Asparagine, Proline
NCBI	National Center for Biotechnology Information
NPDP	Asparagine, Proline, Aspartic Acid, Proline
NPNA	Asparagine, Proline, Asparagine, Alanine
NPNV	Asparagine, Proline, Asparagine, Valine
NTD	N-Terminal Domain
NVDP	Asparagine, Valine, Aspartic Acid, Proline
PDB	Protein Database
PfCSP	*Plasmodium falciparum* Circumsporozoite Surface Protein
PfHop	*Plasmodium falciparum* Heat Shock Protein 90-Heat Shock Protein 70 Organizing Protein
PfHsp90	*Plasmodium falciparum* Heat Shock Protein 90

PlasmoDB	*Plasmodium* Database
PV	Parasitophorous Vacuole
rPfCSP	Recombinant PfCSP
RMSD	Root Means Square Deviation
SPZ	Sporozoites
TFN	Tumour Necrosis Factor
TPR	Tetratricopeptide Repeat
TV	Transient Vacuole
Uniprot	Universal Protein Resource
WHO	World Health Organization

DEFINITION OF TERMS

In-Silico:	Using a computer to perform an experiment
Pharmacological Properties:	Therapeutic characteristics of a particular molecule or compound
Molecular Dynamics Simulation:	A computer approach for assessing the physical movements of molecules and atoms
Hierarchical Virtual Screening:	Searching small molecules' libraries to identify structures that can bind a particular protein target of interest
In Vitro:	An experiment taking place outside a living organism, especially the laboratory
In Vivo:	An experiment taking place in or on a whole living organism like a person

CHAPTER ONE

INTRODUCTION

1.1 Background Information

Malaria remains a global public health burden, with approximately 241 million confirmed cases and a fatality of approximately 627,000 as at 2020 (World Health Organization (WHO), 2022). These statistics underscore an alarming rise in malaria cases and deaths compared to WHO's 2019 report. In 2019, the World Health Organization (WHO) reported 227 million confirmed cases and approximately 558,000 deaths worldwide (WHO, 2022). Unfortunately, Africa contributes a disproportionally high portion of the global malaria burden, especially sub-Saharan Africa. In 2020, the African region contributed 95% of malaria-confirmed cases and 96% of malaria deaths (Oladipo *et al*., 2022). Children aged five years and below accounted for approximately 80% of all malaria deaths in the African region (Oladipo *et al*., 2022).

Four countries within sub-Saharan Africa, including Mozambique (3.8%), the United Republic of Tanzania (4.1%), the Democratic Republic of the Congo (13.2%), and Nigeria (31.9%) accounted for over half of malaria deaths globally (WHO, 2022). These shockingly high morbidity and mortality rates call for an in-depth understanding of malaria's etiology, transmission, and pathogenesis and how malaria intervention strategies can be more effective. Mosquitoes are the primary vectors of malaria, which primarily affects individuals in tropical and subtropical regions. Obligate protozoan parasites of the genus *Plasmodium* cause the ailment (Sá, Costa, & Tavares, 2022). Mosquito vectors that carry malaria transmit the parasites to people during a blood meal when they bite an individual.

Once within the host, the parasites first infect the liver cells before moving on to the red blood cells. Ramos *et al*. (2021) explain that by altering the infected erythrocytes to make them

cytoadherent, malaria parasites cause malaria pathology at the blood stage. Malaria infection, whose incubation period is 7-14 days, can cause lethargy, fatigue, muscle aches, nausea, stomach aches, fever, and shivering (Laurens, 2020; Nadeem *et al*., 2022). Due to the massive loss of red blood cells, the disease can cause jaundice and anemia. Furthermore, if not appropriately treated, malaria can become lethal and cause coma, mental confusion, seizures, kidney failure, and finally, death (Center for Disease Control and Prevention (CDC), 2022).

To date, *Plasmodium falciparum*, *Plasmodium knowlesi*, *Plasmodium ovale*, *Plasmodium vivax*, and *Plasmodium malariae* are the five species of *Plasmodium* that can infect individuals and cause malaria. *P. falciparum* has the highest morbidity and fatality rates and hence poses a severe threat to public well-being in locations where malaria is endemic (Ayanful-Torgby *et al*., 2018; Chew *et al*., 2022; Laurens, 2020; Nadeem *et al*., 2022). Even so, the devastating effects of the other four *Plasmodium* species on human health should not be underrated. Currently, malaria kills approximately 400,000 individuals yearly, primarily kids in sub-Saharan Africa because they have not yet developed any immunity to the illness. It affects 200-400 million people annually (Chew *et al*., 2022; Gross, 2019; Wang *et al*., 2020).

Developing tools and strategies that can interrupt the transmission of a specified malaria parasite species is a way of reducing the devastating effects of the disease on human health and safeguarding the well-being of the millions of people affected by the illness yearly. The WHO recommended malaria prevention strategies and tools that have been in use for almost two decades. Some of these strategies include the use of anti-malarial drugs and malaria vaccines. Even though such malaria prevention strategies and tools have reduced the global burden of the disease, the increase in the number of malaria's confirmed cases and deaths from 2019 to 2020 underlies the need for more effective intervention strategies (WHO, 2022).

Wang *et al*. (2020) outline that between 2000 and 2015, anti-malarial medications, insecticide-treated mosquito nets, and other public health initiatives helped reduce malaria cases worldwide by 50–75%. The recently developed malaria vaccine is an essential tool to alleviate the enormous socioeconomic burden that malaria causes. Despite these initiatives, malaria incidences have grown since 2015 in numerous places for various reasons (Wang *et al*., 2020). Some of the outstanding reasons include the inefficacy of the existing Mosquirix vaccine and the parasites developing resistance to anti-malarial drugs. The modest efficacy of the existing RTS,S/AS01 vaccine curtails malaria eradication efforts.

The results from RTS,S/AS01 clinical trials demonstrated that after four years of follow-up, the vaccine's effectiveness against malaria was modest, just 36% among kids aged 5 to 17 months who received four doses (Laurens, 2020). Similarly, Arora *et al*. (2021) point out that RTS,S/AS01 is ineffective against types of malaria caused by *P. vivax*, *P. knowlesi*, *P. ovale*, and *P. malariae*. RTS,S/AS01 vaccine's modest efficacy and ineffectiveness against certain types of malaria provide a scientific gap. Vaccines with better efficacies should be developed, or compounds that can increase the effectiveness of the existing Mosquirix vaccine should be discovered to aid in fighting malaria. This study sought to explore and fill this scientific gap by using *in-silico* approaches to find compounds from natural sources (ZINC20 database) that can increase the efficacy of the existing RTS,S/AS01 vaccine.

Similarly, anti-malarial drug resistance has become a menace that casts doubt on the effectiveness of the currently available anti-malarial medications. One of the biggest dangers to controlling malaria is the emergence of drug resistance, which increases malaria morbidity and mortality. Only two of the four human malaria parasite species, *P. falciparum* and *P. vivax*, have been proven to be resistant to anti-malarial medications currently on the market (CDC, 2018). No information is

available on *P. malariae* or *P. ovale* treatment resistance. *P. knowlesi*, a zoonotic monkey malaria that affects people in Southeast Asian forested settings, is completely sensitive to chloroquine and other commonly used medications (CDC, 2018).

P. falciparum and *P. vivax* are resistant to chloroquine. *P. falciparum* is also resistant to other anti-malarial drugs, including quinine, halofrantrine, mefloquine, and sulfadoxine/pyrimethamine (CDC, 2018). Even though resistance to these medications tends to be considerably less geographically prevalent, the effects of such multi-drug resistant malaria can be severe in some parts of the world (CDC, 2018). These findings demonstrate the need for additional malaria control and eradication measures (Cockburn & Seder, 2018). Recently, portions of Southeast Asia have experienced the emergence of resistance to both the artemisinin and non-artemisinin components of artemisinin-based combination therapy, reducing the efficacy of this essential anti-malarial class (CDC, 2018). If this anti-malarial drug resistance trend continues, malaria's adverse effects on human health will be catastrophic.

1.2 Statement of the Problem

Several antimalarial drugs have been developed to help eradicate malaria, including chloroquine, cilexetil, dipyridamole, hydroxychloroquine, and candesartan (Mengist *et al*., 2021). Similarly, the RTS,S/AS01 vaccine was recently developed to assist in containing the spread of the disease. However, these antimalarial drugs and the malaria vaccine have low levels of effectiveness as malaria intervention strategies because of antimalarial drug resistance and the inefficacy of the RTS,S/AS01 vaccine. The RTS,S/AS01 vaccine's modest efficacy for children, between 18% and 36%, does not attain the required effectiveness threshold to significantly reduce malaria's global burden (Laurens, 2020).

While antimalarial drug resistance creates a need for better antimalarial drugs, the efficacy of monoclonal antibodies produced following Mosquirix administration and the possibility of their use have not been documented, offering a wide window for discovering other effective compounds with pharmacological advantages on RTS,S/AS01. Therefore, this study undertook an *in-silico* identification of PfHsp90 and PfCSP inhibitors with pharmacological activity against *Plasmodium* malaria using molecular dynamics simulation (MDS) and hierarchical virtual screening (HVS).

1.3 Justification of the Study

Most drugs already available are ineffective since the parasite is mounting resistance. The PfHsp70-PfHop-Pfhsp90 complex usually aids in the growth and pathogenicity of the malaria parasite *P. falciparum* (Zininga *et al*., 2015). When the parasite invades the unfavorable conditions of the human host, the Hsps maintain proteostasis under such conditions. The two Hsps also enhance the folding of various proteins. Some proteins that rely on this PfHsp70-PfHop-PfHsp90 complex for folding into their fully functional conformation are kinases and steroid hormone receptors (Zininga *et al*., 2015). Since the complex helps in the growth and pathogenesis of malaria, any drug that interferes with its formation can be used to prevent and cure malaria.

This complex, therefore, can be utilized as a potential drug target. Different compounds have been found to interfere with the interaction of PfHop with PfHsp90 by disrupting the binding of PfHsp90 to the TPR2A domain of PfHop. One such compound is a drug known as geldanamycin. It is a possible anti-malarial drug since it can moderate the function of PfHsp90 by interacting with its N-terminal ATP binding domain (NTD) via binding the ATP-binding site (Darby *et al*., 2020). This interaction prevents the assembly of the PfHsp70-PfHop-PfHsp90 complex, eventually destroying the parasite (Stofberg *et al*., 2021).

On the same note, the recent discovery of Mosquirix has identified PfCSP as another essential protein in the development and pathogenesis of malaria. The protein facilitates the sporozoite's invasion and motility as it enters the hepatocyte, leading to malaria disease (Storti-Melo *et al*., 2022). Due to Mosquirix, L9, one of the mAbs that target PfCSP, has been identified as a molecule that can prevent PfCSP from executing its function in malaria development and pathogenesis by binding to it and facilitating the destruction of the parasites' sporozoites.

Due to the several problems malaria presents and the resistance that the parasite is mounting, studying the Hsp90 and CSP proteins and their interaction with geldanamycin and L9, respectively, can lead to the development of better and efficacious anti-malarial medicines and vaccines. The drugs or vaccines can be discovered by searching for natural compounds that target and preferentially bind to the active sites of PfHsp90 and PfCSP, thereby preventing their functions in malaria growth and pathogenesis.

1.4 Scope of the Study

This study seeks to mine PfHsp90 and PfCSP inhibitors with pharmacological activity against *Plasmodium* malaria. The research will involve the use of *in-silico* approaches, including evolutionary analysis, virtual screening, pharmacokinetics analysis, and molecular docking to determine and characterize PfHsp90 and PfCSP inhibitors with pharmacological activity against *Plasmodium* malaria. The study will also assess the stability of complexes formed between these inhibitors with their respective target proteins, PfHsp90 and PfCSP, using MDS. Ultimately, the study will perform an experimental assay, *in vitro* validation, to determine the inhibitory levels of the PfHsp90 and PfCSP inhibitors against their respective target proteins. The study aims to find novel antimalarial drugs and adjuvants that can aid malaria eradication and assist in mitigating antimalarial drugs resistance.

1.5 Significance of the Study

Malaria remains a public health burden affecting millions of people annually, making this study necessary. The significance of this study is multifaceted, ranging from the cost element to health impacts. Discovery of novel antimalarial drugs and malaria vaccine adjuvants will expand the arsenal of malaria treatment options. The new antimalarial candidates might not only provide effective therapies but also overcome the antimalarial drug resistance problem that is derailing the fight against *Plasmodium* malaria. The vaccine adjuvants might improve the efficacy of Mosquirix, further aiding the fight against *Plasmodium* malaria.

1.6 Objectives

1.6.1 General Objective

To perform an *in-silico* screening and *in-vitro* validation of PfHsp90 and PfCSP inhibitors with pharmacological activity against *Plasmodium* malaria.

1.6.2 Specific Objectives

1. To identify novel PfHsp90 and PfCSP inhibitors with pharmacological activity against *Plasmodium* malaria and potential to enhance Mosquirix efficacy, respectively.
2. To determine the stability of the molecularly docked target protein-inhibitors complexes.
3. To determine an *in vitro* validation of the inhibitory levels of the selected PfHsp90 and PfCSP inhibitors.

1.7 Research Questions

1. Which natural compounds from databases such as ZINC20 exhibit superior pharmacological activity as PfHsp90 inhibitors against *Plasmodium* malaria, and as PfCSP inhibitors with potential to enhance Mosquirix efficacy, compared to benchmark agents geldanamycin and monoclonal antibody L9, respectively?

2. How stable are the discovered PfHsp90 and PfCSP inhibitors when complexed with their target proteins?
3. Are the discovered PfHsp90 and PfCSP inhibitors capable of preventing the growth of the *Plasmodium* parasite *in vitro*?

CHAPTER TWO

LITERATURE REVIEW

2.1 Introduction

Malaria is a global health burden with approximately 241 million cases and 627,000 deaths in 2020 and 227 million cases and roughly 558,000 deaths in 2019 (WHO, 2022). Stofberg *et al*. (2021) projected 229 million infections and more than 419,000 fatalities worldwide in 2019. The figures for malaria deaths in 2019 surpassed this projection, indicating that the disease persists as a significant public health burden. Africa contributed 95% of malaria cases and 96% of deaths to the global malaria figures in 2020 (WHO, 2022). 95% of malaria-related deaths occur in sub-Saharan Africa, and 67% involve kids aged five years and below (Sarfo *et al*., 2023). Malaria is caused by the *Plasmodium* species, a single-celled eukaryote protozoan parasite in the phylum Apicomplexa. The conventional methods of developing drugs and vaccines are expensive and time-consuming (Onyango *et al*., 2022). Therefore, there is a paradigm shift from these traditional drug and vaccine development techniques to the rapidly emerging *in-silico* approaches that are revolutionizing vaccine and drug discovery. Some *in-silico* tools for developing vaccines include ANTIGENpro, AllergenFP, AllerTOP, and others (Shiragannavar & Madagi, 2021). Researchers have used such *in-silico* vaccine design tools and techniques to develop vaccine candidates. For instance, Khalid *et al*. (2022) created a rational vaccine design utilizing the method of epitope mapping against the infections caused by *Acinetobacter baumannii*. The authors combined epitopes of an outer membrane protein with immunogenic potential (target protein) to form a 240 amino-acid vaccine sequence that underwent different processes to act as a vaccine candidate (Khalid *et al*., 2022). Using *in-silico* approaches to designing vaccines can lead to an effective fight against infectious diseases.

On the same note, drug development increasingly relies on computer-aided drug design (CADD) approaches, which are essential for efficiently identifying viable drug candidates. These computational techniques help medicinal chemists and pharmacologists during the drug discovery process by reducing the usage of animal models in pharmacological research, assisting in the rational design of novel and safe drug candidates, and repurposing already-marketed medications (Brogi, 2020).

Some *in-silico* drug design and development approaches include pharmacophore modeling, drug design visualization, hierarchical visual screening, molecular docking, molecular dynamics simulations, and others (Onyango *et al*., 2022). Several researchers have used some of these *in-silico* techniques to develop drug candidates. For instance, Onyango *et al*. (2022) used *in-silico* methods to discover potential anti-SARS-CoV-2 main protease (M^{pro}) drugs. In the study, the protein SARS-CoV-2 M^{pro} was used as the target.

In most *in-silico* drug discovery processes, a target protein is usually used to assist in identifying its potential inhibitors. Two of the most desirable drug targets in the fight to eradicate malaria are PfHsp90 and PfCSP. The formation of the PfHsp70-*P*. *falciparum* Heat Shock Protein 90-Heat Shock Protein 70 Organizing Protein (PfHop)-PfHsp90 complex within a host facilitates the onset and progression of malaria. PfHop is a protein molecule that functions as a link between the two Heat Shock Proteins (Hsps), 70 and 90. The protein molecule has three significant domains referred to as tetratricopeptide repeat (TPR) domains (Hatherley *et al*., 2015). They include TPR1, TPR2A, and TPR2B. The TPR2A and TPR1 domains have sites where the conserved C termini amino acid residues EEVD of both Hsp90 and Hsp70 can bind, respectively (Hatherley *et al*., 2015; Zininga *et al*., 2015). The EEVD of Hsp90 usually interacts with amino acids positively charged in Heat Shock Protein 90-Heat Shock Protein 70 Organizing Protein (Hop). The positively

charged amino acids are carboxylate clamps (Krysztofinska *et al*., 2017; Mishra *et al*., 2018). Any single point mutation at the carboxylate clamps can affect Hsp90 binding and destabilize the global conformation of Hop (Krysztofinska *et al*., 2017).

However, the TPR domains are usually not affected. Between TPR1 and TPR2A exists a DP (Degree of Polymerization) domain referred to as DP1. Another DP domain exists between TPR2B and Hop's C terminus. It is alluded to as DP2 (Hatherley *et al*., 2015). The association between Hsp90 and Hop takes place in the TPR2A domain. TPR2A binds to the MEEVD motif situated at the C terminal residues of Hsp90. The concave interface of TPR2A is involved in this interaction, but it does not explain the strong affinity of the TPR domain to the Hsp90 molecule. The convex surfaces of TPR2A and TPR2B can form an interaction with the Hsp90 molecule (Hatherley *et al*., 2015). However, this kind of interaction is believed to prevent the activity of ATPase, an Hsp90 enzyme, by forcing the heat shock protein to change its conformation (Hatherley *et al*., 2015; Krysztofinska *et al*., 2017; Zininga *et al*., 2015). Therefore, Hsp90 often binds to the concave interface of TPR2A. Preventing this linkage using anti-malarial compounds like geldanamycin (GDM) can assist in eradicating malaria (Zininga *et al*., 2015). However, GDM is not being used because of its hepato-toxicity and poor solubility. Therefore, discovering other PfHsp90 inhibitors with better pharmacokinetic properties than GDM can help eliminate malaria.

Apart from Hsp90, circumsporozoite surface protein (CSP) is also a malaria vaccine and drug target. It is the most prevalent polypeptide in the sporozoite covering. This protein functions in the sporozoite's motility and invasion as it enters the hepatocyte (Storti-Melo *et al*., 2022). Fernández-Arias *et al*. (2015) outline that a scientific team discovered circumsporozoite as a significant surface protein of *P. berghei* sporozoites. Following this, CSPs of additional plasmodial species were found and demonstrated to have comparable structural and immunological characteristics.

An immunodominant B cell epitope's random repeat surrounded by C- and N-terminal domains make up the CSP, which has an estimated size of 40–60 Kilodalton (kDa) (Fernández-Arias *et al*., 2015).

In the salivary invasion and maturation process in the vector and human liver cells, the CSP of the infective sporozoite of all *Plasmodium* species can be evidenced. The finding of sequence variation in the repeated sequence of its core part gene forced a re-evaluation of this strategy. However, it has been a prominent target in creating recombinant malaria vaccines (Storti-Melo *et al*., 2022). The central repeat region (CRR) and the conserved domains RI (positioned in the amino-terminal) and RII (situated in the carboxyl-terminal) are present in all CSPs (Storti-Melo *et al*., 2022). Being an essential component of *P. falciparum* sporozoites, CSP has been used to create a malaria vaccine (Mosquirix) that generates monoclonal antibodies (mAbs) against CSP. L9 is one of the mAbs that target PfCSP or can be considered anti-PfCSP. Discovery of other molecules that target PfCSP can help eradicate malaria by improving the efficacy of the Mosquirix vaccine.

2.2 *P. falciparum* Life Cycle

Within the vertebrate human host and the vector, the female Anopheles mosquito, *P. falciparum,* leads a highly complex life cycle, **Figure 2.1** (Nadeem *et al*., 2022). After a blood meal, an infected mosquito injects the sporozoites into the dermis, where they travel to the bloodstream and cause the unicellular protozoan parasites to infect people. The sporozoites travel through the blood and enter hepatocytes, where they begin to reproduce asexually for the first time (Langlois *et al*., 2020). Merozoites are finally delivered into the bloodstream when the infested hepatocytes burst. They infect RBCs to start the intra-erythrocytic growth phase. The *P. falciparum* first develops into the ring phase, then into trophozoites, and finally, schizonts, which burst to release merozoites that

reinvade fresh RBCs (Stofberg *et al*., 2021). A tiny number of the ring-stage parasites in the infected RBC (iRBC) may also mature sexually to become gametocytes.

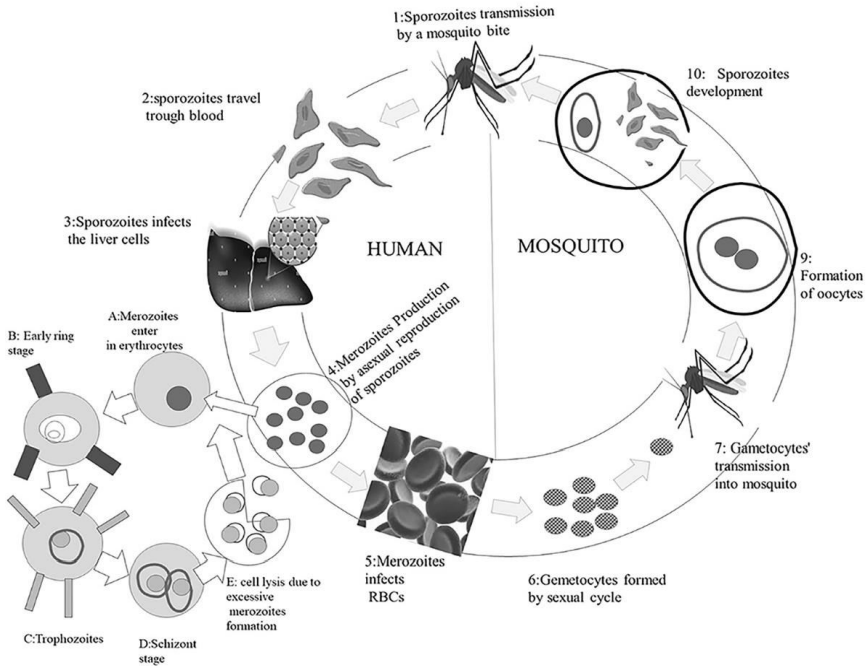

Figure 2.1: *P. falciparum* life cycle. The cycle shows how malaria is transmitted from infected mosquitoes to humans (Nadeem *et al*., 2022).

By ingesting them during a blood meal, mosquitoes continue the cycle of transmission by producing gametes that initiate the cycle of sporogony inside the mosquito (Stofberg *et al*., 2021). The erythrocytic cycle of the parasite's life cycle is mainly linked to malaria symptoms; for instance, in *P. falciparum*, the adhesion phenomenon is connected to the severity of the illness (Lee *et al*., 2019). This is explained by the fact that the parasite and iRBC intracellular material are released when schizonts burst. The intracellular substances and exposed parasites trigger immunological reactions that aid in the pathogenesis of malaria (Sarfo *et al*., 2023). The change from the 25°C poikilothermic vectors to the 37°C homoeothermic host places the parasites in a harsh environment that they must withstand to complete their intricate life cycle. Thermal stress is

created as a result and exacerbated during fever episodes marked by temperature increases up to 41°C (Uwimana *et al*., 2020).

P. falciparum upregulates several molecular chaperones' expression to preserve its proteome because it requires a robust protein quality control mechanism to withstand these alterations (Bratt, 2024). Some of these molecular chaperones include Hsp90 and Hsp70. Inhibitors to such molecular chaperones can compromise the functional integrity of the Hsps and assist in destroying the parasite and preventing or treating malaria; thus, the need to determine novel PfHsp90 inhibitors with pharmacological activity against *Plasmodium* malaria through HVS using geldanamycin (GDM) as the ligand/reference structure.

2.3 Antimalarial Drug Resistance

Researchers have argued that Artemisinin-based Combination Therapy (ACT) is the only efficacious malaria treatment (Maiga *et al*., 2021; Pousibet-Puerto *et al*., 2016). However, Stofberg *et al*. (2021) explain that the extended ACTs clearance times, which are linked to the emergence of artemisinin monotherapy resistance, have been recorded most recently in Africa and the Great Mekong region, pose a danger to its efficacy. This trend in drug resistance is comparable to the medicine chloroquine's fate, where drug resistance first appeared in the early 2000s in the Mekong region before spreading widely to many areas, including Africa and East Asia. Genotypes of parasites resistant to the artemisinin medication have recently been discovered in Rwanda, indicating extensive artemisinin compound resistance (Tintó-Font *et al*., 2021). It is well known that parasite-targeted gene mutations cause the development of medication resistance (Stofberg *et al*., 2021). Antiparasitic drug concentrations are influenced by the proper operation of mutant genes connected to the inflow and efflux pumps; for instance, molecular chaperones such as the Hsps are responsible for the proper folding of mutated chloroquine resistance transporter (CRT).

All proteins can fold naturally when under stress, including pressure from drugs, thanks to these Hsps. Therefore, the Hsps are invaluable antimalarial drug targets.

Additionally, due to their crucial function in protein quality regulation, the genes, such as the CRT gene linked to multidrug resistance, are situated in the same Hsp90 gene cluster (Zininga *et al*., 2015). This implies that the expression of the mutant CRT gene and the chaperone may be similarly co-regulated by cis-regulatory elements like transcription factors. Furthermore, it has been established that various molecular chaperones interact directly and indirectly with CRT through an unknown mechanism (Sarfo *et al*., 2023). We hypothesize that Hsps' chaperoning function on proteins might facilitate drug resistance during the stress response. Since the 1600s, attempts have been made to control and manage anti-malaria drug resistance in vain (Chakrabarti *et al*., 2019). Reported malaria cases have always been in millions, as displayed in **Figure 2.2** (Chakrabarti *et al*., 2019). Therefore, Hsp90 can be considered a drug target whose inhibition prevents its role in protein folding and facilitates malaria treatment by reducing the level of antimalarial drug resistance that the parasite can mount within the body. In this regard, Hsp90 can be used as a target protein to discover inhibitors against *Plasmodium* malaria with geldanamycin (GDM) as the ligand/reference structure using computational approaches like HVS.

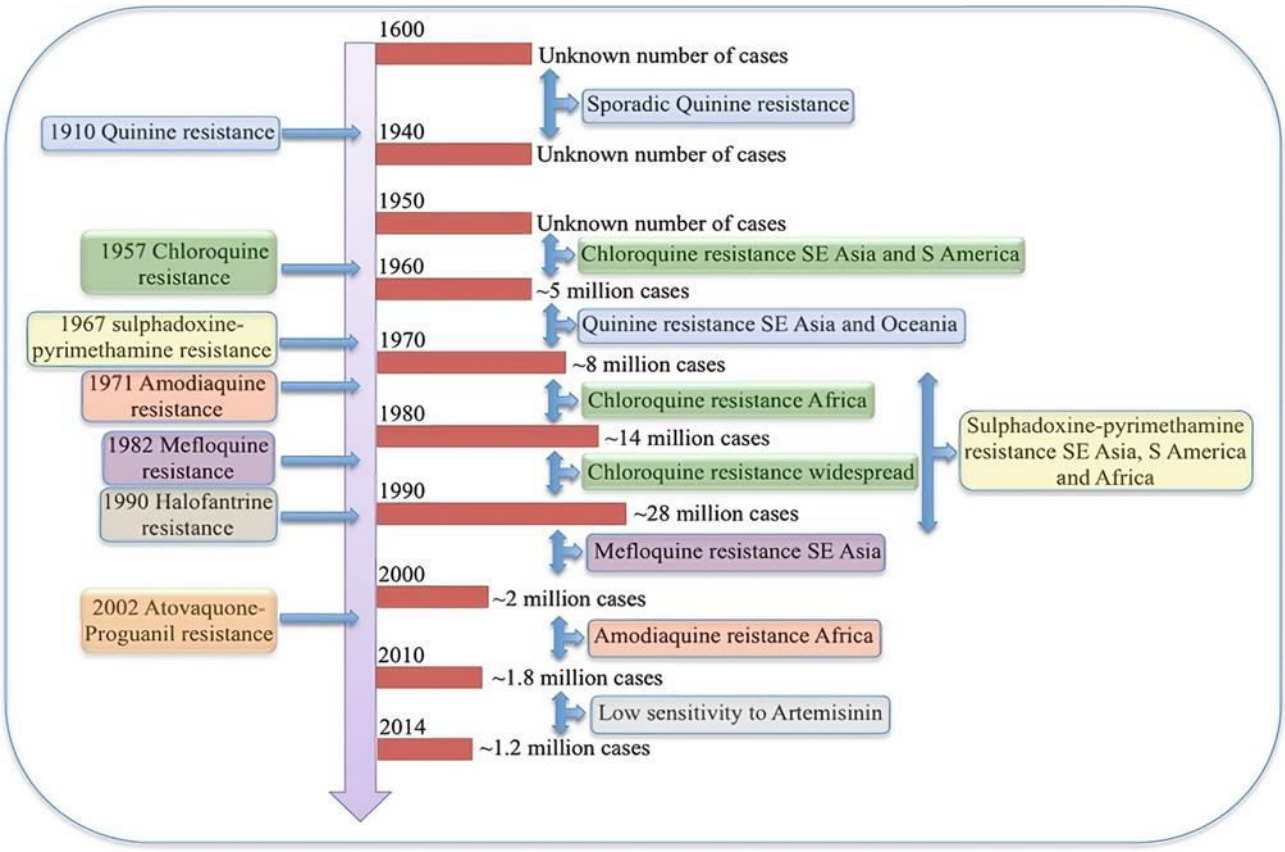

Figure 2.2: Antimalarial drug resistance. This timeline shows how *P. falciparum* has been mounting resistance to various antimalarial drugs over the years (Chakrabarti *et al*., 2019).

2.4 Malaria Vaccines

Even though numerous new drug compounds have been found to treat malaria, drug resistance development raises concerns about the effectiveness of the currently available medications (Islam *et al*., 2017; Shehzad *et al*., 2019). Creating a potential malaria vaccine is crucial to addressing such issues and is anticipated to effectively eradicate malaria worldwide (Nadeem *et al*., 2022). A vaccine that functions with maximum efficacy and efficiency, acting in a manner that first inhibits the pathogen's earliest growth phase before its subsequent stages, is the most efficient strategy to stop the spread of malaria. **Figure 2.3** (Laurens, 2020) shows the three major phases of the *P. falciparum* life cycle that can be broken using vaccines to prevent transmission and eliminate

malaria. The three phases include pre-erythrocytic, blood-stage, and transmission-blocking phases (Laurens, 2020). Making individuals immune to infectious diseases is one of the essential aspects of international health measures, especially in comparison to other human activities like cleanliness and sanitation (Draper *et al*., 2018). According to a recent phase IIb clinical trial with the identifier NCT03896724, the antigen R-21, a malaria vaccine candidate developed using Matrix-M adjuvant from Novavax Inc. by the University of Oxford, showed 77% effectiveness in children (Datoo *et al*., 2021).

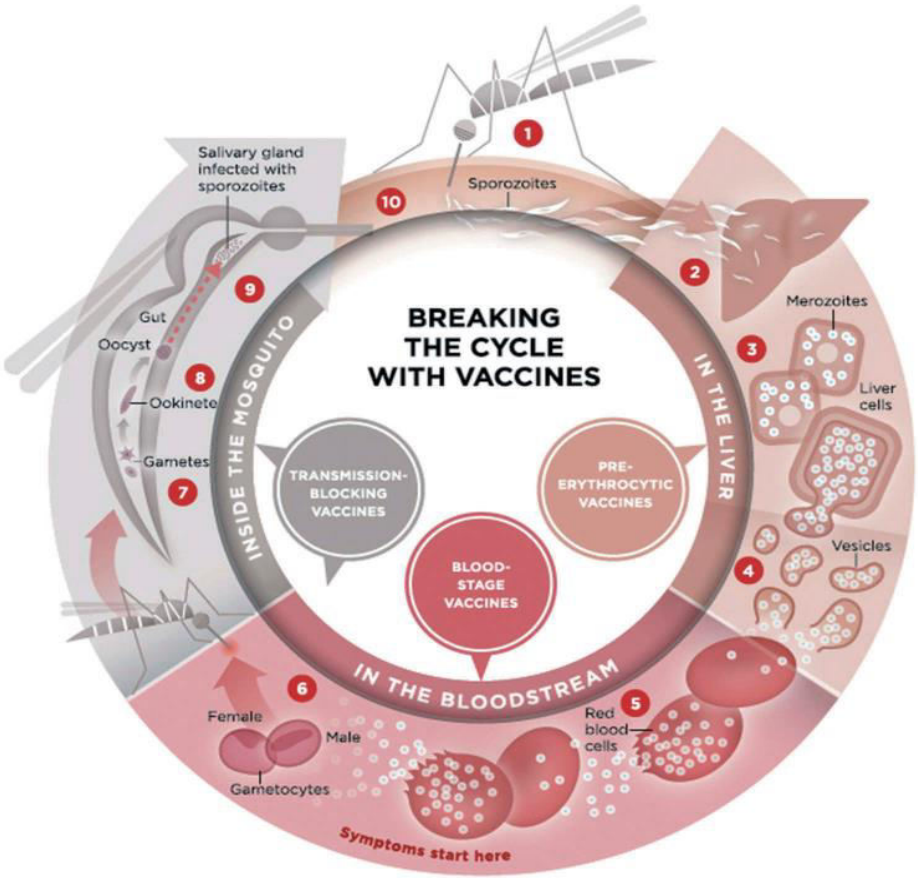

Figure 2.3: Malaria vaccine targets. The three major phases of the *P. falciparum* life cycle that can be broken using vaccines to aid in eliminating malaria include pre-erythrocytic, blood-stage, and transmission-blocking phases (Laurens, 2020).

However, the research on implementing the first malarial vaccine ordered by WHO is the most noteworthy undertaking that has been completed in this respect (Draper *et al*., 2018). The most

progressive malaria vaccine is the RTS,S vaccine (Nadeem *et al*., 2022), with only around 36% efficacy. It is acknowledged that vaccines can induce defense from novel infections by inducing robust cellular and humoral immune reactions against *Plasmodium*'s sporozoite phase in the mammal host. However, the fundamental mechanisms provoking immune reactions to malaria pre-erythrocytic phases are not entirely comprehended.

While the vaccinated host produces sporozoite-specific antibodies that prevent sporozoite invasion of the hepatocytes (Marques-da-Silva *et al*., 2020), satisfactory amounts of sporozoite antigen-specific T lymphocytes aid in the elimination of the liver cells infected with the *Plasmodium* parasites that display these epitopes (Kurup *et al*., 2019). The associations between the host hepatocytes and sporozoite depend on the Circumsporozoite Protein (CSP), a crucial component of the sporozoites' surface coat (Nadeem *et al*., 2022). As a result, the CSP can potentially be a target antigen in anti-malarial vaccines for the pre-erythrocytic stage. This study used CSP as a target molecule to discover compounds that can enhance the RTS,S vaccine's efficacy and its public health benefits.

2.5 Hsp90, CSP, and their Functional Cycles

Hsp90 and CSP have been well-characterized in the existing literature. Understanding their functional cycle is essential to identifying their active sites or binding pockets in which inhibitors can be docked. Spiegelberg *et al*. (2020) consider the Hsp90 an evolutionary conserved and widely expressed molecular chaperones group that accounts for around 2% of the cellular proteome. Almost all organisms possess Hsp90 proteins, which are necessary for eukaryotes to survive but optional for some eubacterial species to survive under normal circumstances (Honoré *et al*., 2017; Schopf *et al*., 2017). Hsp90 chaperone is essential in reducing stress and preserving cellular homeostasis.

Schopf *et al*. (2017) explain that as a critical regulator of vital physiological functions, including protein folding, stress control, DNA repair, growth, signaling pathways, and immunological response, Hsp90 cooperates with a wide range of client proteins. Hsp90s are desirable pharmacological targets for numerous illnesses, including neurological conditions, cancer, and infectious illnesses like malaria, because of their crucial role in cell survival (Schopf *et al*., 2017). The Hsp90 family members are ATP-dependent chaperones involved in numerous biological functions (Schopf *et al*., 2017). Adenosine triphosphate (ATP) binding and subsequent hydrolysis power the Hsp90, which occurs as a V-shaped homodimer functional cycle (**Figure 2.4**) (Stofberg *et al*., 2021).

The release of the appropriately folded client protein is then made possible by the dissociation of the NTDs brought on by ATP hydrolysis (Radli & Rüdiger, 2018; Rashid *et al*., 2020). Therefore, Hsp90's active site is found within the NTD, where ATP can bind and initiate the folding of different client proteins. Finding compounds that can bind to Hsp90's N-terminal ATP binding site can help curtail the protein's function of assisting the folding of other client proteins.

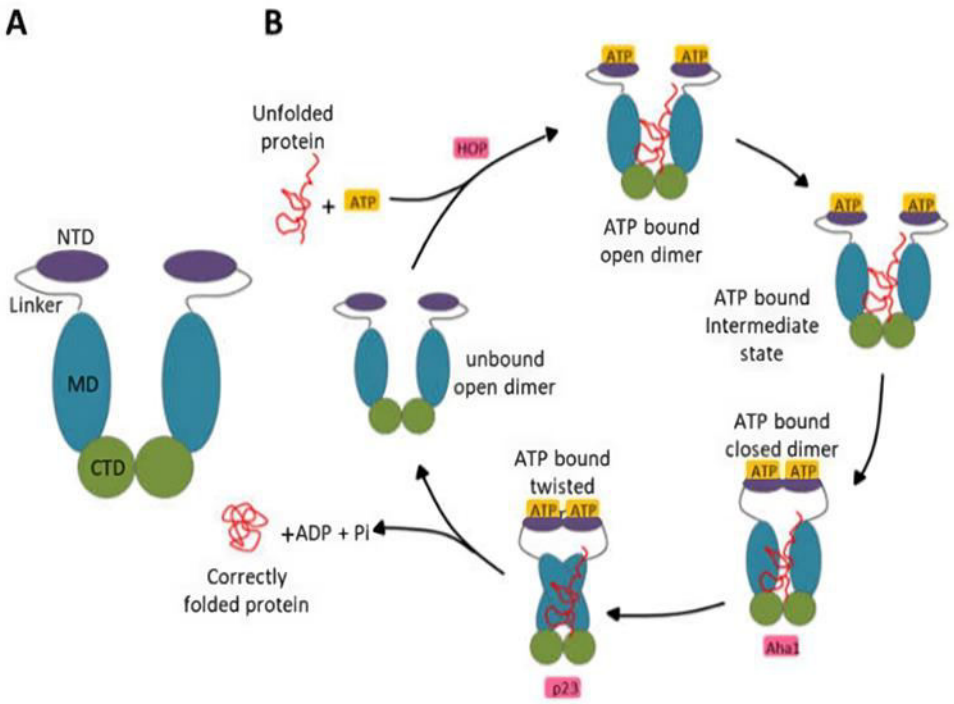

Figure 2.4: Hsp90 domain organization and functional cycle. (**A**) Schematic representation of the V-shaped domain organization of the Hsp90 protein. (**B**) Schematic representation of the Hsp90 functional cycle begins with the binding of ATP to Hsp90, provoking the association of the protein with a client/unfolded protein. Consequently, a closed conformation is adopted following the NTD dimerization after the lid region of Hsp90 closes over the ATP binding pocket. ATP hydrolysis occurs after repositioning the catalytic loop when the MDs associate. The correctly folded client protein is released upon ATP hydrolysis. This protein folding and ATP hydrolysis cycle reoccur after the Hsp90 homodimer regains its unbound open configuration and is primed. Aha1, HOP, and p23 are other co-chaperones that modulate this functional cycle (Stofberg *et al*., 2021).

Apart from Hsp90, several scholars have also identified PfCSP as a malaria drug and vaccine target. Therefore, it is not surprising that the RTS,S/AS01 recombinant, CSP-based vaccine is one of the most well-known anti-malarial subunit vaccines. A lesser amount of aspartic acid and valine residues can be found in the 58 kDa CSP protein, which also has 37–49 NANP (N, asparagine; A, alanine; P, proline) amino acid repeats (Marques-da-Silva *et al*., 2020). Marques-da-Silva *et al*. (2020) outline that Multiple Human Leukocyte Antigens DR Isotype (HLA-DR) compounds can detect the T cell epitopes of the CSP C-terminal region.

In human trials, it was discovered that the RTS,S/AS01 vaccine produced cellular and humoral responses that protected mosquito bite challenge infections (Marques-da-Silva *et al*., 2020). Along with protecting against malaria, the vaccine also produced defensive immune reactions against Hepatitis B because it was intentionally designed to include a portion of the Hepatitis B surface antigen (HBsAg) as part of its molecular structure (Valéa *et al*., 2020). Different researchers have developed some monoclonal antibodies against CSPs of other plasmodial species using Mosquirix (Valéa *et al*., 2020). Most of them have been demonstrated to identify CSP immunodominant repeat domain and to counteract parasite infection *in vitro* and, in some instances, *in vivo* (Fernández-Arias *et al*., 2015).

Notably, one study used a phage display library to successfully recover a monoclonal antibody against CSP from a person exposed to *P. falciparum* sporozoites (Fernández-Arias *et al*., 2015). This study seeks to explore the possibility of discovering other effective compounds that can increase the efficacy of the RTS,S/AS01 vaccine by characterizing novel PfCSP inhibitors with pharmacological properties on Mosquirix through HVS using monoclonal antibody L9 as the ligand/reference structure. **Plate 1** (Loubens *et al*., 2021) displays the functional cycle of CSP in malaria development, providing avenues that can be exploited to discover anti-CSP compounds.

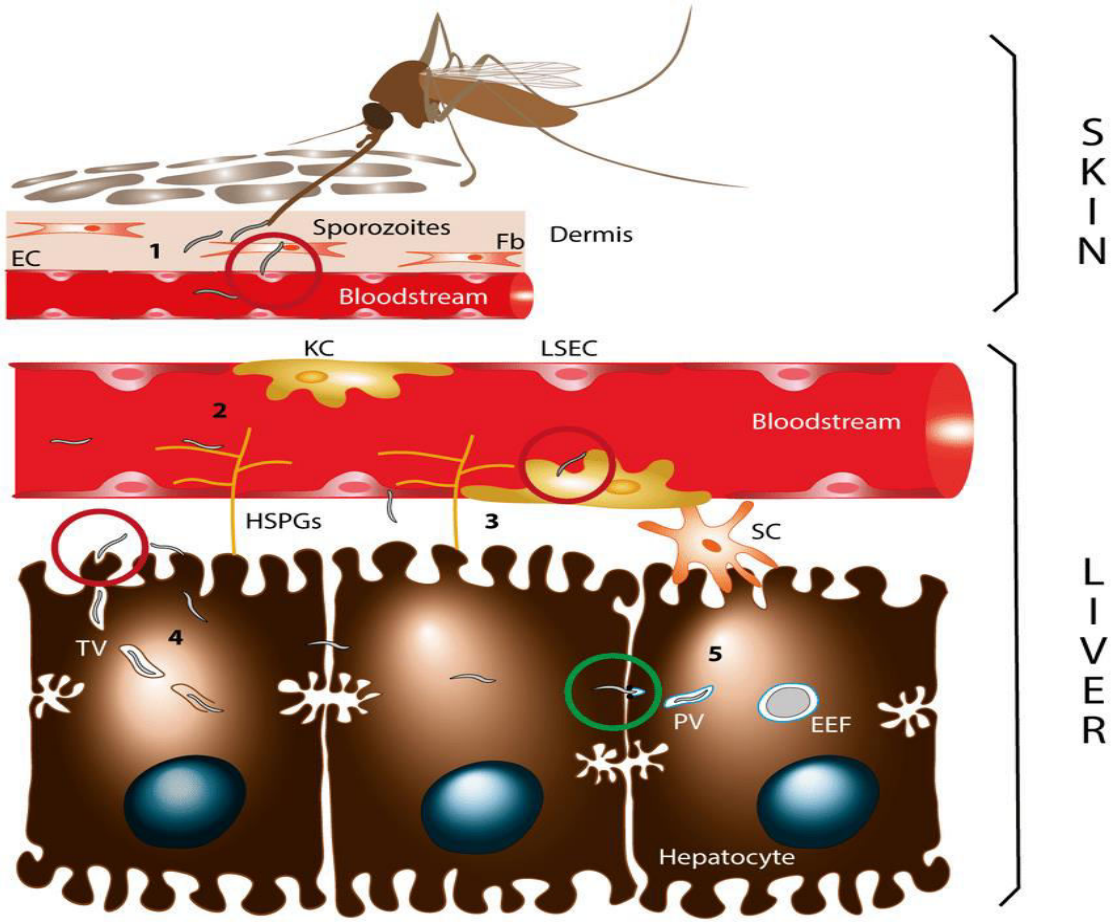

Plate 1: CSP functional cycle. (**1**) An infected mosquito deposits sporozoites in the mammalian host dermis via a bite. (**2**) The sporozoites enter the bloodstream by crossing the dermal fibroblasts (Fb) and endothelial cells (EC). They then traffic to the liver. The sporozoites are sequestered in the liver sinusoids through the association between hepatic heparan sulfate proteoglycans (HSPGs) and CSP. (**3**) Those sporozoites, through Kupffer cells (KCs) and liver sinusoidal endothelial cells (LSECs), cross the sinusoidal cellular barrier into the liver parenchyma. (**4**) The sporozoites traverse through numerous liver cells, sometimes inside a transient vacuole (TV). (**5**) A parasitophorous vacuole (PV) formation, in which the parasite matures into a replicative exoerythrocytic form (EEF), enables the sporozoites to switch to the productive invasion of a final hepatocyte (Loubens *et al*., 2021).

2.6 *P. falciparum* Hsp90 as a Drug Target

In early studies, Hsp90 inhibitors were primarily used to treat cancer (Koren & Blagg, 2020). Due to the cancer cells' insatiable addiction to Hsp90 (Koren & Blagg, 2020), these inhibitors mainly

targeted Hsp90 NTD's ATP binding pocket (Stofberg *et al*., 2021). These characteristics make Hsp90 a promising target for anti-cancer medications (Han *et al*., 2018). In *P. falciparum*, similar to other eukaryotes, all four Hsp90s may be necessary for parasite persistence and changes in erythrocytic stage transitions (Stofberg *et al*., 2021). Hsp90 proteins are desirable therapeutic targets for several reasons. First, Hsp90s are ATPases with differing activity levels in various organisms (Whitesell *et al*., 2019), and diseased cells have higher ATP hydrolysis rates, making them more vulnerable to ATPase inhibitors (Stofberg *et al*., 2021).

Numerous crystal structures of various Hsp90 NTDs in complex with inhibitors and nucleotides have been resolved (Que *et al*., 2018). Additionally, Hsp90's complete structural characterization has prompted the creation of inhibitors targeting its MD (Silva *et al*., 2020; Zhang *et al*., 2018; Mak *et al*., 2021) and CTD (Bopp *et al*., 2016). **Figure 2.5** (Dutta *et al*., 2022) shows PfHsp90's domain organization and structure. Through targeting Hsp90, some inhibitors have been demonstrated to be efficient at reducing the parasite's development (Posfai *et al*., 2018; Wang *et al*., 2016; Zininga & Shonhai, 2019). Therefore, PfHsp90 was used as the target protein to determine novel PfHsp90 inhibitors with pharmacological activity against *Plasmodium* malaria through HVS using GDM as the ligand/reference structure.

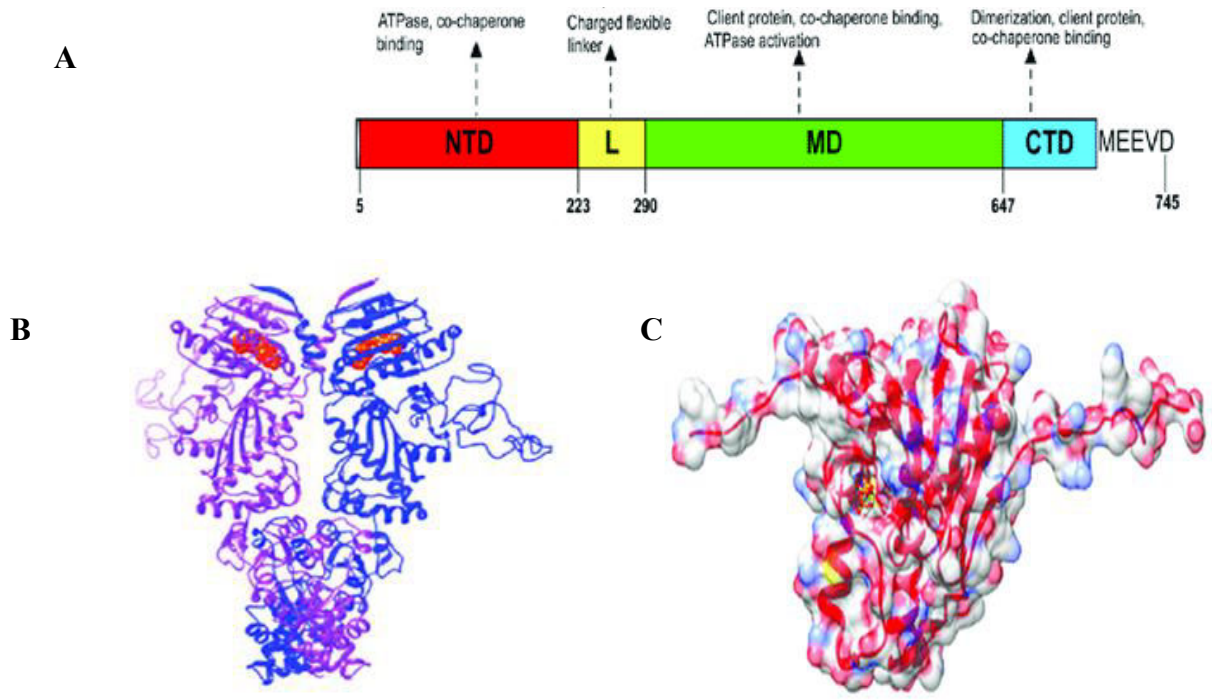

Figure 2.5: PfHsp90 domain organization and structure view. (**A**) Schematic model of the different PfHsp90 domains labeled NTD (N-Terminal Domain), L (Linker Region), MD (Middle Domain), and CTD (C-Terminal Domain). (**B**) Cartoon representation of PfHsp90 proteins. Red spheres represent ATP bound to NTD. The purple and blue colors in the model depict the two PfHsp90 monomers. (**C**) Surface representation of PfHsp90's NTD with 60% transparency and colored according to element type (Dutta *et al*., 2022).

2.7 *P. falciparum* CSP as a Vaccine Target

Since PfCSP is necessary for the central surface protein on infectious sporozoites (SPZ) to infect hepatocytes, it is the ideal vaccine target. As shown in **Figure 2.6** (Draper *et al*. 2018), a C-terminus, a repeated tetrapeptide core domain, and an N-terminus are the three domains that makeup PfCSP (Wang *et al*., 2022). The region at the intersection of the repeat domain and N-terminus in the Pf3D7 reference strain begins with NPDP and is followed by three repeats that alternate between NANP and NVDP. 35 NANP repeats follow this "junctional zone," with a fourth NVDP added after the twentieth NANP (Cockburn & Seder, 2018).

According to structural analyses, the three tetrapeptides joined to form DPNA, NPNV, and NPNA are the motifs that PfCSP mAbs recognize in the repetition domain (Oyen *et al*., 2018). Notably,

RTS,S only has the C-terminus and 19 NANP repeats (Wang *et al*., 2022). All counteracting PfCSP mAbs described in existing literature target the immunodominant NANP repeats (Julien & Wardemann, 2019). Nonetheless, identifying uncommon and powerful mAbs that bind NPDP (Kisalu *et al*., 2018; Tan *et al*., 2018) or the NVDP repeats (Wang *et al*., 2020) highlighted these subdominant epitopes as weak spots on PfCSP. These discoveries resulted in the creation of next-generation vaccines against the junctional area because these epitopes are not seen in RTS,S (Atcheson *et al*., 2021; Calvo-Calle *et al*., 2021; Francica *et al*., 2021).

Scholars have lately identified which epitopes can enhance immunogen design and choose the most effective mAb for medical progress by examining the binding and efficacy of a panel of defensive human PfCSP mAbs. The panel's most effective protective mAb was mAb L9, which primarily binds NVDP repeats and cross-reacts with NANP repeats (Wang *et al*., 2020). Isothermal titration calorimetry (ITC) revealed that L9 and other powerful mAbs bound recombinant PfCSP (rPfCSP) in two binding occurrences with different attractions, raising the possibility that this *in vitro* hallmark of "two-step binding" might be associated with *in vivo* sporozoites neutralization (Wang *et al*., 2020). Therefore, PfCSP was used as the target protein to characterize novel PfCSP inhibitors with pharmacological properties on Mosquirix through HVS using monoclonal antibody L9 as the ligand/reference structure.

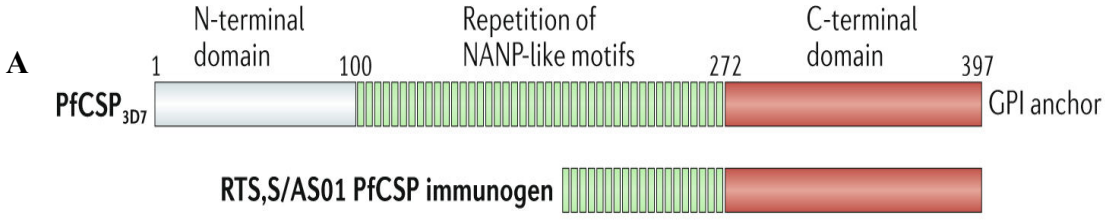

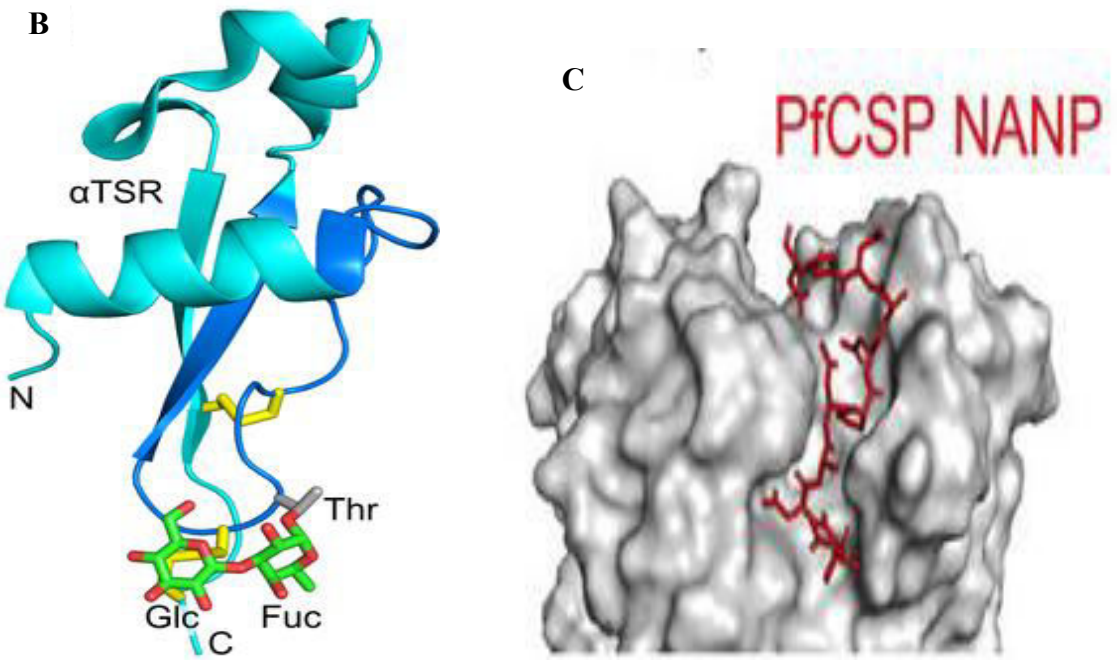

Figure 2.6: PfCSP domain organization and structure view. (**A**) Schematic model of the different PfCSP domains labeled as N-terminal domain, NANP repetition domain, and C-terminal domain. The figure also shows the Mosquirix PfCSP immunogen that shares structural similarities to PfCSP (Julien & Wardemann, 2019). (**B**) Mass spectrometry observed a 3D model of the TSR domain of CSP displaying glycosylation location. Glycans are represented using sticks with green denoting carbon and red signifying oxygens. Silver carbons and blue nitrogens represent amino acid side chains attached to glycans. Yellow denotes disulfide bonds (Swearingen *et al*. 2016). (**C**) Surface representation of how antibodies interact with PfCSP by binding to its NANP repeats to prevent sporozoites from invading hepatocytes (Draper *et al*. 2018).

2.8 Overview of Inhibitors in *In-Silico* Drug Discovery

In *in-silico* drug discovery, inhibitors can be defined as molecules that disrupt the biological activity of target proteins by binding to their active or allosteric sites and altering their function (Brogi *et al*., 2020; Onyango *et al*., 2022). In diseases including cancer, infectious diseases, and autoimmune disorders, where pathology is driven by dysregulated protein activity, inhibitors are crucial to the development of therapeutics. Clinical efficacy and safety depend on the selectivity and potency of inhibitors, which might be small compounds, peptides, or biologics (Wankhede *et al*., 2024).

In-silico techniques have made it possible to rationally create inhibitors that target important *Plasmodium* proteins like PfHsp90 and PfCSP in the context of malaria research. Prior to moving on to *in vitro* or *in vivo* testing, researchers can rank drugs with high selectivity and anti-parasitic potential by simulating molecular interactions and comparing binding efficiencies (Wankhede *et al*., 2024). In this study, two such inhibitors were examined: monoclonal antibody L9, which binds to PfCSP, and geldanamycin, a small chemical that targets PfHsp90. Both of these inhibitors were employed as reference ligands in virtual screening procedures to find new anti-malarial compounds.

2.9 Geldanamycin (GDM) and L9 as Inhibitors

One of the first Hsp90 inhibitors discovered was geldanamycin (GDM), a benzoquinone ansamycin molecule naturally generated by *Streptomyces hygroscopicus* (Stofberg *et al*., 2021). GDM was initially believed to be an antibiotic that inhibited kinases, but it was later discovered that it had a high degree of selectivity in its binding to Hsp90 (Sarfo *et al*., 2023). Some of these initial studies targeted Hsp90 in tumor cells and eventually adapted their findings to treat other illnesses, such as malaria. As a result, it was demonstrated that some cancer treatments and inhibitors have strong anti-plasmodial efficacy (Posfai *et al*., 2018).

GDM competitively binds to the PfHsp90's ATPase domain (Stofberg *et al*., 2021). The unfolded client protein is then degraded due to GDM's ability to prevent PfHsp90-client protein interaction (Bratt, 2024). In a study at an IC_{50} similar to the well-known anti-malarial chloroquine (20 nM and 15 nM, respectively), GDM suppressed *in vitro* parasite development (Stofberg *et al*., 2021). PfHsp90 may be crucial for the growth of parasites because its inhibition causes a stage evolution arrest for intra-erythrocytic parasite phases, primarily the transition from the ring to the trophozoite

stages (Sarfo *et al*., 2023). Furthermore, GDM has been noted to be similarly effective against strains that are sensitive to and resistant to chloroquine (Stofberg *et al*., 2021).

Compared to human HSPC2, independent research found GDM to be extra efficacious at decreasing PfHsp90's ATPase action (Bratt, 2024). This shows that GDM is more selective in abrogating PfHsp90's enzymatic role than its human counterpart. Therefore, it was used as the reference ligand during virtual screening to determine novel PfHsp90 inhibitors with pharmacological activity against *Plasmodium* malaria. **Plate 2** shows the interaction between PfHsp90 and GDM.

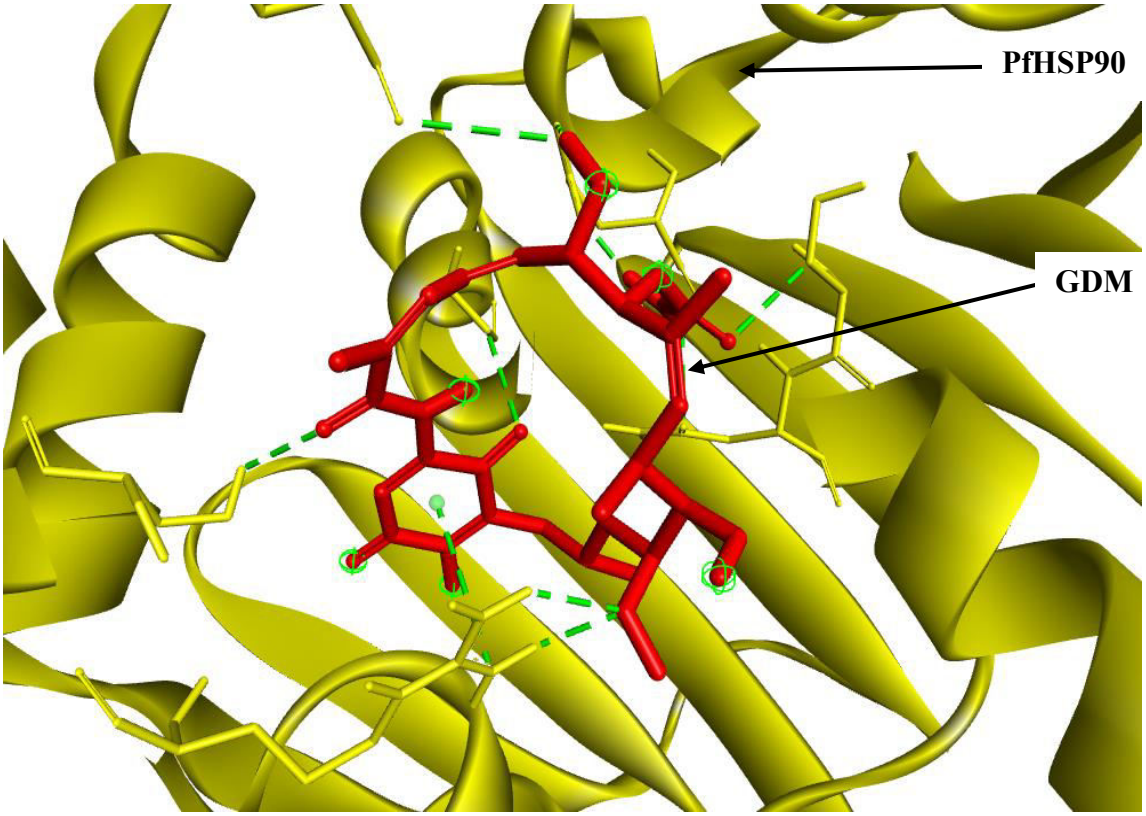

Plate 2: Geldanamycin (GDM) as a PfHsp90 inhibitor. The red stick-like structure represents GDM. The green dotted lines display the interaction points between GDM and PfHsp90. The structure is available in the PDB database (https://www.rcsb.org/) (Berman *et al*., 2000) and can be retrieved using the PDB ID 1YET. BIOVIA Discovery Studio 2021 (BIOVIA, 2021) was used to find the suitable binding pocket pose and show the points of interaction between the two molecules.

Similarly, L9 is another inhibitor that can assist in eradicating malaria. It is a powerful human monoclonal antibody (mAb) that binds to PfCSP on malaria-infective sporozoites and cross-reacts with significant NANP repeats (Wang *et al*., 2022). It is easier to develop vaccines if the ontogeny and PfCSP binding mechanisms of this mAb are understood. Wang *et al*. (2022) isolated mAbs with a clonal affinity for L9 and demonstrated how this B-cell lineage initially exhibits NVDP affinity before developing NANP reactivity. Combining the L9 kappa light chain (L9) with clonally-associated heavy chains creates chimeric mAbs that cross-link two NVDP, react with NANP, and kill sporozoites *in vivo* more effectively than their light chain-only counterparts (Wang *et al*., 2022). The chimeric mAbs bound minor repeats in a type-1-turn similar to other repeat-specific antibodies, according to structural studies undertaken by Wang *et al*. (2022). These findings demonstrate the critical role L9 plays in binding NVDP to PfCSP to kill sporozoites and imply that PfCSP-based immunogens may benefit from the presentation of 2 NVDP (Wang *et al*., 2022). In this regard, mAb L9 was essential in the study as a reference ligand for virtual screening to characterize novel PfCSP inhibitors with pharmacological properties on Mosquirix. **Plate 3** shows monoclonal antibody L9 as a PfCSP inhibitor and its interaction with PfCSP.

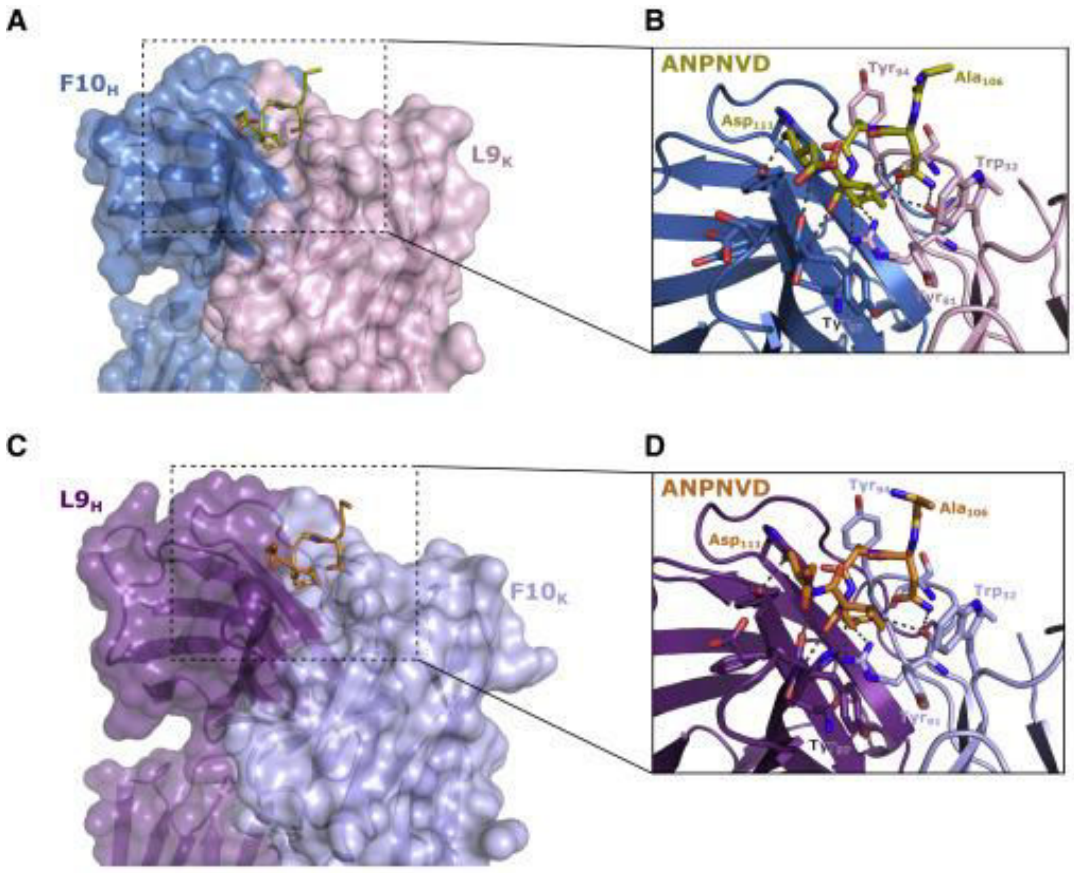

Plate 3: L9 as a PfCSP inhibitor. (**A & C**) Transparent surface representation with a visible cartoon representation of F10HL9k Fab (**A**) structures and L9HF10k Fab (**C**) bound to NANPNVDP. (**B & D**) Zoomed-in images of the binding sites in F10HL9k Fab (**B**) and L9HF10k Fab (**D**). The stick representations show the peptide interacting residues, with the dashed lines signifying hydrogen bonds (Wang *et al*., 2022).

2.10 *In-Silico* Drug Discovery

In-silico techniques can be used to test the anti-plasmodial activity of synthetic compounds *in vivo* through molecular binding. For instance, Tahghighi *et al*. (2020) used *in-silico* methods to ascertain that the synthetic derivatives of 1-(heteroaryl)-2-((5-nitroheteroaryl) methylene) hydrazine that showed anti-plasmodial activities *in vitro*, also possessed the same capability *in vivo*. From the molecular docking results in the study, the authors verified *Pf* lactate dehydrogenase (LDH) inhibition and the inhibitory effect on the haemozoin formation for the

studied compounds (Tahghighi *et al*., 2020). In a similar study, Sachdeva *et al*. (2020) used *in-silico* approaches to assess the capability of repurposing approved antimalarial drugs against COVID-19. The researchers discovered that the antimalarial drug doxycycline (DOX) could be an ideal candidate for repurposing for COVID-19 because it bound effectively to the spike protein of SARS-CoV-2 (Sachdeva *et al*., 2020). These studies prove that *in-silico* methodologies are ideal complements to drug design, development, and discovery.

Similarly, computational methods have been used in vaccine design and development (Shiragannavar & Madagi, 2021). In fact, as evident in existing literature, the use of *in-silico* techniques to design and develop vaccines is gaining popularity at a tremendous rate. Some *in-silico* tools for developing vaccines include ANTIGENpro, AllergenFP, and AllerTOP (Shiragannavar & Madagi, 2021). Several researchers have used *in-silico* tools and approaches to create vaccine candidates. For instance, to prevent illnesses caused by *A. baumannii*, Khalid *et al*. (2022) developed a logical vaccine design using the epitope mapping technique. The authors created a 240 amino acid vaccine sequence from epitopes of an outer membrane protein with immunogenic potential (target protein) that underwent various procedures to function as a vaccine candidate (Khalid *et al*., 2022). On the same note, Rodrigues-da-Silva *et al*. (2016) used *in-silico* methods to validate *P. vivax* malaria vaccine candidate Merozoite Surface Protein-9 (MSP9) and support its inclusion in future subunit vaccines. This study is in tandem with those reported by Takashima *et al*. (2021), all of which use *in-silico* processes to narrow down the candidate list of novel transmission-blocking vaccines discovered directly using human malaria parasites. The development of vaccines using *in-silico* methods can help combat infections and diseases more successfully (Takashima *et al*., 2021).

This study used two *in-silico* approaches, HVS and MDS. HVS is a multi-step process that combines several computational screening techniques. It involves pharmacophore or ligand-based screening, drug-likeness test, ADMET analysis, and molecular docking to identify promising therapeutic candidates from large chemical libraries. HVS is efficient, cost-effective, customizable, and diversified in terms of scaffold or small molecules identification (Duay *et al*., 2023; Ibrahim *et al*., 2022). It quickly creates a workable shortlist from thousands to millions of chemicals; lessens the need for costly wet-lab tests in the beginning; can be modified to incorporate shape-based filters, docking precision levels, and pharmacophore models; and promotes the discovery of new chemical scaffolds that go beyond well-known inhibitors (Duay *et al*., 2023). Conversely, HVS is prone to false negatives/positives, bias risk, and docking limitations. Preliminary screenings may keep non-binders or reject good prospects; induced-fit effects may be missed by strict receptor assumptions; and results may be distorted by an over-reliance on established pharmacophores or grading systems (Duay *et al*., 2023). Regardless, HVS was used because it enables ranking of substances according to their anticipated binding affinity and pharmacological significance.

MDS offers insights into the stability, flexibility, and conformational changes of protein-ligand complexes under physiological settings by simulating the physical movements of atoms and molecules over time. It can be used in conjunction with MM-PBSA or MM-GBSA to estimate binding free energies, reveals how ligands act in a realistic, time-evolving environment, evaluates whether a molecule stays bound over time or dissociates, and catches protein movements that static docking lacks (Durrant & McCammon, 2011). However, it is not the best option for screening huge chemical libraries, it takes a lot of time and resources for lengthy simulations, and the results are highly dependent on force fields and simulation configuration (Durrant & McCammon, 2011).

In any case, it was selected for this study because it can reveal water-mediated interactions and allosteric effects that are invisible in docking, helps validate docking poses and evaluate real-world binding behavior, and boosts confidence in lead compounds by demonstrating sustained interactions, hydrogen bonding, and hydrophobic contacts over time.

2.11 *In Vitro* Validation of Drug and Vaccine Candidates

Using *in-silico* techniques to discover drug and vaccine candidates often occur during the pre-clinical stage of vaccine and drug design and development. After identifying the potential drug and vaccine candidates, it is essential to undertake further *in vitro* and *in vivo* validation of their therapeutic potential. For instance, Sachdeva *et al*. (2020) recommended further *in vitro* and *in vivo* studies to ascertain the actual potential of DOX against COVID-19. In most cases, the *in vitro* drug sensitivity assays are used depending on the pathogen and disease of interest. Sinha *et al*. (2017) undertook a systematic review highlighting the various drug sensitivity assay used for antimalarial drug efficacy testing targeting different stages of the parasite's development. Some of those assays include blood stages assays (Schizont maturation, microscopic assay, radioisotopic assay, and enzymatic assay), gametocytes stage assays (oxido-reduction indicator, Alamar blue, and SMFA), liver stage assays (infrared fluorescence detection method), and HTS (fluorescence-based assay and *in vitro* beta-hematin formation assay) (Sinha *et al*., 2017).

One of the most common antimalarial drug sensitivity assays is the SYBR green assay. It is considered the gold standard for *in vitro* malaria drug sensitivity testing because of its reliability as a drug screening and surveillance tool (Cheruiyot *et al*., 2016). It is also described as a simple and cost-effective methodology that has been used to determine the 50% inhibitory concentrations (IC_{50}) of clinical isolates (Cheruiyot *et al*., 2016). Researchers have used this assay in their studies, including Traoré *et al*. (2019) when assessing the susceptibility of *P. falciparum* isolates to

antimalarial drugs in Mali. Similarly, Duan *et al*. (2022) determined susceptibilities of *P. falciparum* isolates to 11 antimalarial drugs using the SYBR green assay. The antimalarial drugs included PND, lumefantrine (LMF), quinine (QN), artemether (AM), DHA, artesunate (AS), pyrimethamine (PY), NQ, mefloquine (MFQ), PPQ, and chloroquine (CQ) (Duan *et al*., 2022). Therefore, this assay determined the inhibitory capability of the selected PfHsp90 and PfCSP inhibitors.

2.12 Need for Better Antimalarial Drugs and Efficacious Vaccines

Studies have identified the need for better antimalarial drugs and more efficacious malaria vaccines in existing studies, creating a gap that should be explored and filled. The threat of antimalarial drug resistance raises questions about the efficacy of the antimalarial drugs already on the market. Drug resistance, which raises malaria morbidity and death, is one of the main threats to malaria control. The parasite has mounted resistance to antimalarial drugs like chloroquine, quinine, halofrantrine, mefloquine, and sulfadoxine/pyrimethamine (CDC, 2018). This occurrence has led to the development of antimalarial drugs with better effectiveness on the parasite through both *in-silico* and traditional means. For instance, even though GDM was initially developed as an anti-tumor drug, it has also been repurposed to function as an antimalarial medication. However, from existing studies, the main barriers to the approval of GDM in clinical testing as an anti-cancer and anti-malarial medication were its poor solubility and severe hepatotoxicity (Hoter *et al*., 2018).

Due in part to these drawbacks, many GDM derivatives have been created with enhanced drug-like properties, including stability, higher *in vivo* action, and low toxicity profiles. A change in the carbon 17 position of the Ansa ring gives the GDM derivative 17-allylamino-17-demethoxy geldanamycin (17-AAG, KOS-953; CNF; tanespimycin), which has a higher potency and lower toxicity than GDM (Meyer *et al*., 2018). In many phase I trials reported by Yuno *et al*. (2018) and

a phase II clinical trial against HER-2 breast cancer, this substance, 17-AAG, demonstrated encouraging outcomes against several malignancies (Stofberg *et al*., 2021). Because 17-AAG lacked selectivity for parasite Hsp90s, it was not highly successful when used to treat malaria. Therefore, PfHsp90 at 4.54 M and PfGrp94 at 28.5 M of parasite Hsp90 had a lower affinity for 17-AAG than human HSPC2 (0.09 M) (Murillo-Solano *et al*., 2017). Similar to GDM, 17-AAG demonstrated lower IC_{50} values in parasite cultures (Stofberg *et al*., 2021).

These results necessitated repurposing and modifying 17-AAG and developing other anti-malarial drugs with better solubility and low toxicity. Furthermore, it illuminated the need to create malaria drugs with the required effectiveness and efficacy that most existing medications do not possess (Murillo-Solano *et al*., 2017). It also encouraged the development of vaccines. However, to date, Mosquirix is the only approved vaccine. Unfortunately, its efficacy and effectiveness against malaria are low, just 36% among kids aged 5 to 17 months who received four doses (Laurens, 2020). This low efficacy percentage necessitates developing better efficacious malaria vaccines or finding ways of increasing the effectiveness of the already existing Mosquirix vaccine. The lack of effective antimalarial drugs and efficacious malaria vaccines presents a gap worth exploring. Therefore, this study sought to undertake an *in-silico* screening and *in-vitro* validation of novel compounds with pharmacological activity against *Plasmodium* malaria.

CHAPTER THREE

MATERIALS AND METHODS

3.1 Design and Software

A computer-based design was used to find PfHsp90 and PfCSP inhibitors. A computer with the following specifications was used in this research: 11th Gen Intel(R) Core(TM) i7-11800H @ 2.30GHz. Some software was downloaded and installed on the computer. The particular software included BioEdit (Hall, 1999), BIOVIA Discovery Studio 2021 (BIOVIA, 2021), PyRx (Dallakyan & Olson, 2015), and GROMACS 2022 (Van Der Spoel *et al*., 2005). Furthermore, the web-based servers and databases that were used included PlasmoDB (Aurrecoechea *et al*., 2009), UniProt (The UniProt Consortium, 2023), NCBI (NCBI Resource Coordinators, 2023), PDB (Berman *et al*., 2000), PubChem (Kim *et al*., 2021), and SwissADME (Daina *et al*., 2017).

3.2 Retrieval of PfHsp90 and PfCSP Accession Numbers

Retrieving the accession numbers of PfHsp90 and PfCSP was done towards determining novel PfHsp90 inhibitors with pharmacological activity against *Plasmodium* malaria and characterizing novel PfCSP inhibitors with pharmacological properties on Mosquirix, respectively. The subsequent steps, until drug-likeness test, were discussed in tandem when dealing with PfHsp90 and PfCSP because they are similar and lead to determining novel PfHsp90 inhibitors with pharmacological activity against *Plasmodium* malaria through HVS using GDM as the ligand/reference structure and characterizing novel PfCSP inhibitors with pharmacological properties on Mosquirix through HVS using monoclonal antibody L9 as the ligand/reference structure. The accession numbers of PfHsp90 and PfCSP were retrieved from the PlasmoDB database (https://plasmodb.org/plasmo/app) (Aurrecoechea *et al*., 2009) and were essential for retrieving the sequences of PfHsp90 and PfCSP in the subsequent sections of the research.

3.3 Retrieval of PfHsp90 and PfCSP Sequences

The accession numbers of PfHsp90 and PfCSP were used to retrieve their protein sequences from the UniProt database (https://www.uniprot.org/) (The UniProt Consortium, 2023). The retrieved protein sequences were downloaded in the fasta file format and stored for use in other processes. The protein sequences were necessary to perform a BLAST query search for homologous sequences.

3.4 BLAST Query Search for PfHsp90 and PfCSP Homologs

Several organisms possess the Hsp90 and CSP proteins. The PfHsp90 and PfCSP sequences retrieved from UniProt were used to perform a BLAST search using NCBI (https://www.ncbi.nlm.nih.gov/) (NCBI Resource Coordinators, 2023), a process that yielded PfHsp90 and PfCSP homologous sequences from other organisms. The organisms of interest were *Plasmodium* species that can infect people and cause malaria: *P. malariae*, *P. vivax*, *P. ovale*, and *P. knowlesi*. Other organisms like *Homo sapiens*, *Toxoplasma gondii*, *Cryptosporidium parvum*, *Babesia bovis*, and *Theileria annulate* were considered outgroups during phylogenetic tree construction in the subsequent processes.

Where a BLAST search for either PfHsp90 or PfCSP homologous sequences did not produce homologous sequences from the desired organisms; the precise protein sequences of those specific organisms were individually searched in UniProt using their names (for the outgroup organisms) or accession numbers initially retrieved from PlasmoDB (for *Plasmodium* species). The sequences were used to perform multiple sequence alignment, identify their conserved regions, and determine their similarity and homology in other research processes.

3.5 Multiple Sequence Alignment

This step involved performing a multiple sequence alignment (MSA) of PfHsp90 and their homologous sequences and those of the individual CSP sequences. The PfHsp90 homologous sequences were edited in one flat file. The file was used to carry out multiple sequence alignment using Bio-Edit software (Hall, 1999), which contains an inbuilt Clustal W Programme. The result received from the alignment was used to determine the identity, similarity, and homology of those homologous sequences, assess the conserved sequence patterns, and identify the three domains of the PfHsp90 protein, which include the middle domain (MD), C-terminal domain (CTD), and N-terminal domain (NTD).

NCBI's BLAST (NCBI Resource Coordinators, 2023) was used to calculate the percentages of identity and similarity of the Hsp90 sequences. Maximum likelihood in MEGA 11 (Tamura *et al*., 2021) was used to construct a phylogenetic tree to show the evolutionary relationship of the organisms of interest. Maximum likelihood was preferred to maximum parsimony because it is more accurate, recovering the true tree, especially when sequences are divergent or when substitution rates vary and robust, handling rate heterogeneity, transition/transversion biases, and unequal base frequencies, which maximum parsimony ignores (Tamura *et al*., 2021). The same process was performed in the case of CSP sequences. The CSP sequences of the five parasites and those of other organisms were edited in one flat file, and the file was used to carry out multiple sequence alignment. The multiple sequence alignment result was used to determine the identity, similarity, and homology level of the CSP sequences and examine any conserved sequence patterns that might exist. NCBI's BLAST (NCBI Resource Coordinators, 2023) was used to calculate CSP sequences' identity and similarity percentages, and maximum likelihood in MEGA 11 (Tamura *et al*., 2021) utilized to construct a phylogenetic tree.

3.6 PfHsp90 and PfCSP 3D Structures Retrieval and Preparation

The 3D structures of PfHsp90 and PfCSP were retrieved from the Protein Data Bank (PDB) database (https://www.rcsb.org/) (Berman *et al*., 2000). PfHsp90's domain of interest (NTD) was retrieved using PDB ID 3K60 and downloaded in the PDB format. The 3D structure of PfCSP was retrieved using the PDB ID 3VDL and downloaded in the PDB format. These two 3D structures were essential during molecular docking. Their use as target proteins in molecular docking necessitated preparing them for the process. Therefore, they were prepared for molecular docking after retrieval using BIOVIA Discovery Studio 2021 (BIOVIA, 2021). All side chains and bound ligands were removed, leaving only the A chains of the two target proteins.

Similarly, all water molecules and heteroatoms were removed as well. These compounds were removed because they did not participate in the binding of the ligands of interest to the target protein. Deleting them presented a desirable pose search and eased computations that would otherwise have proven challenging if such compounds clouded the binding pocket of the target proteins. Another preparation step involved adding polar hydrogens to aid in locating hydrogen bond interactions in the 3D structures. The hydrogen bond interactions are essential to ascertain the ligands' binding affinity to the two target proteins. The prepared 3D structures of PfHsp90 and PfCSP were saved as .pdb files.

3.7 Retrieval of Geldanamycin (GDM) Structures

The PubChem library database (https://pubchem.ncbi.nlm.nih.gov/) (Kim *et al*., 2021) was utilized to retrieve the 2D and 3D structures of GDM, an inhibitor of interest. The 3D structure of the ligand was crucial during virtual screening to identify structurally similar compounds with antimalarial properties or activities.

3.8 Retrieval and Preparation of Monoclonal Antibody L9 Structure

The 3D structure of L9 was retrieved from PDB (https://www.rcsb.org/) (Berman *et al*., 2000) and downloaded in the PDB format. Being a monoclonal antibody produced in the human body following Mosquirix injection, its structure might not be available in the PubChem library database. The 3D structure from PDB was used as a ligand for the virtual screening of natural compounds database, ZINC20 database (https://zinc.docking.org/) (Irwin et al., 2020), to identify compounds with a similar structure possessing anti-malarial properties or activities. It was loaded into BIOVIA Discovery Studio 2021 (BIOVIA, 2021), and all side chains and ligands were removed, leaving behind only the chain involved in binding PfCSP. The prepared 3D structure of the L9 antibody was saved as .pdb files.

3.9 Pharmacophore-Based Virtual Screening

Through two independent virtual screening processes, the 3D structures of GDM and L9 antibody were used to locate active compounds with similar structures that can inhibit PfHsp90 and PfCSP, respectively. The ZINCPHARMER web server (http://zincpharmer.csb.pitt.edu/pharmer.html) (Koes & Camacho, 2012) was used in the process. These active compounds were subjected to further processes to ascertain whether or not they could be used as antimalarial compounds or drugs.

3.10 Drug-Likeness and Pharmacokinetics Test

The compounds retrieved from the virtual screening process were subjected to a drug-likeness test to determine their drug-likeness properties and pharmacokinetics analysis to ascertain their oral bioavailability. SwissADME web tool (http://www.swissadme.ch/) (Daina *et al*., 2017) was used to perform the drug-likeness test and pharmacokinetics analysis. The SMILES of the virtual screening hits were copy-pasted into the SwissADME web server (http://www.swissadme.ch/)

(Daina *et al*., 2017). The various drug-likeness filters that were used include Muegge (Muegge *et al*., 2001), Egan (Egan *et al*., 2000), Veber (Veber *et al*., 2002), Ghose (Ghose *et al*., 1999), and Lipinski's Rule of Five (Lipinski *et al*., 2001).

These filters assisted in selecting the compounds with desirable drug properties. Similarly, pharmacokinetic results were analyzed in the form of bioavailability radars and the Brain Or IntestinaL EstimateD permeation (BOILED-Egg) diagram. The molecules that satisfied all the bioavailability and permeation and at least four drug-likeness filters' requirements were selected for molecular docking studies.

3.11 Molecular Docking

The selected molecules, potential PfHsp90 and PfCSP inhibitors, were docked with their respective target proteins using Autodock Vina (Trott & Olson, 2010), an inbuilt tool within the PyRx software (Dallakyan & Olson, 2015). The format of the target proteins, PfHsp90 and PfCSP, was converted from .pdb to .pdbqt using the PyRx software (Dallakyan & Olson, 2015). The .pdbqt format is the desirable molecular docking format. The chosen ligand compounds were prepared for molecular docking by minimizing their energies to optimize their geometry for binding and converting them to .pdbqt format using the PyRx software (Dallakyan & Olson, 2015).

Molecular docking was then performed, and all protein-ligand complexes with the lowest binding energies were selected as the final potential drug candidates. This molecular docking process was also undertaken using the reference ligands, GDM and L9 antibody. Their binding energies were compared to those of the final potential drug candidates to ascertain whether or not the selected drug candidates preferentially bind to PfHsp90 and PfCSP.

3.12 Molecular Dynamics Simulation (MDS)

The docked complexes of the final drug candidates and their respective target proteins were subjected to MDS to confirm the docking outcomes and perform an in-depth examination of the behavior of the ligands within the target proteins' binding pocket. GROMACS 2022 (Van Der Spoel *et al*., 2005) was used during the MDS process because of its exceptional computational speed, algorithmic efficiency, and versatility in simulations types. The GROMACS MDS files, which include topology files for the ligand and protein and parameter files for the ligand, were first generated using Charmm 36 Force Field from the CHARMM-GUI web server (Jo *et al*., 2008).

The CHARMM-GUI web server's default settings were preferred, including water box size options, number of ions to be added to the protein-ligand complexes, method of ions addition (Monte-Carlo ion placing method), and system temperature (300.00K). During the GROMACS energy minimization process, the number of steps was set at 5000. The minimized system was equilibrated via a 100ps run. The final MDS run, the production run, was set at 100ns. After the last run, the number of hydrogen bonds, root mean square fluctuation (RMSF), and root mean square deviation (RMSD) were calculated using GROMACS (Van Der Spoel *et al*., 2005).

3.13 *In Vitro* Validation of PfHsp90 and PfCSP Inhibitors

The final PfHsp90 and PfCSP inhibitors were purchased and underwent an *in vitro* validation to ascertain their inhibitory capability. Their antimalarial activity was measured using the WWARN SYBR Green I-based drug sensitivity assay (Procedure INV02) (WWARN In Vitro Module, 2011). To get the inhibitors to a final concentration of 200 ng/mL, they were first dissolved in 300 µL of Dimethyl Sulfoxide (DMSO). Following that, 11 wells of a 96-well plate (12 columns × 8 rows) were serially diluted using a particular growth medium that was optimized for *P. falciparum*

culture (as detailed in WWARN INV02) (**Appendix 1**). Each dilution (150 µL) was put into a brand-new 96-well plate that was intended for parasite exposure.

Appropriate controls were incorporated throughout the plate arrangement to guarantee the assay's dependability and interpretability. *P. falciparum* cultures in drug-free positive control wells represented the highest possible parasite growth (WWARN In Vitro Module, 2011). In order to account for background fluorescence from host DNA and medium components, negative control wells included uninfected red blood cells. To identify any reagent or instrumental noise, blank wells containing just growth medium and lysis buffer were employed. To confirm test performance, reference drug controls utilizing chloroquine at known inhibitory doses were also added. To guarantee reproducibility and statistical robustness, each condition was run three times (WWARN In Vitro Module, 2011).

P. falciparum was cultivated in a synchronized ring-stage with a 2% hematocrit and 1% parasitemia. Each well holding the drug dilutions received 150 µL of this culture, for a total volume of 300 µL per well. The plates were incubated in a closed gas environment (5% CO_2, 5% O_2, and 90% N_2) at 37°C for 72 hours, which corresponds to the full intra-erythrocytic developmental cycle of *P. falciparum*, from ring stage to schizont (WWARN In Vitro Module, 2011). Each well received 150 µL of lysis buffer containing SYBR Green I dye following incubation. The parasite DNA is released when the red blood cells are lysed by this buffer, and it attaches itself to the dye to enable quantification. To ensure full staining, the plate was incubated for an hour at room temperature (25°C) in the dark.

A Tecan microplate reader with excitation at 485 nm and emission at 535 nm was used to measure fluorescence. The degree of fluorescence indicates the vitality of the parasite since it is correlated with its DNA content. For analysis, the generated data was exported to Microsoft Excel. The Four-

Parameter Logistic (4PL) non-linear regression was used to get IC_{50} values and create dose-response curves using the 4PL equation below. The goodness of fit was evaluated using the coefficient of determination (R^2); values nearer 1 would suggest a robust relationship between the model and the observed data, confirming the accuracy of the IC_{50} estimations.

$$Y = \text{Bottom} + \frac{\text{Top} - \text{Bottom}}{1 + \left(\frac{X}{IC_{50}}\right)^{HillSlope}}$$

$Where\ Y = RFU\ (response)$
$X = drug\ concentration$
$Top = maximum\ RFU\ (untreated\ control)$

$Bottom = minimum\ RFU\ (maximum\ inhibition)$
$IC_{50} = concentration\ where\ response = halfway\ between\ top\ and\ bottom$
$HillSlope = steepness\ of\ the\ curve$

CHAPTER FOUR

RESULTS

Specific Objective 1

4.1 PfHsp90 and PfCSP Accession Numbers

The accession numbers or gene names of PfHsp90 and PfCSP were obtained and recorded as **PF3D7_0708400** and **PF3D7_0304600**, respectively. This information is summarized in **Table 4.1**.

Table 4.1: The PlasmoDB Accession Numbers or Gene Names of PfHsp90 and PfCSP

No.	Organism	Accession Number/Gene Name (Hsp90)	Accession Number/Gene Name (CSP)
1.	*Plasmodium falciparum*	PF3D7_0708400	PF3D7_0304600

4.2 PfHsp90 and PfCSP Sequences

The sequences of PfHsp90 and PfCSP were retrieved from UniProt (The UniProt Consortium, 2023) using their accession numbers. The isolate 3D7 of *P. falciparum* Hsp90 had 745 amino acids while that of CSP had 397 amino acids. The sequences of PfHsp90 and PfCSP were as follows:

PfHsp90

>tr|Q8IC05|Q8IC05_PLAF7 Heat shock protein 90 OS=*Plasmodium falciparum* (isolate 3D7) OX=36329 GN=PF3D7_0708400 PE=1 SV=1
MSTETFAFNADIRQLMSLIINTFYSNKEIFLRELISNASDALDKIRYESITDTQKLSAEPEFFIRIIPDK
TNNTLTIEDSGIGMTKNDLINNLGTIARSGTKAFMEAIQASGDISMIGQFGVGFYSAYLVADHVV
VISKNNDDEQYVWESAAGGSFTVTKDETNEKLGRGTKIILHLKEDQLEYLEEKRIKDLVKKHSEF
ISFPIKLYCERQNEKEITASEEEEGEGEGEREGEEEEEKKKKTGEDKNADESKEENEDEEKKEDNE
EDDNKTDHPKVEDVTEELENAEKKKKEKRKKKIHTVEHEWEELNKQKPLWMRKPEEVTNEEY
ASFYKSLTNDWEDHLAVKHFSVEGQLEFKALLFIPKRAPFDMFENRKKRNNIKLYVRRVFIMDD
CEEIIPEWLNFVKGVVDSEDLPLNISRESLQQNKILKVIKKNLIKKCLDMFSELAENKENYKKFYE
QFSKNLKLGIHEDNANRTKITELLRFQTSKSGDEMIGLKEYVDRMKENQKDIYYITGESINAVSNS
PFLEALTKKGFEVIYMVDPIDEYAVQQLKDFDGKKLKCCTKEGLDIDDSEEAKKDFETLKAEYE
GLCKVIKDVLHEKVEKVVVGQRITDSPCVLVTSEFGWSANMERIMKAQALRDNSMTSYMLSKK
IMEINARHPIISALKQKADADKSDKTVKDLIWLLFDTSLLTSGFALEEPTTFSKRIHRMIKLGLSID
EEENNDIDLPPLEETVDATDSKMEEVD

PfCSP

>sp|Q7K740|CSP_PLAF7 Circumsporozoite protein OS=*Plasmodium falciparum* (isolate 3D7) OX=36329 GN=CSP PE=1 SV=1
MMRKLAILSVSSFLFVEALFQEYQCYGSSSNTRVLNELNYDNAGTNLYNELEMNYYGKQENWY
SLKKNSRSLGENDDGNNEDNEKLRKPKHKKLKQPADGNPDPNANPNVDPNANPNVDPNANPN
VDPNANPNANPNANPNANPNANPNANPNANPNANPNANPNANPNANPNANPNANPNANPNAN
PNANPNANPNVDPNANPNANPNANPNANPNANPNANPNANPNANPNANPNANPNANPNANPN
ANPNANPNANPNANPNANPNANPNKNNQGNGQGHNMPNDPNRNVDENANANSAVKNNNNEE
PSDKHIKEYLNKIQNSLSTEWSPCSVTCGNGIQVRIKPGSANKPKDELDYANDIEKKICKMEKCSS
VFNVVNSSIGLIMVLSFLFLN

4.3 BLAST Query Search for PfHsp90 and PfCSP Homologous Sequences

The homologous sequences from *P. knowlesi*, *P. malariae*, *P. vivax*, and *P. ovale* had a percentage identify of over 90% and an E-value of 0.0. The Hsp90 accession numbers of the other four *Plasmodium* species included XP_038969368.1 (*P. knowlesi*), SCO64938.1 (*P. vivax*), XP_028859990.1 (*P. malariae*), and SBT30398.1 (*P. ovale*). The strain H of *P. knowlesi* had 739 amino acids. The malaria parasite *P. ovale* had 734 amino acids. *P. malariae* had 741 amino acids. The malaria parasite *P. vivax* had 748 amino acids.

The Hsp90 accession numbers of the organisms considered outgroups included NP_005339.3 (*Homo sapiens*), XP_002368278.1 (*Toxoplasma gondii*), XP_626924.1 (*Cryptosporidium parvum*), XP_001611554.1 (*Babesia bovis*), and XP_952473.1 (*Theileria annulate*). The alpha isoform 2 of *H. sapiens* had 732 amino acids. *Toxoplasma gondii* ME49 had 708 amino acids. *Cryptosporidium parvum* Iowa II had 711 amino acids. *Babesia bovis* T2Bo had 712 amino acids and *Theileria annulata* had 722 amino acids. This information is summarized in **Table 4.2**. The sequences of these nine organisms were downloaded from NCBI in the FASTA format as displayed in **Appendix 2**.

Table 4.2: The NCBI Accession Numbers of the Different *Plasmodium* Species and Outgroups

No.	Organism	Accession Number (Hsp90)	Amino Acids
1.	*P. knowlesi*	XP_038969368.1	739
2.	*P. ovale*	SBT30398.1	734
3.	*P. malariae*	XP_028859990.1	741
4.	*P. vivax*	SCO64938.1	748
5.	*Homo sapiens*	NP_005339.3	732
6.	*Toxoplasma gondii*	XP_002368278.1	708
7.	*Cryptosporidium parvum*	XP_626924.1	711
8.	*Babesia bovis*	XP_001611554.1	712
9.	*Theileria annulate*	XP_952473.1	722

In the case of PfCSP, the accession numbers and sequences of the four *Plasmodium* species included AEJ33939.1 (*P. knowlesi*), QCZ35286.1 (*P. ovale*), QWO71690.1 (*P. malariae*), and AAG43992.1 (*P. vivax*). The CSP sequence from *P. knowlesi* had 297 amino acids, *P. ovale* had 328 amino acids, *P. malariae* had 310 amino acids, and *P. vivax* had 263 amino acids. This information is summarized in **Table 4.3**. The CSP sequences from these four *Plasmodium* species are displayed in **Appendix 3**. Therefore, the CSP accession numbers and sequences of the organisms included in the study as outgroups could not be retrieved or found from the BLAST results.

Table 4.3: The NCBI Accession Numbers of the Different *Plasmodium* Species

No.	Organism	Accession Number (CSP)	Amino Acids
1.	*P. knowlesi*	AEJ33939.1	297
2.	*P. ovale*	QCZ35286.1	328
3.	*P. malariae*	QWO71690.1	310
4.	*P. vivax*	AAG43992.1	263

4.4 Multiple Sequence Alignment

PfHsp90 and its homologous sequences from other *Plasmodium* species were aligned and the result obtained (**Figure 4.1**). The multiple sequence alignment shows a high level of similarity, identity, and homology of Hsp90 from the five *Plasmodium* species, portrayed by the differently colored

dotted lines. The results were edited to display the different domains of Hsp90 protein, which include N-terminal domain (NTD), middle domain (MD), and C-terminal domain (CTD). The red box shows the NTD, which runs from amino acid number 5-223 (**Figure 4.1A**) (Dutta *et al*., 2022).

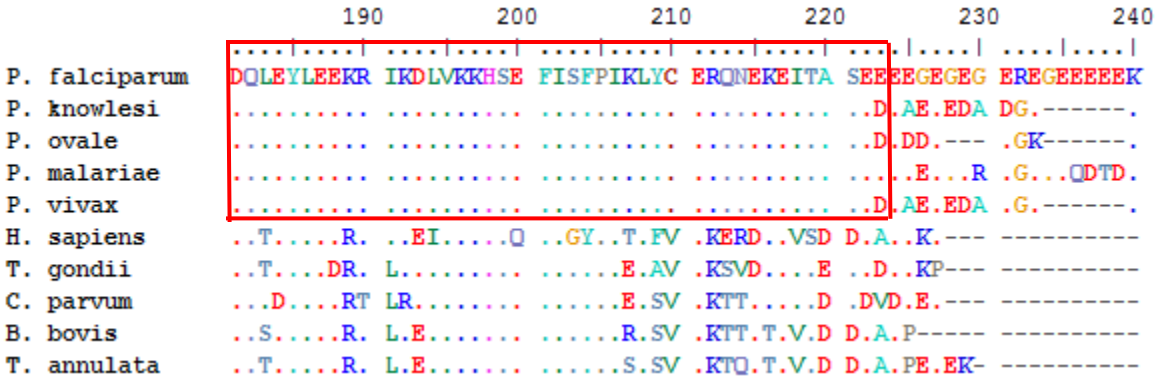

Figure 4.1A: Hsp90 Multiple sequence alignment. It shows the NTD (red box) of Hsp90 from the different organisms. It displays the homology of the Hsp90 sequences from the five *Plasmodium* species and the evolutionary diversity of the Hsp90 sequences from the outgroup organisms.

The green box illuminates the MD that runs from amino acid number 290-647 (**Figure 4.1B**)

(Dutta *et al*., 2022).

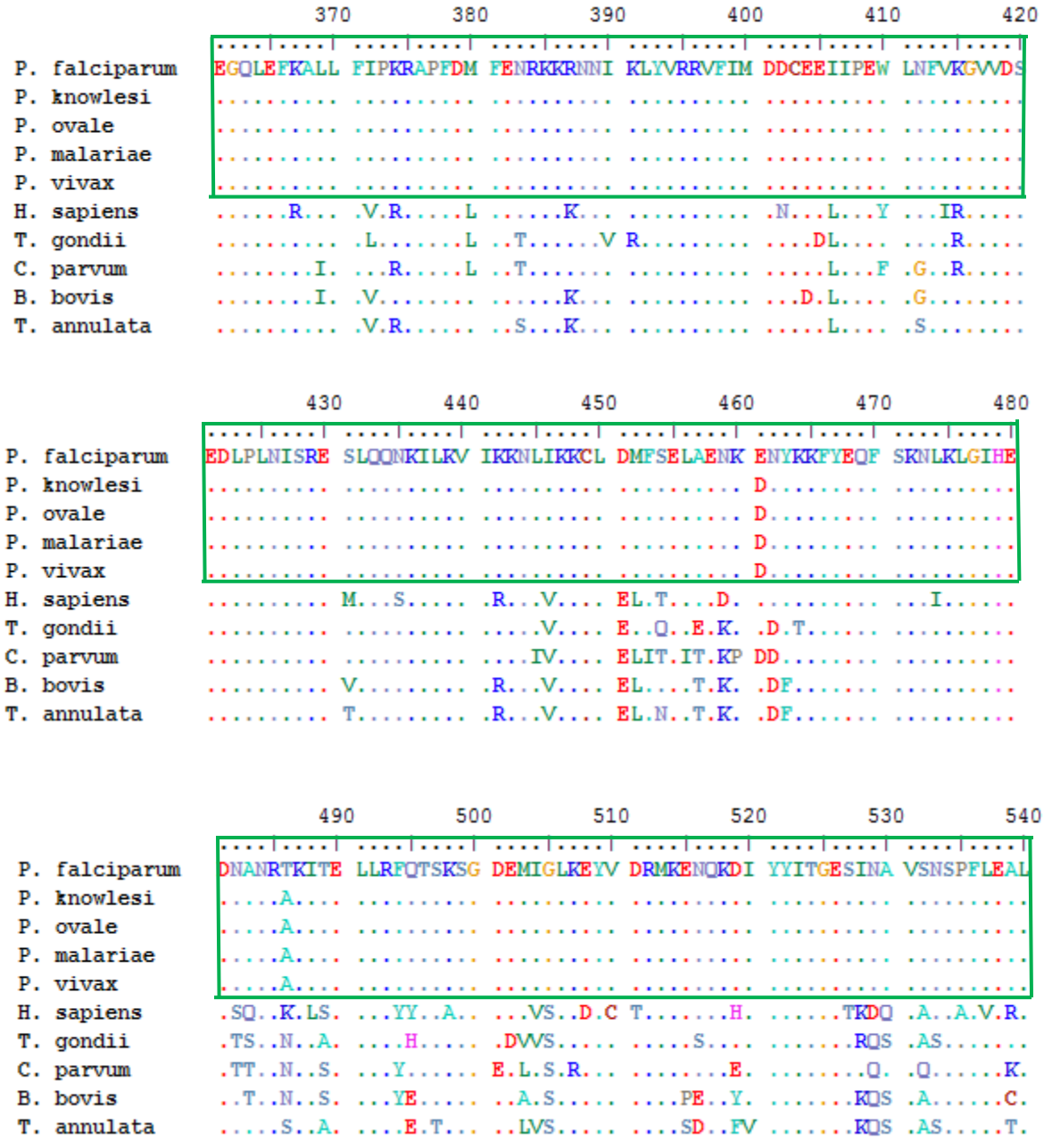
370 380 390 400 410 420
P. falciparum EGQLEFKALL FIPKRAPFDM FENRKKRNNI KLYVRRVFIM DDCEEIIPEW LNFVKGVVDS
P. knowlesi
P. ovale
P. malariae
P. vivax
H. sapiens
T. gondii
C. parvum
B. bovis
T. annulata
430 440 450 460 470 480
P. falciparum EDLPLNISRE SLQQNKILKV IKKNLIKKCL DMFSELAENK ENYKKFYEQF SKNLKLGIHE
P. knowlesi
P. ovale
P. malariae
P. vivax
H. sapiens
T. gondii
C. parvum
B. bovis
T. annulata
490 500 510 520 530 540
P. falciparum DNANRTKITE LLRFQTSKSG DEMIGLKEYV DRMKENQKDI YYITGESINA VSNSPFLEAL
P. knowlesi
P. ovale
P. malariae
P. vivax
H. sapiens
T. gondii
C. parvum
B. bovis
T. annulata

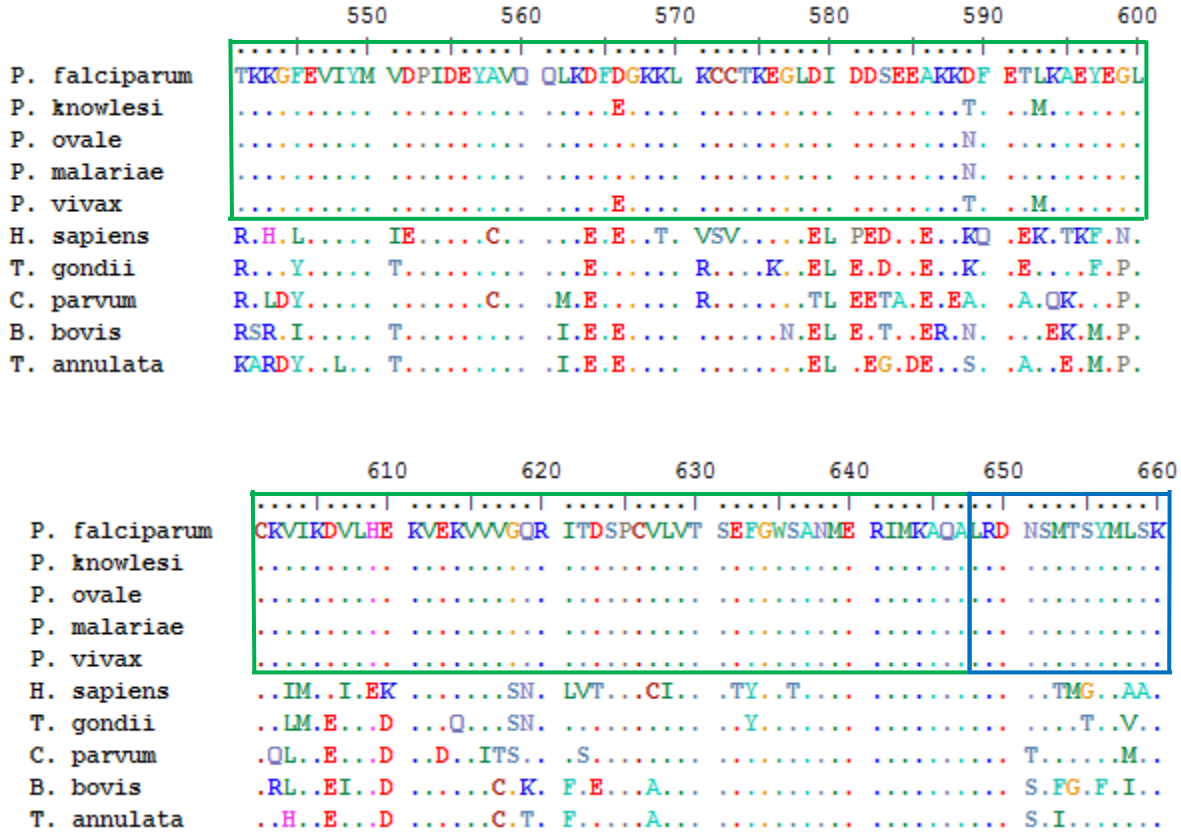

Figure 4.1B: Hsp90 Multiple sequence alignment. It shows the MD (green box) of Hsp90 from the different organisms. It displays the homology of the Hsp90 sequences from the five *Plasmodium* species and the evolutionary diversity of the Hsp90 sequences from the outgroup organisms.

The blue box displays the CTD, which occupies amino acid number 647-745 (**Figure 4.1C**) (Dutta *et al*., 2022). It was possible to identify the Hsp90 domains using PfHsp90 as a template since it is well characterized in Dutta *et al*. (2022).

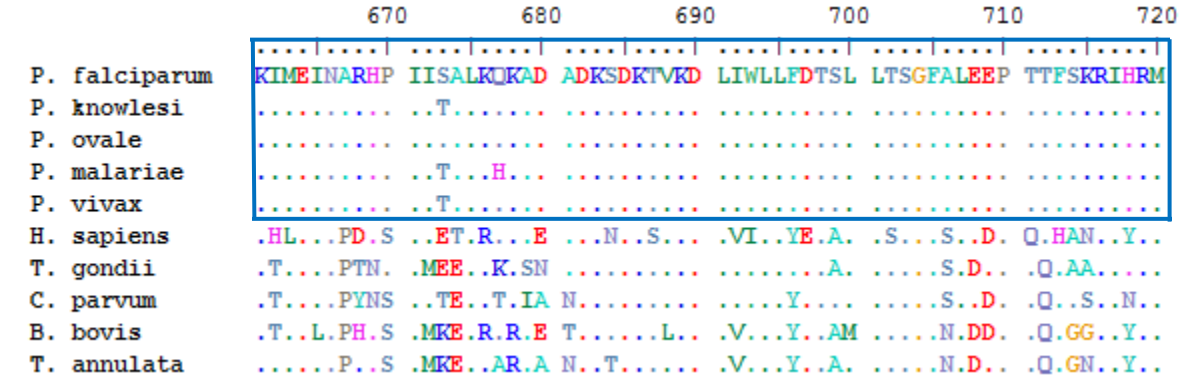

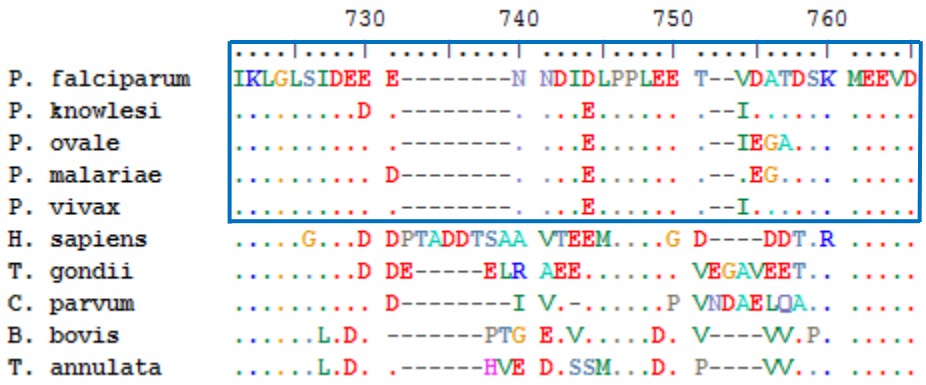

Figure 4.1C: Hsp90 Multiple sequence alignment. It shows the CTD (blue box) of Hsp90 from the different organisms. It displays the homology of the Hsp90 sequences from the five *Plasmodium* species and the evolutionary diversity of the Hsp90 sequences from the outgroup organisms.

The multiple sequence alignment results confirmed the high percentages of similarity and identity of the Hsp90 sequences from the four *Plasmodium* species (above 90%) to PfHsp90 as opposed to those from the outgroup organisms (below 90%) as displayed in **Table 4.4**.

Table 4.4: NCBI's PfHsp90 Homologous Sequences Alignment Results Displaying the Identity, Similarity, and Gap Percentages of the PfHsp90 Homologous Sequences

Alignment	Alignment Length	Identical Residues	Percent Identity	Similar Residues	Percent Similarity	Gaps	Gaps Percent
P. falciparum vs. *P. knowlesi*	739	687/746	92%	715/746	95%	8/746	1%
P. falciparum vs. *P. ovale*	734	688/745	92%	712/745	95%	11/745	1%
P. falciparum vs. *P. malariae*	741	697/747	93%	719/747	96%	8/747	1%
P. falciparum vs. *P. vivax*	748	698/749	93%	722/749	96%	5/749	0%
P. falciparum vs *H. sapiens*	732	304/447	68%	372/447	83%	10/447	2%
P. falciparum vs T. gondii	708	175/227	77%	198/227	87%	1/227	0%
P. falciparum vs *C. parvum*	711	175/219	80%	197/219	89%	0/219	0%
P. falciparum vs *B. bovis*	712	511/743	69%	605/743	81%	38/743	5%

P. falciparum vs *T. annulate*	722	521/744	70%	617/744	82%	34/744	4%

The phylogenetic tree (**Figure 4.2**) confirms the homology or evolutionary relationship between the five *Plasmodium* species.

A

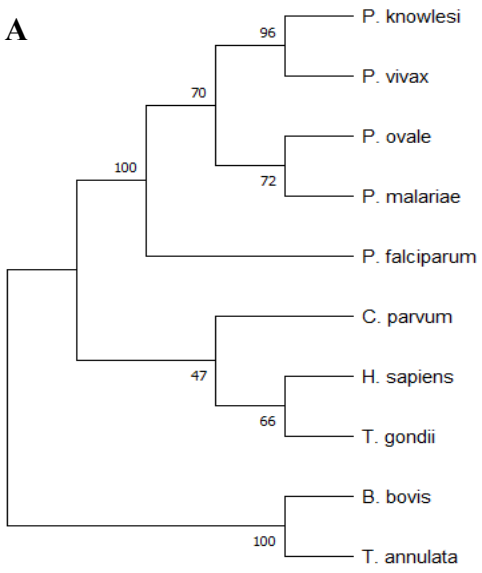

B

	P._falciparum	P._knowlesi	P._ovale	P._malariae	P._vivax	H._sapiens	T._gondii	C._parvu	B._bovis	T._annulata
P._falciparum										
P._knowlesi	0.0574									
P._ovale	0.0547	0.0451								
P._malariae	0.0528	0.0492	0.0334							
P._vivax	0.0624	0.0191	0.0489	0.0586						
H._sapiens	0.3894	0.3915	0.3866	0.3900	0.3915					
T._gondii	0.2721	0.2777	0.2702	0.2707	0.2777	0.3725				
C._parvum	0.2753	0.2810	0.2753	0.2701	0.2829	0.3827	0.2782			
B._bovis	0.3322	0.3365	0.3302	0.3299	0.3345	0.4248	0.3282	0.3145		
T._annulata	0.3158	0.3162	0.3105	0.3125	0.3162	0.4168	0.3181	0.3267	0.1772	

Figure 4.2: Hsp90s Bootstrapped Rectangular Cladogram & Pairwise Distance Matrix. (**A**) The maximum likelihood method was used to construct the phylogenetic tree. The tree confirms the homology or evolutionary relationship between the five *Plasmodium* species that are distantly or diversely related to the other organisms. (**B**) Pairwise distances showing the distances between different sequences. PfHsp90 is closely related to Hsp90 from the other four *Plasmodium* species with distances below 0.10 while it is distantly related to Hsp90 from the outgroup organisms with distances above 0.25.

The CSP sequences from the five *Plasmodium* species were also aligned. Even though PfCSP has no homologous sequences from other organisms other than different *Plasmodium* species, multiple sequence alignment was performed to ascertain the lack of similarity, identity, conserved sequence patterns, and homology of CSP sequences from the five parasites. The results (**Figure 4.3**) suggest that CSP sequences of the five parasites have extremely low levels of identity and similarity, denoted by the extremely few differently colored dotted lines.

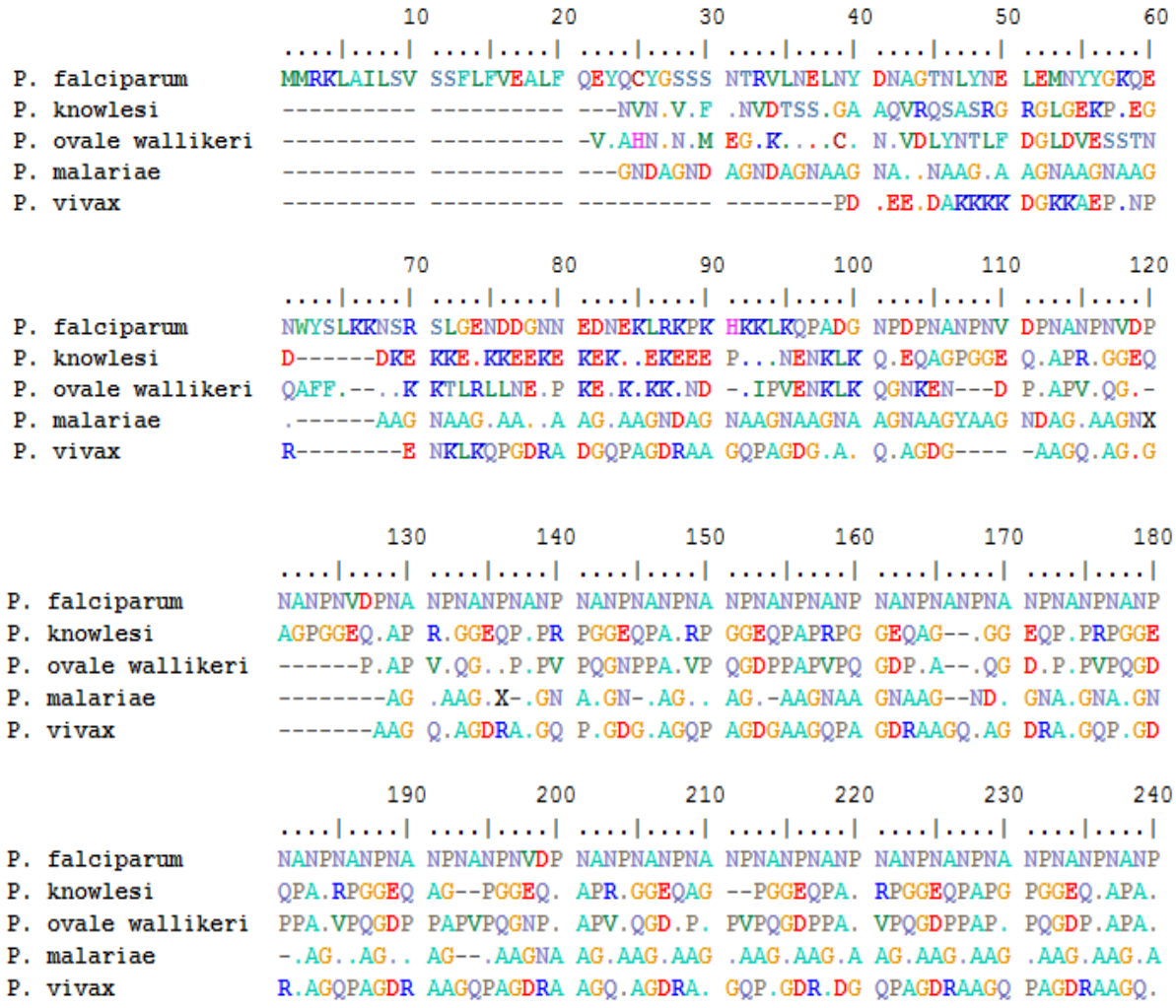

Figure 4.3: CSP Multiple sequence alignment indicates the diversity in the CSP sequences of the five *Plasmodium* species.

Table 4.5, showing the identity, similarity, and gap percentages of CSP sequences alignment from NCBI, confirmed **Figure 4.3** results. It displays the low identity and similarity percentages or scores of the CSP sequences.

Table 4.5: NCBI's PfCSP Homologous Sequences Alignment Results Displaying the Identity, Similarity, and Gap Percentages of the PfCSP Homologous Sequences

Alignment	Alignment Length	Identical Residues	Percent Identity	Similar Residues	Percent Similarity	Gaps	Gaps Percent
P. falciparum vs. *P. knowlesi*	297	20/37	54%	34/37	91%	0/37	0%
P. falciparum vs. *P. ovale*	328	50/93	54%	69/93	74%	4/93	4%
P. falciparum vs. *P. malariae*	310	44/84	52%	59/84	70%	8/84	9%
P. falciparum vs. *P. vivax*	263	20/35	57%	31/35	88%	0/35	0%

The phylogenetic tree (**Figure 4.4**) confirms the evolutionary diversity of the five *Plasmodium* species. The five *Plasmodium* species do not share a common ancestral origin or ancestor with respect to the CSP protein.

A

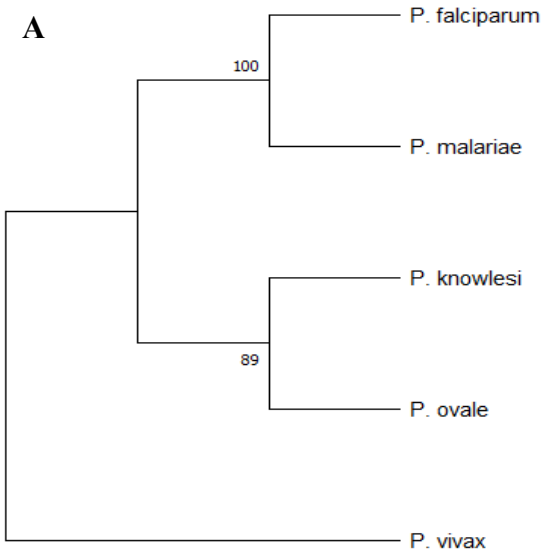

B

	P._falciparum	P._knowlesi	P._ovale	P._malariae	P._vivax
P._falciparum					
P._knowlesi	1.7188				
P._ovale	1.5541	0.9226			
P._malariae	1.1787	1.4594	1.5678		
P._vivax	1.7220	0.9303	1.0280	1.1027	

Figure 4.4: CSPs Bootstrapped Rectangular Cladogram & Pairwise Distance Matrix. (A) The maximum likelihood method was used to construct the phylogenetic tree. The tree confirms the diverse evolutionary relationship between the five *Plasmodium* species. (**B**) Pairwise distances showing the distances between different sequences. PfCSP is not closely related to CSPs from the other four *Plasmodium* species with high distances of above 1.00.

4.5 PfHsp90 and PfCSP Structure Retrieval and Preparation

The 3D structures of PfCSP and the NTD of PfHsp90 were retrieved from PDB database (Berman *et al*., 2000) using PDB IDs 3VDL and 3K60, respectively. They were loaded into BIOVIA

Discovery Studio 2021 (BIOVIA, 2021) and prepared for molecular docking. It was discovered that the NTD of PfHsp90 contains two chains, A and B, as shown in **Plate 4**. Several active sites of the NTD were within chain A. Therefore, during preparation, chain B was deleted, leaving behind a prepared chain A of PfHsp90 NTD, also presented in **Plate 4**. PfCSP was also prepared for molecular docking. It was discovered that it has three chains, A, B, and C as displayed in **Plate 5**.

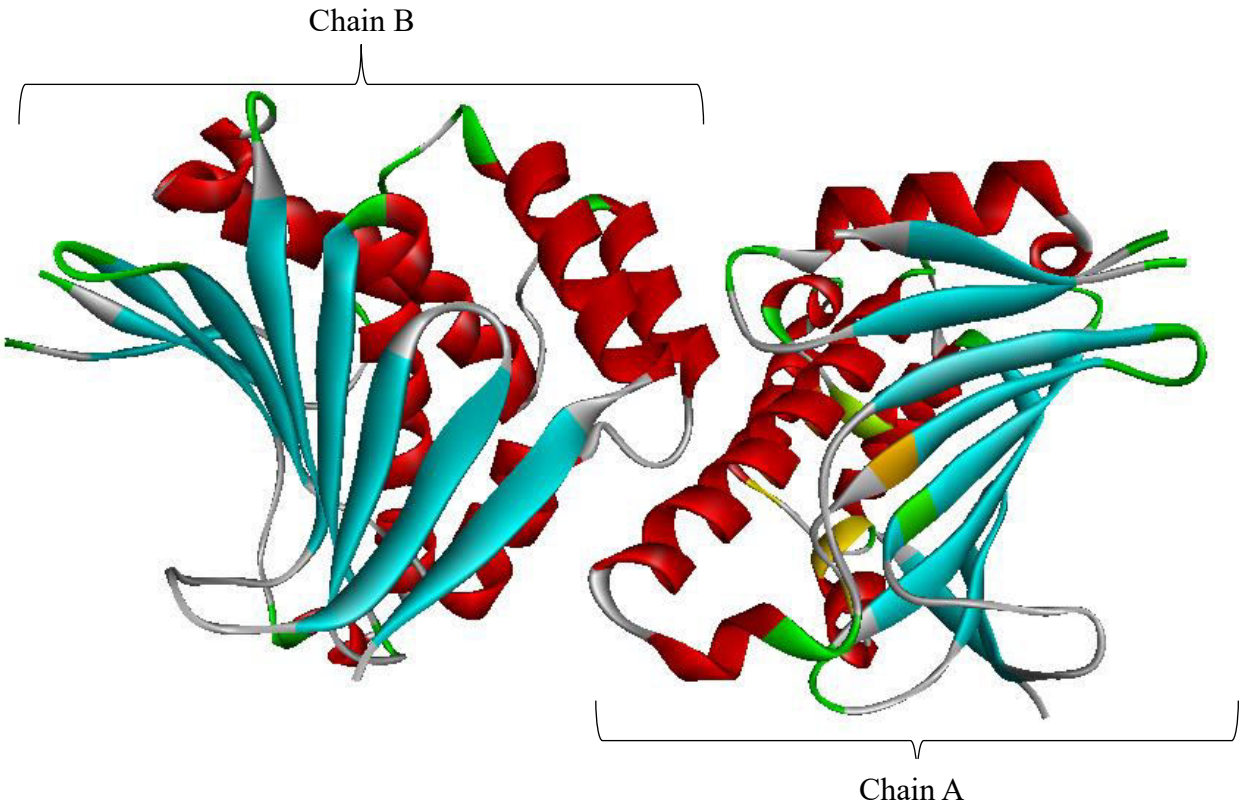

Plate 4: The 3D structure of prepared PfHsp90 NTD. PfHsp90 NTD retrieved from PDB, ID 3K60. All heteroatoms and water molecules removed and polar hydrogens added. The two chains, A and B, are indicated.

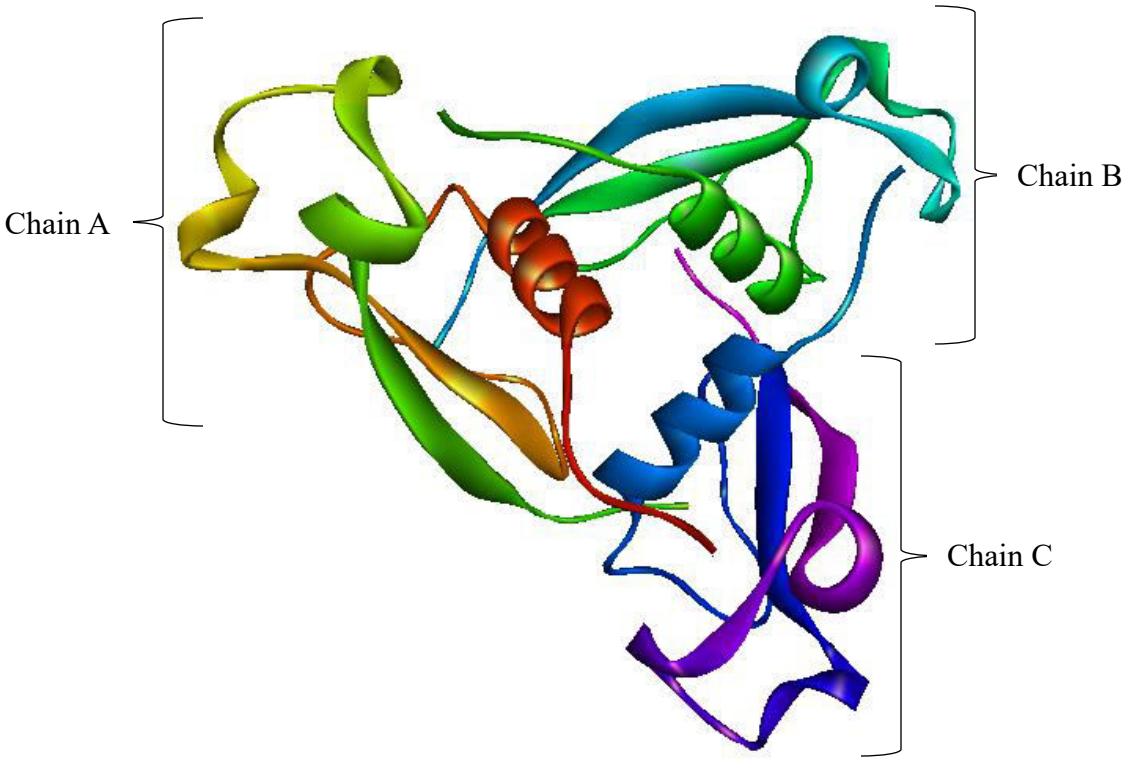

Plate 5: The 3D structure of prepared PfCSP. PfCSP retrieved from PDB, ID 3VDL. All heteroatoms and water molecules removed and polar hydrogens added. The three chains, A, B, and C, are indicated.

4.6 Retrieval of Geldanamycin (GDM) Structures

From the PubChem library database, the 2D and 3D structures of GDM were retrieved. The molecular weight, molecular formular, and PubChem CID of the compound were collected. This information is summarized in the **Table 4.6** and **Plate 6**.

Table 4.6: Basic Information on GDM Retrieved from PubChem Library Database

Molecule	Name	PubChem CID	Molecular Formular (MF)	Molecular Weight (MW)
1.	Geldanamycin (GDM)	5288382	$C_{29}H_{40}N_2O_9$	560.6

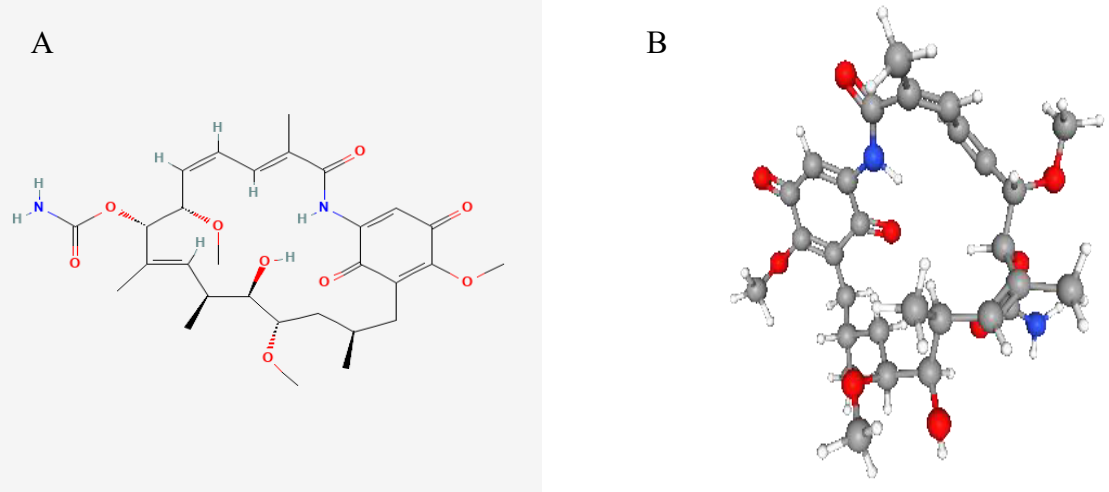

Plate 6: 2D and 3D Structures of GDM. (**A**) 2D structure. (**B**) 3D structure.

4.7 Retrieval and Preparation of Monoclonal Antibody L9 Structure

The 3D structure of L9 antibody was retrieved from PDB database using PDB ID 7RQP. It was loaded into BIOVIA Discovery Studio 2021 and prepared for molecular docking. It was discovered that L9 antibody has two chains, A (L9 Heavy Chain) and B (L9 Light Kappa Chain). Wang *et al*. (2022) outline that the L9 light chain is crucial for binding the minor repeats in PfCSP and preventing malaria. Therefore, chain A was deleted from the 3D structure, leaving behind only chain B, shown in **Plate 7**.

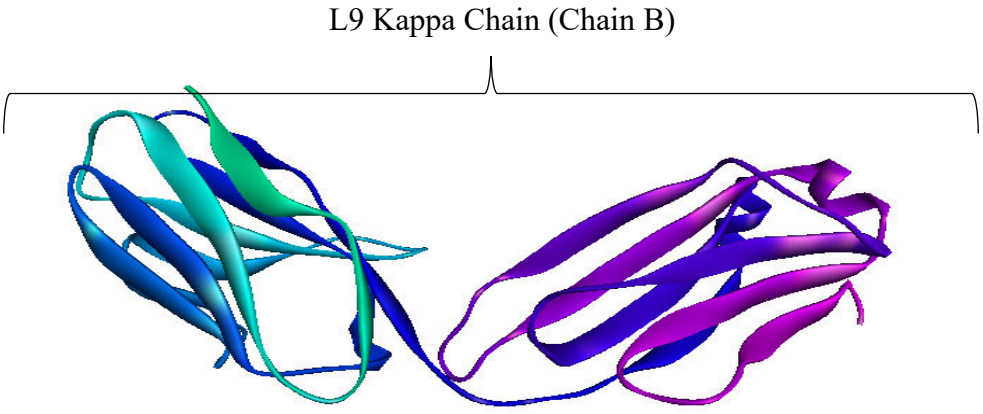

Plate 7: The 3D structure of prepared L9 Kappa chain. It was retrieved from PDB, ID 7RQP. All side chains and ligands removed.

4.8 Pharmacophore-Based Virtual Screening

The 3D structure of GDM was loaded into the ZINCPHARMER web server. Four of GDM's features, namely two hydrogen donors (interacting with GLU 33 and ASN 37 and one freely available) and two hydrogen acceptors (interacting with SER 36 and GLY 123) that are integral in the interaction between GDM and PfHsp90 were selected to act as the preferred pharmacophore features. The virtual screening process was then initiated, resulting in 17 hits (**Table 4.7**). The 17 hits were downloaded and saved in a .sdf file.

Table 4.7: Basic Information on the Virtual Screening Results using GDM as Ligand or Reference Structure with the RMSD Values, Mass, and Number of Rotatable Bonds of the Molecules

No.	Molecule	RMSD	Mass	RBnds
1	ZINC09060002	0.363	394	4
2	ZINC32537723	0.380	305	5
3	ZINC92700801	0.291	296	5
4	ZINC71617232	0.257	244	6
5	ZINC63526364	0.342	332	6
6	ZINC71617229	0.270	244	6
7	ZINC22325332	0.352	473	7
8	ZINC72358557	0.332	394	7
9	ZINC72358537	0.331	410	7
10	ZINC77271253	0.240	300	7
11	ZINC72133064	0.279	329	8
12	ZINC72163401	0.410	315	8
13	ZINC91416974	0.373	353	8
14	ZINC72358880	0.330	368	9
15	ZINC32796276	0.300	453	10
16	ZINC70981147	0.245	336	15
17	ZINC70981147	0.249	336	15

Similarly, the 3D structure of L9 antibody was loaded into the ZINCPHARMER web server. Six of L9's features, namely one aromatic ring (interacting with THR 172), one hydrogen donor (interacting with SER 12), two hydrogen acceptors (interacting with LEU 11 and SER 12), and two hydrophobic amino acids (interacting with THR 172 and THR 10) were selected to act as the

preferred pharmacophore features. The virtual screening process was then initiated, resulting in 23 hits (**Table 4.8**). The 23 hits were downloaded and saved in a .sdf file.

Table 4.8: Basic Information on the Virtual Screening Results using L9 as Ligand or Reference Structure with the RMSD Values, Mass, and Number of Rotatable Bonds of the Molecules

No.	Molecule	RMSD	Mass	RBnds
1	ZINC04529323	0.286	493	8
2	ZINC32780968	0.625	493	7
3	ZINC32780968	0.625	493	7
4	ZINC22939614	0.642	534	9
5	ZINC40144754	0.441	395	5
6	ZINC13152865	0.362	485	8
7	ZINC40144754	0.440	395	5
8	ZINC39933536	0.666	472	8
9	ZINC07948710	0.434	377	5
10	ZINC67103919	0.658	370	8
11	ZINC25374360	0.582	449	8
12	ZINC25374360	0.574	449	8
13	ZINC22938754	0.643	492	8
14	ZINC32735690	0.434	396	7
15	ZINC71998971	0.288	433	6
16	ZINC57991640	0.571	448	9
17	ZINC67410702	0.678	374	8
18	ZINC67410702	0.675	374	8
19	ZINC70705715	0.651	618	12
20	ZINC12530088	0.494	472	8
21	ZINC17588493	0.383	446	7
22	ZINC71996727	0.427	420	4
23	ZINC09125912	0.487	460	9

4.9 Drug-Likeness and Pharmacokinetics Test

The hits were then subjected to a drug-likeness test and pharmacokinetics analysis using the SwissADME web server (http://www.swissadme.ch/) (Daina *et al*., 2017). The drug-likeness test results are as displayed in **Table 4.9** (GDM) and **Table 4.10** (L9 Antibody). In the case of GDM, 11 of the 17 hits satisfied at least four of the five drug-likeness filters. Therefore, they were selected for further pharmacokinetics analysis.

Table 4.9: Drug-Likeness Test Results of the 17 Molecules using Five Drug-Likeness Filters, Including Lipinski, Ghose, Veber, Egan, and Muegge

No.	Molecule	Lipinski	Ghose	Veber	Egan	Muegge	Drug-Like?
1	**ZINC09060002**	**Yes**	**Yes**	**Yes**	**Yes**	**Yes**	**Yes**
2	ZINC32537723	Yes	Yes	No	No	No	No
3	**ZINC92700801**	**Yes**	**Yes**	**Yes**	**Yes**	**Yes**	**Yes**
4	ZINC71617232	Yes	No	Yes	No	Yes	No
5	**ZINC63526364**	**Yes**	**No**	**Yes**	**Yes**	**Yes**	**Yes**
6	ZINC71617229	Yes	No	Yes	No	Yes	No
7	ZINC22325332	Yes	No	No	No	Yes	No
8	**ZINC72358557**	**Yes**	**Yes**	**Yes**	**Yes**	**Yes**	**Yes**
9	**ZINC72358537**	**Yes**	**No**	**Yes**	**Yes**	**Yes**	**Yes**
10	ZINC77271253	Yes	No	Yes	No	Yes	No
11	**ZINC72133064**	**Yes**	**Yes**	**Yes**	**Yes**	**Yes**	**Yes**
12	**ZINC72163401**	**Yes**	**No**	**Yes**	**Yes**	**Yes**	**Yes**
13	**ZINC91416974**	**Yes**	**No**	**Yes**	**Yes**	**Yes**	**Yes**
14	**ZINC72358880**	**Yes**	**Yes**	**Yes**	**Yes**	**Yes**	**Yes**
15	ZINC32796276	Yes	Yes	No	No	Yes	No
16	**ZINC70981147**	**Yes**	**No**	**Yes**	**Yes**	**Yes**	**Yes**
17	**ZINC70981147**	**Yes**	**No**	**Yes**	**Yes**	**Yes**	**Yes**

As for L9 Antibody (**Table 4.10**), 12 of the 23 hits satisfied at least four of the five drug-likeness filters. From the 12, it was discovered that three were duplicates: ZINC40144754, ZINC25374360, and ZINC67410702, which were removed. The remaining 9 hits were subjected to pharmacokinetics properties analysis.

Table 4.10: Drug-Likeness Test Results of the 23 Molecules

No.	Molecule	Lipinski	Ghose	Veber	Egan	Muegge	Drug-Like?
1	ZINC04529323	Yes	No	Yes	No	Yes	No
2	ZINC32780968	Yes	No	No	No	No	No
3	ZINC32780968	Yes	No	No	No	No	No
4	ZINC22939614	Yes	No	No	Yes	No	No
5	**ZINC40144754**	**Yes**	**Yes**	**Yes**	**Yes**	**Yes**	**Yes**
6	ZINC13152865	Yes	No	No	Yes	Yes	No
7	**ZINC40144754**	**Yes**	**Yes**	**Yes**	**Yes**	**Yes**	**Yes**
8	ZINC39933536	Yes	No	No	Yes	Yes	No
9	**ZINC07948710**	**Yes**	**Yes**	**Yes**	**Yes**	**Yes**	**Yes**
10	**ZINC67103919**	**Yes**	**Yes**	**No**	**Yes**	**Yes**	**Yes**
11	**ZINC25374360**	**Yes**	**Yes**	**No**	**Yes**	**Yes**	**Yes**
12	**ZINC25374360**	**Yes**	**Yes**	**No**	**Yes**	**Yes**	**Yes**

13	ZINC22938754	Yes	No	No	Yes	Yes	No
14	ZINC32735690	Yes	No	No	Yes	Yes	No
15	**ZINC71998971**	**Yes**	**No**	**Yes**	**Yes**	**Yes**	**Yes**
16	**ZINC57991640**	**Yes**	**Yes**	**No**	**Yes**	**Yes**	**Yes**
17	**ZINC67410702**	**Yes**	**Yes**	**No**	**Yes**	**Yes**	**Yes**
18	**ZINC67410702**	**Yes**	**Yes**	**No**	**Yes**	**Yes**	**Yes**
19	ZINC70705715	No	No	No	No	No	No
20	ZINC12530088	Yes	No	No	Yes	Yes	No
21	**ZINC17588493**	**Yes**	**Yes**	**Yes**	**Yes**	**Yes**	**Yes**
22	**ZINC71996727**	**Yes**	**Yes**	**Yes**	**Yes**	**Yes**	**Yes**
23	ZINC09125912	Yes	No	No	Yes	Yes	No

In the case of GDM, two of the 11 hits were excluded because of their unfavorable pharmacokinetics properties as evident in BOILED-Egg analysis chart **Figure 4.5**.

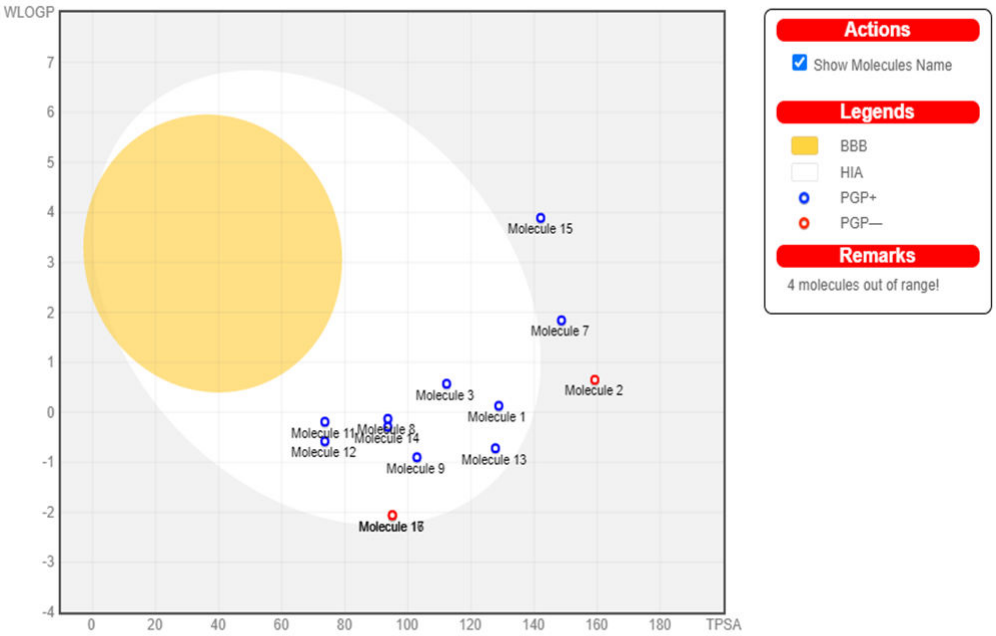

Figure 4.5: BOILED-Egg Analysis (GDM). Boiled egg prediction of blood brain barrier permeability and gastrointestinal absorption for the 17 hits. 4 molecules (15, 7, 2, and 16) are out of range, thus excluded. The other molecules are P-glycoprotein (P-gp) substrate, indicated by the blue dot, depicting their ease of excretion from the body.

Only 9 hits (**Figure 4.6**) were selected for docking studies after the drug-likeness test and the pharmacokinetics properties analysis.

A

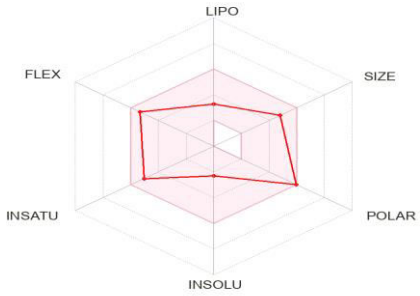
LIPO
SIZE
POLAR
INSOLU
INSATU
FLEX

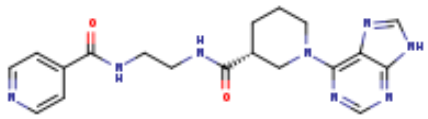

B

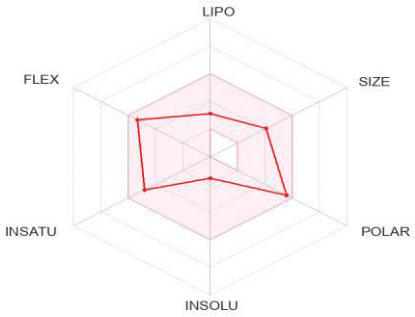
LIPO
SIZE
POLAR
INSOLU
INSATU
FLEX

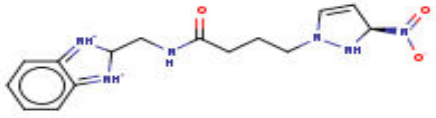

C

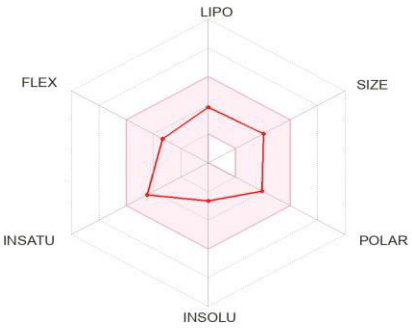
LIPO
SIZE
POLAR
INSOLU
INSATU
FLEX

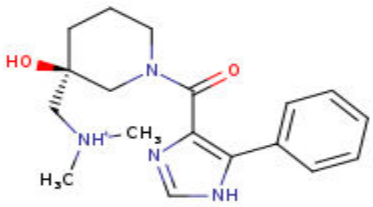
HO
O
N
NH
CH3
H3C
N
NH

D

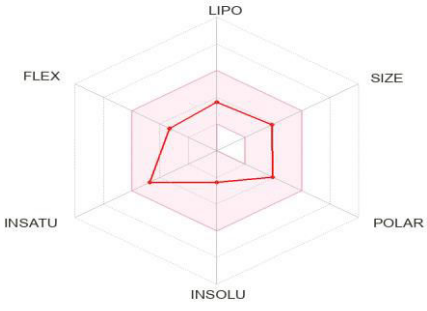
LIPO
SIZE
POLAR
INSOLU
INSATU
FLEX

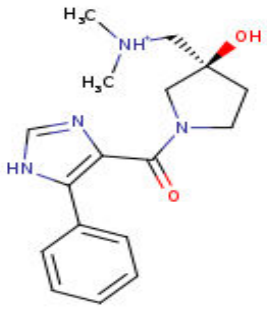
H3C
NH
H3C
OH
N
HN
N
O

E

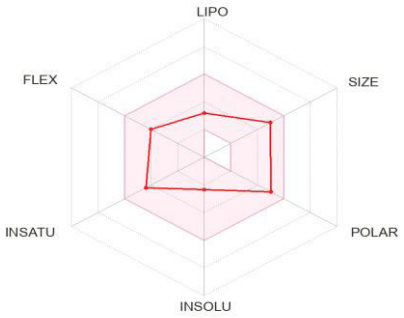
LIPO
SIZE
POLAR
INSOLU
INSATU
FLEX

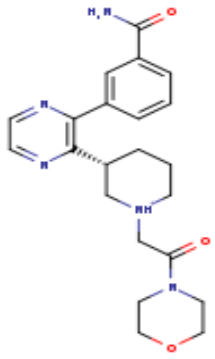

F

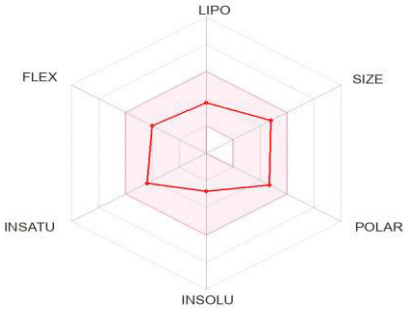
LIPO
SIZE
POLAR
INSOLU
INSATU
FLEX

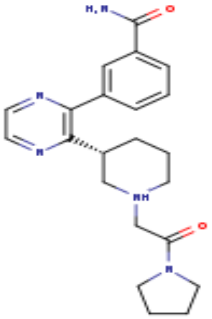

G

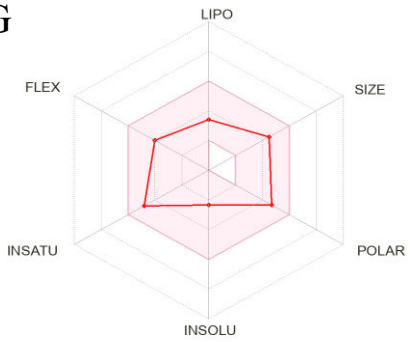
LIPO
SIZE
POLAR
INSOLU
INSATU
FLEX

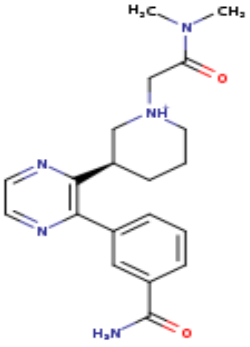

H

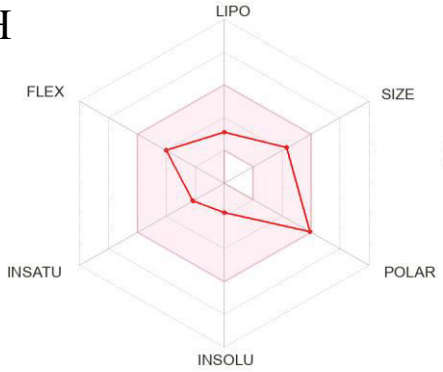
LIPO
SIZE
POLAR
INSOLU
INSATU
FLEX

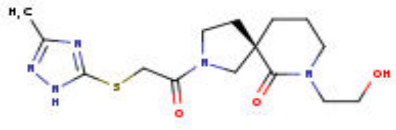

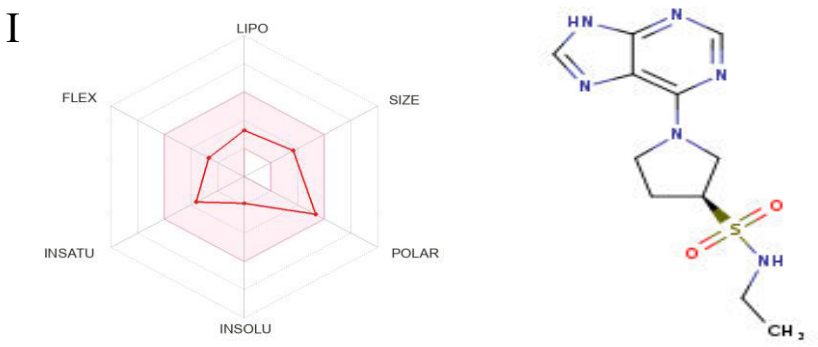

Figure 4.6: The Structures and Oral Bioavailability Radars of the 9 Hits (GDM). (**A**) ZINC09060002, (**B**) ZINC63526364, (**C**) ZINC72133064, (**D**) ZINC72163401, (**E**) ZINC72358537, (**F**) ZINC72358557, (**G**) ZINC72358880, (**H**) ZINC91416974, (**I**) ZINC92700801

When subjected to pharmacokinetics analysis, ZINC04529323, ZINC32780968, ZINC32780968, and ZINC70705715 were out of the required range, as evident in the BOILED-Egg analysis chart (**Figure 4.7**). These four molecules had already been excluded from further analysis because they did not satisfy the drug-likeness requirements.

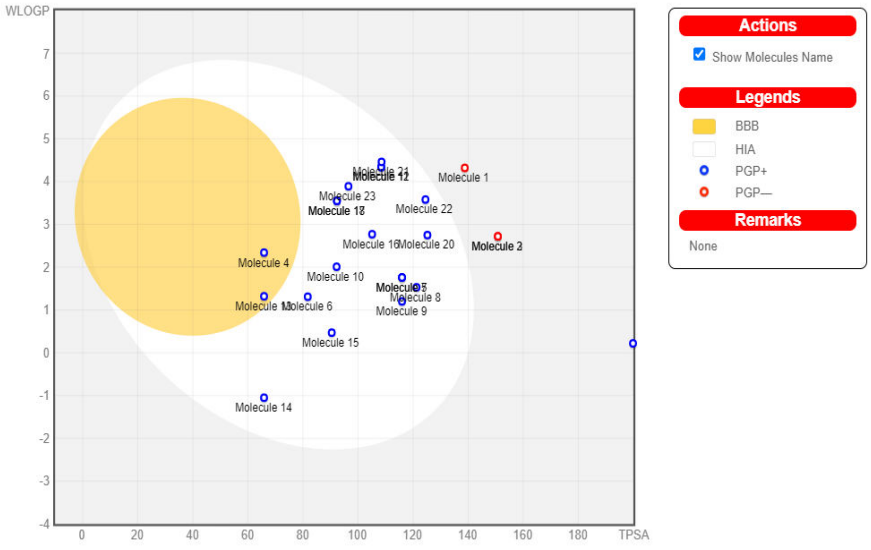

Figure 4.7: BOILED-Egg Analysis (L9 Antibody). Boiled egg prediction of blood brain barrier permeability and gastrointestinal absorption for the 23 hits. 4 molecules (1, 2, 3, and 19) are out of range, thus excluded. The other molecules are P-glycoprotein (P-gp) substrate, indicated by the blue dot, depicting their ease of excretion from the body.

The 9 hits that remained after drug-likeness test and pharmacokinetics properties analysis (**Figure 4.8**) were used for molecular docking.

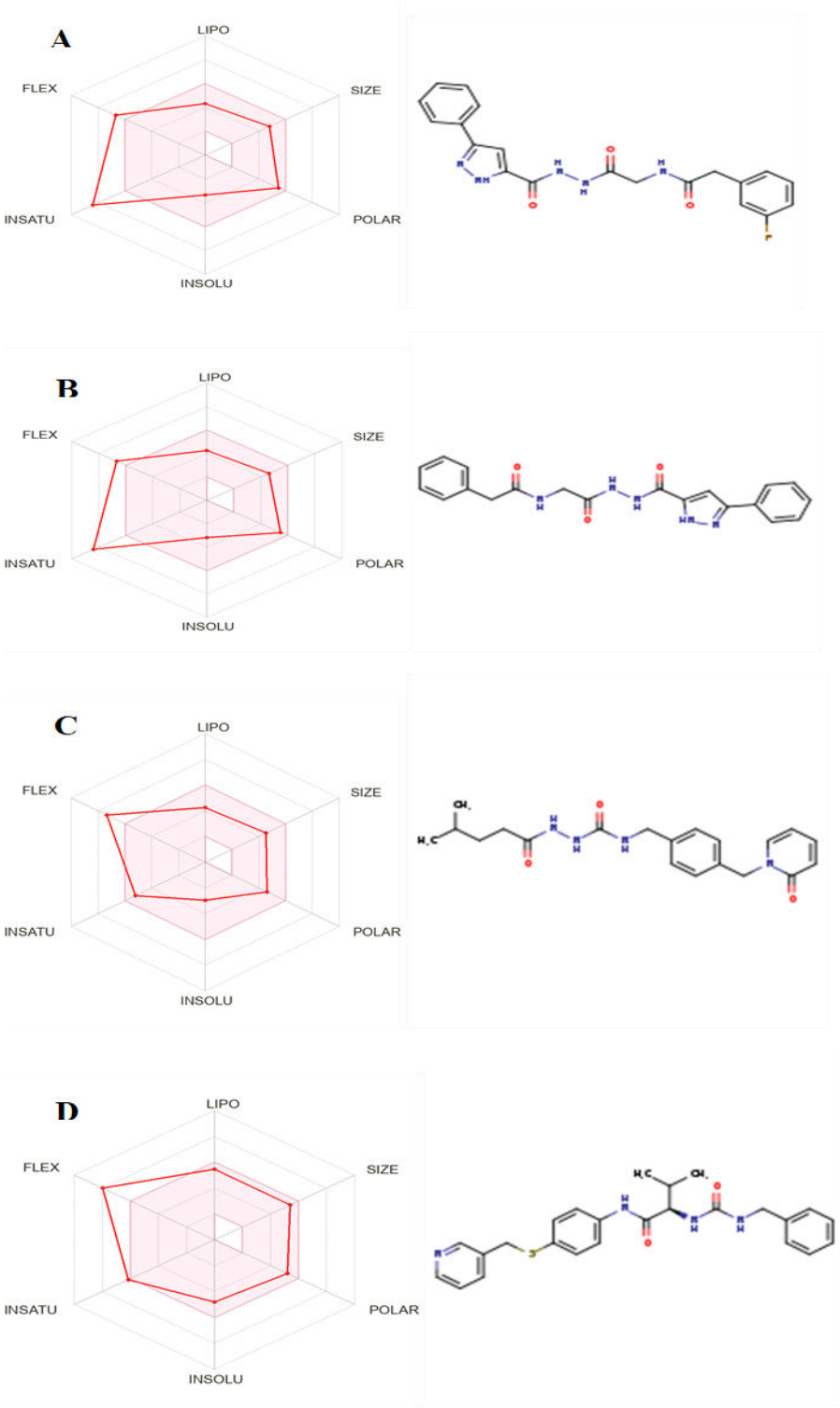

E

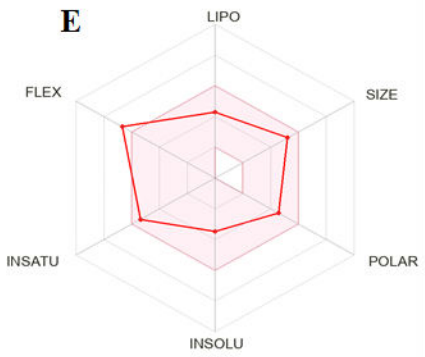
LIPO
SIZE
POLAR
INSOLU
INSATU
FLEX

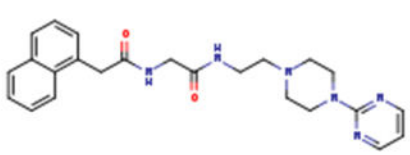

F

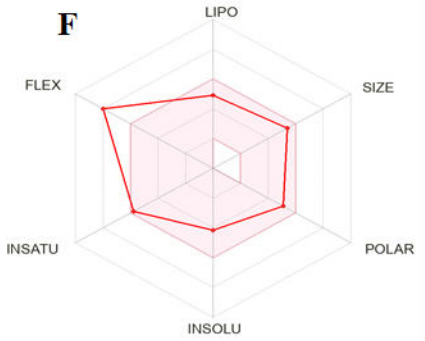
LIPO
SIZE
POLAR
INSOLU
INSATU
FLEX

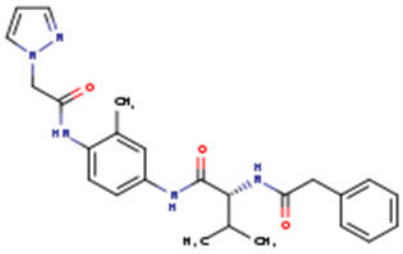

G

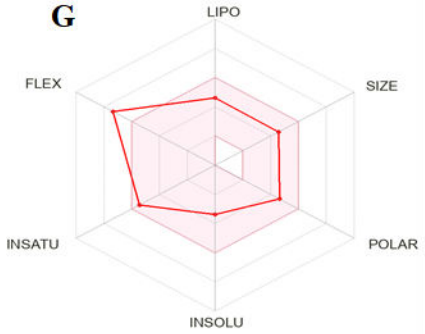
LIPO
SIZE
POLAR
INSOLU
INSATU
FLEX

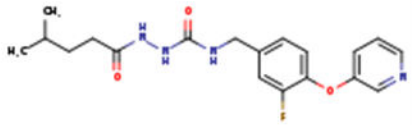

H

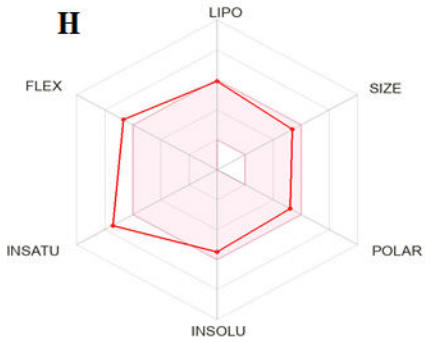
LIPO
SIZE
POLAR
INSOLU
INSATU
FLEX

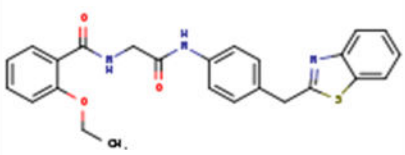

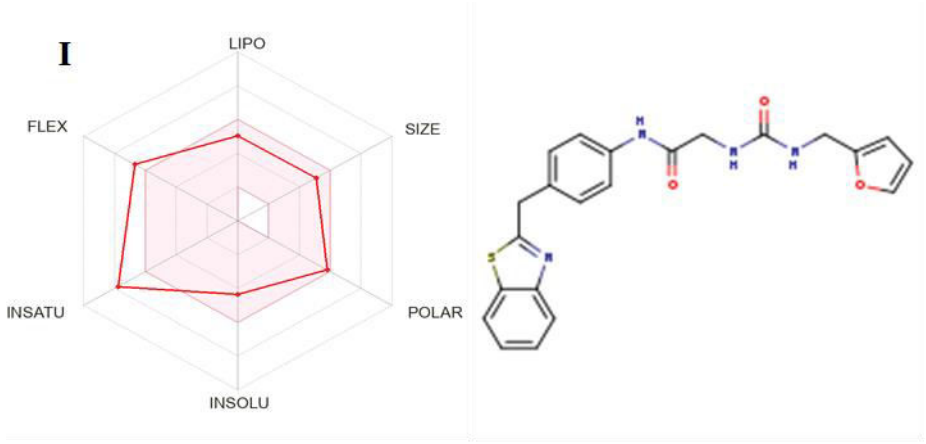

Figure 4.8: The Structures and Oral Bioavailability Radars of the 9 Hits (L9 Antibody). (**A**) ZINC40144754, (**B**) ZINC07948710, (**C**) ZINC67103919, (**D**) ZINC25374360, (**E**) ZINC71998971, (**F**) ZINC57991640, (**G**) ZINC67410702, (**H**) ZINC17588493, (I) ZINC71996727

4.10 Molecular Docking

The binding affinity of GDM to PfHsp90 was -7.5 kcal/mol. ZINC72163401 (-7.7 kcal/mol), ZINC72133064 (-7.8 kcal/mol), ZINC09060002 (-8.2 kcal/mol), ZINC72358557 (-7.6 kcal/mol), and ZINC72358537 (-8.1 kcal/mol) had better binding affinities to PfHsp90 than GDM. The other 4 molecules had -6.7 kcal/mol (ZINC92700801), -7.1 kcal/mol (ZINC63526364), -7.0 kcal/mol (ZINC91416974), and -7.1 kcal/mol (ZINC72358880). Therefore, the five ligands with better binding affinities than GDM were considered for MDS. **Figure 4.9** shows the interaction between PfHsp90 and GDM with binding affinity of -7.5 kcal/mol.

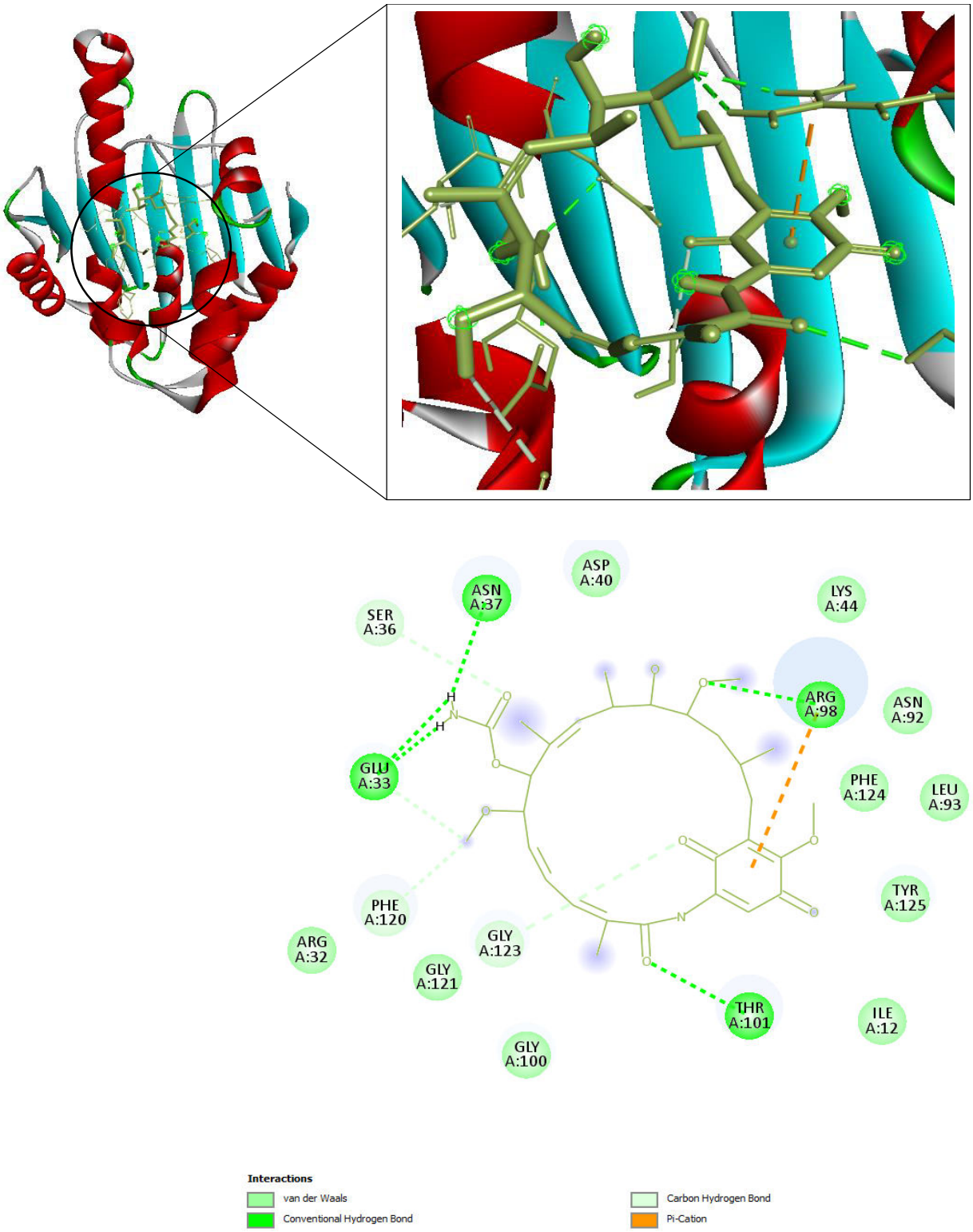

Figure 4.9: 3D and 2D Interactions of PfHsp90 and GDM. The interaction between PfHsp90 and GDM, with binding affinity of -7.5 kcal/mol.

Figure 4.10 shows the interaction between PfHsp90 and ZINC09060002 with binding affinity of -8.2 kcal/mol.

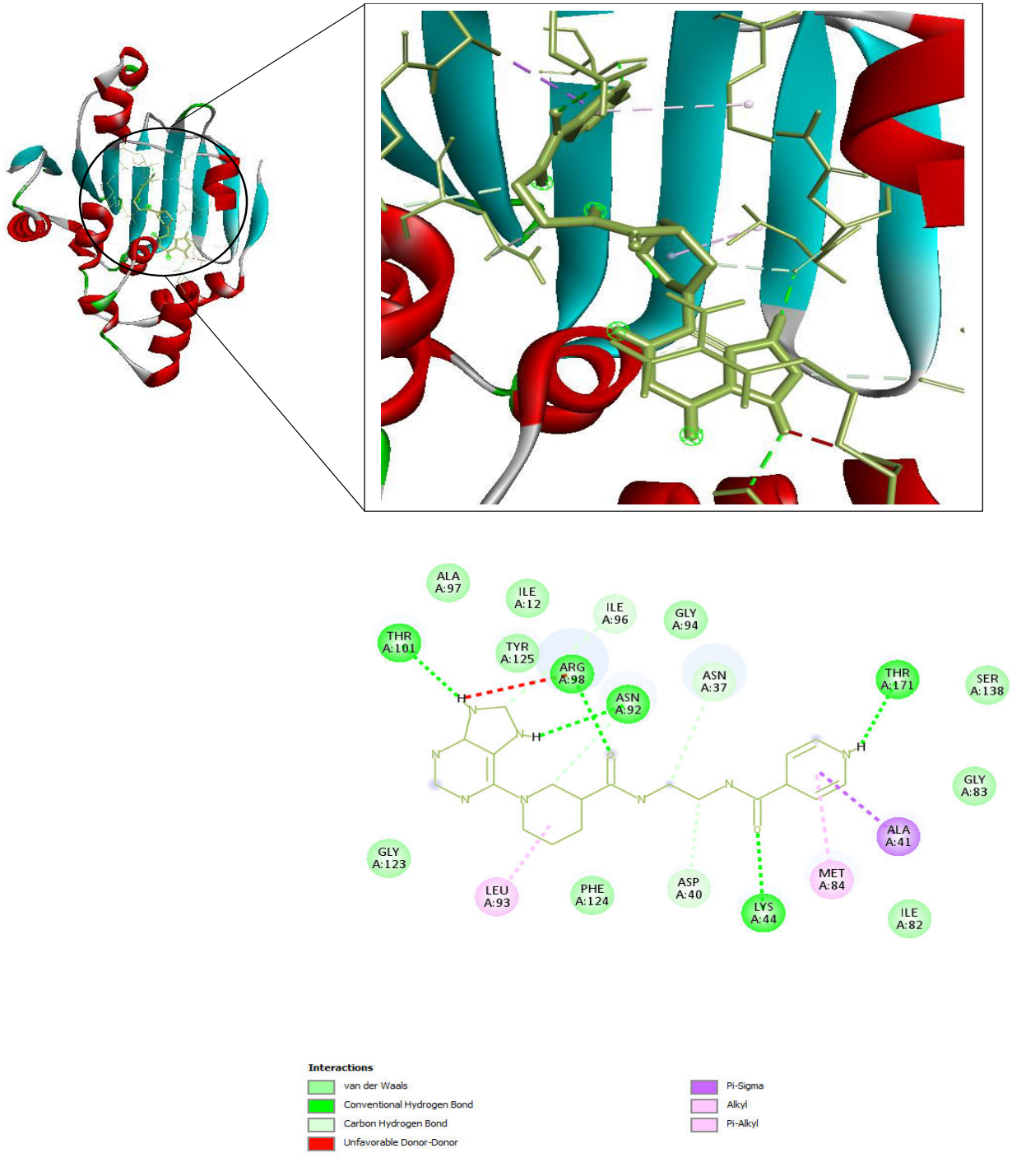

Figure 4.10: 3D and 2D Interactions of PfHsp90 and ZINC09060002. The interaction of PfHsp90 and ZINC09060002, with binding affinity of -8.2 kcal/mol.

Figure 4.11 shows the interaction between PfHsp90 and ZINC72133064 with binding affinity of -7.8 kcal/mol.

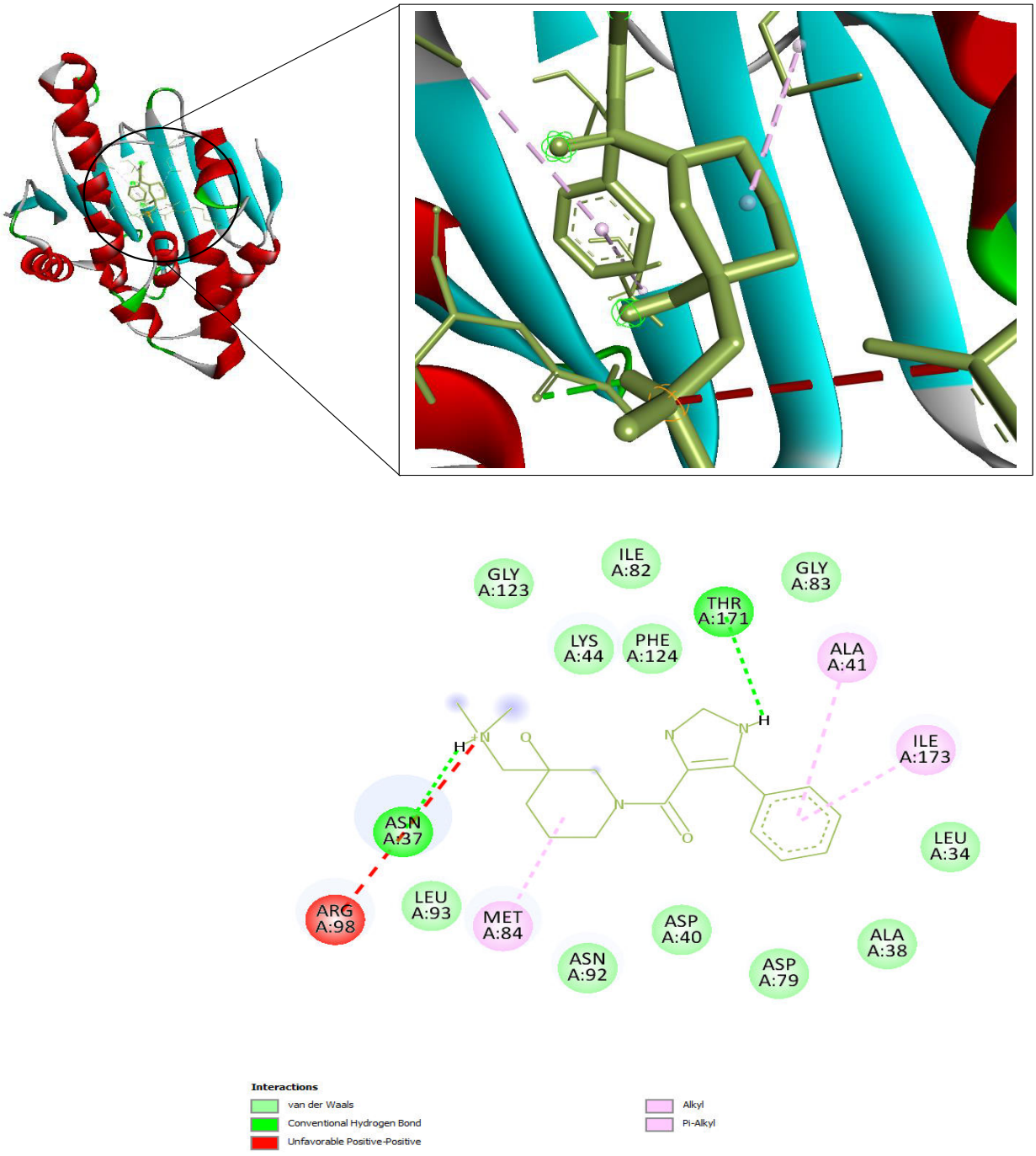

Figure 4.11: 3D and 2D Interactions of PfHsp90 and ZINC72133064. The interactions of PfHsp90 and ZINC72133064, with binding affinity of -7.8 kcal/mol.

Figure 4.12 shows the interaction between PfHsp90 and ZINC72163401 with binding affinity of -7.7 kcal/mol.

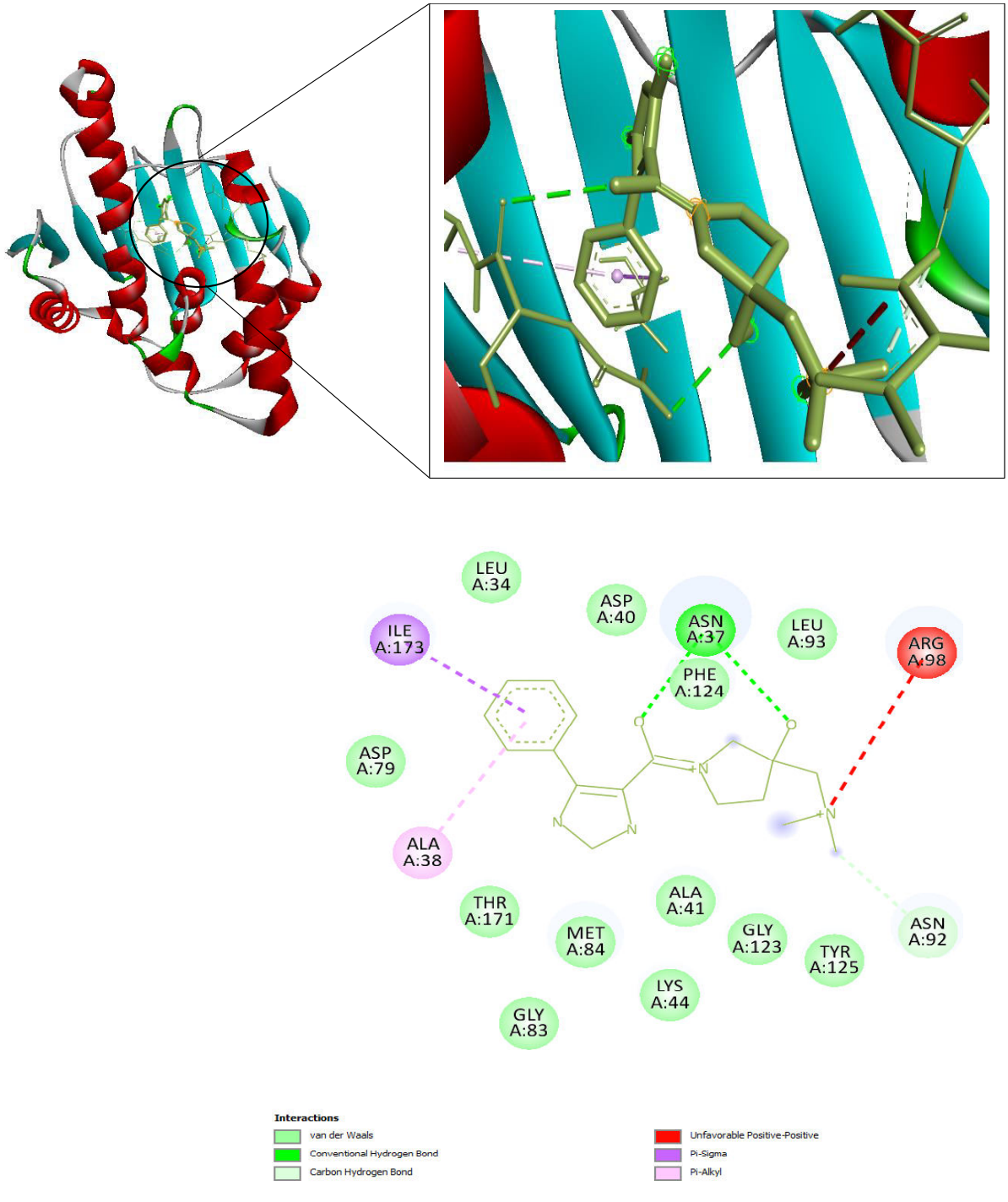

Figure 4.12: 3D and 2D Interactions of PfHsp90 and ZINC72163401. The interaction of PfHsp90 and ZINC72163401, with binding affinity of -7.7 kcal/mol.

Figure 4.13 shows the interaction between PfHsp90 and ZINC72358537 with binding affinity of -8.1 kcal/mol.

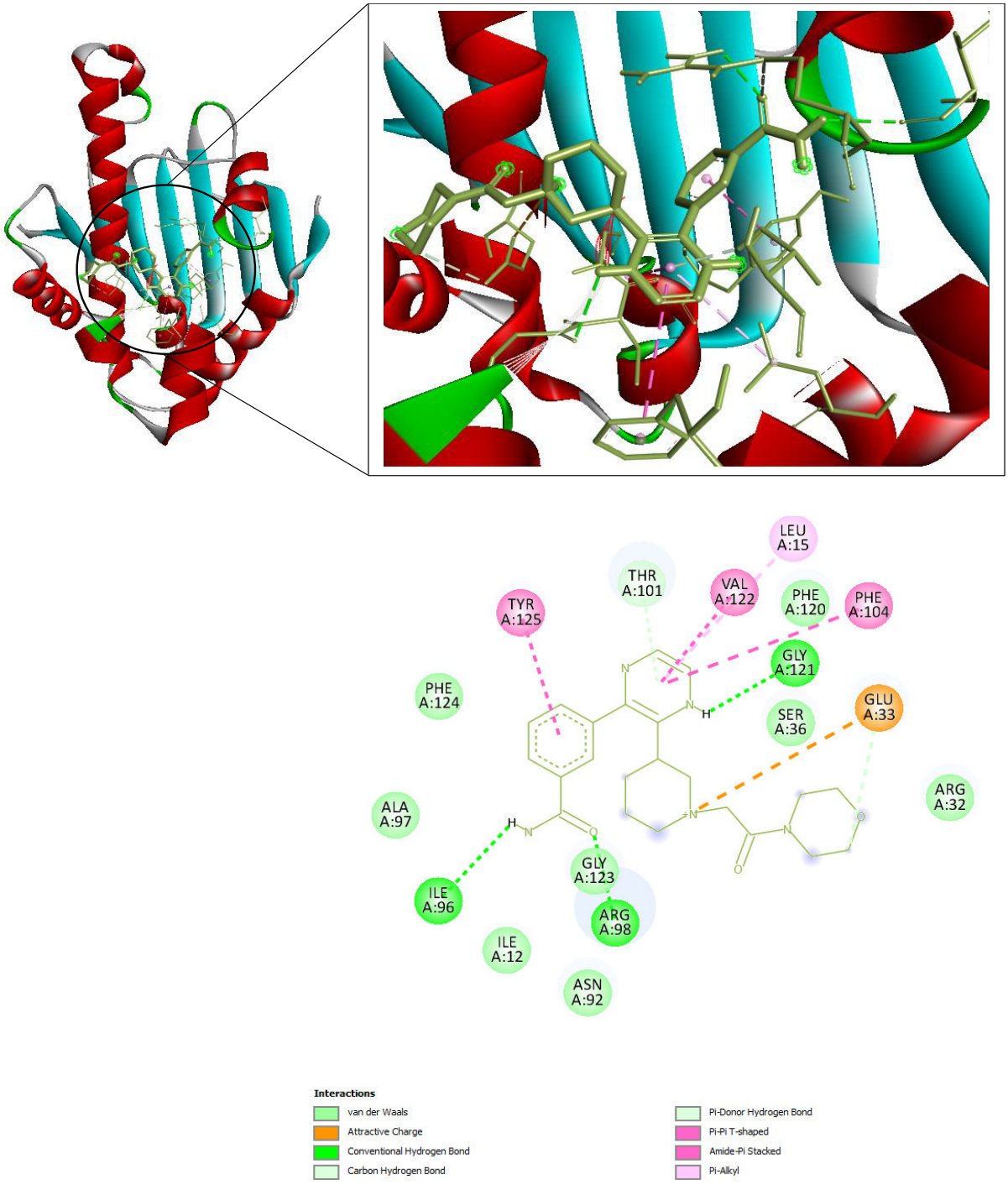

Figure 4.13: 3D and 2D Interactions of PfHsp90 and ZINC72358537. The interaction of PfHsp90 and ZINC72358537, with binding affinity of -8.1 kcal/mol.

Figure 4.14 shows the interaction between PfHsp90 and ZINC72358557 with binding affinity of -7.6 kcal/mol.

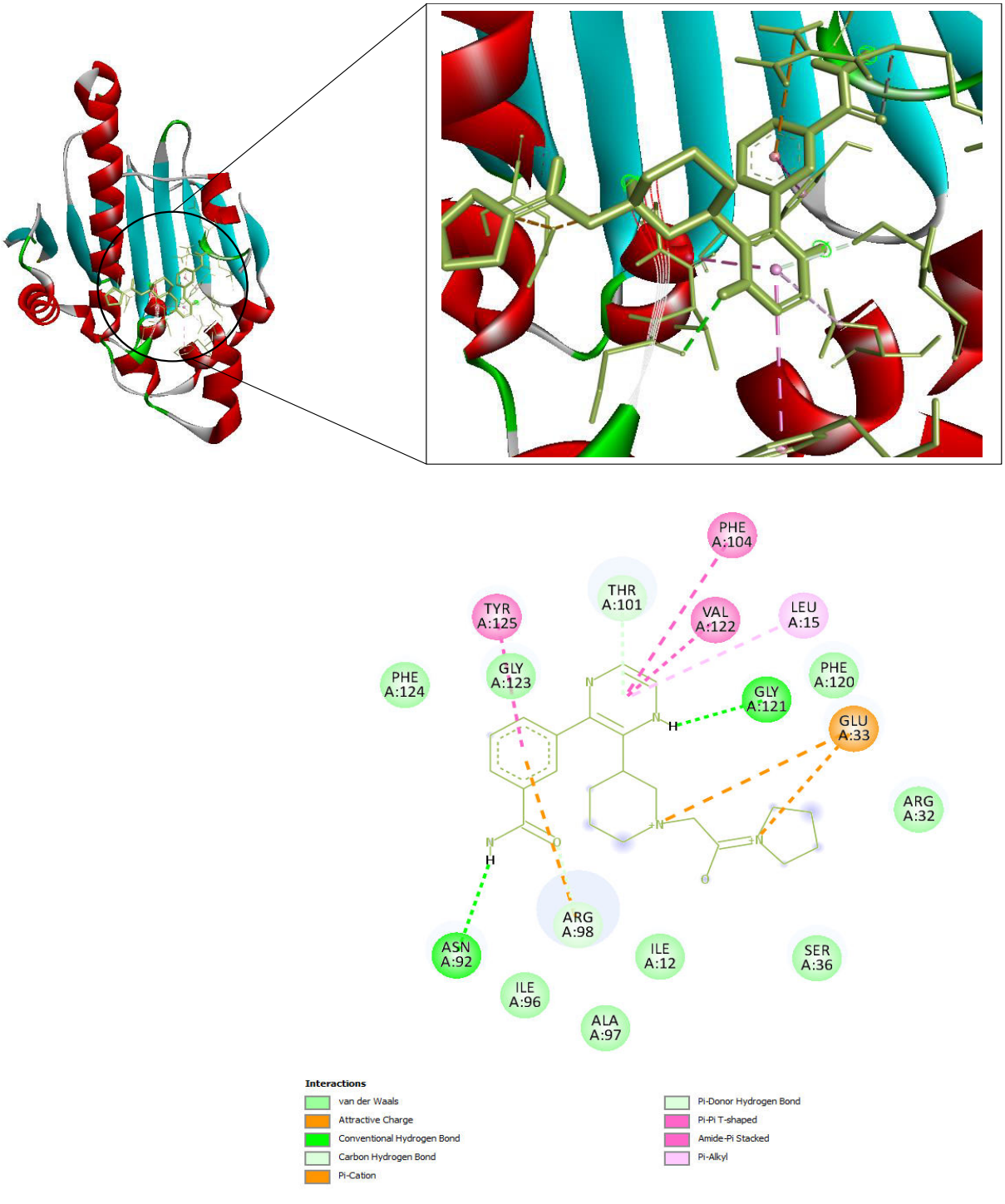

Figure 4.14: 3D and 2D Interactions of PfHsp90 and ZINC72358557. The interaction of PfHsp90 and ZINC72358557, with binding affinity of -7.6 kcal/mol.

The same molecular docking process was performed in the case of PfCSP. The prepared PfCSP (PDB ID 3VDL) was loaded into the PYRX software as a .pdb file and converted into a .pdbqt molecule for docking purposes. A file containing the 9 lead compounds in the .sdf format was then loaded into the PYRX software. Energy of all the 9 ligands was minimized. The ligands were then converted into the preferred .pdbqt format. Docking was then done and the results were as follows: ZINC40144754 (-8.3), ZINC07948710 (-7.7), ZINC67103919 (-7.5), ZINC25374360 (-8.1), ZINC71998971 (-8.0), ZINC57991640 (-7.7), ZINC67410702 (-6.9), (H) ZINC17588493 (-7.8), and ZINC71996727 (-8.9). No docking conformation was found when docking mAb L9 to PfCSP was attempted. Regardless, three lead compounds were chosen for molecular dynamics simulation based on their binding affinities, which was below -8.0. They include ZINC40144754 (-8.3), ZINC25374360 (-8.1), and ZINC71996727 (-8.9). However, when the interaction between PfCSP and the three lead compounds was assessed using BIOVIA Discovery Studio 2021, it was discovered that ZINC40144754 does not interact with chain A (**Figure 4.15**). Furthermore, as evident in **Figure 4.15**, it was also discovered that ZINC40144754 forms unfavorable donor-donor interactions with PfCSP. Therefore, it was excluded from the molecular dynamics simulation process.

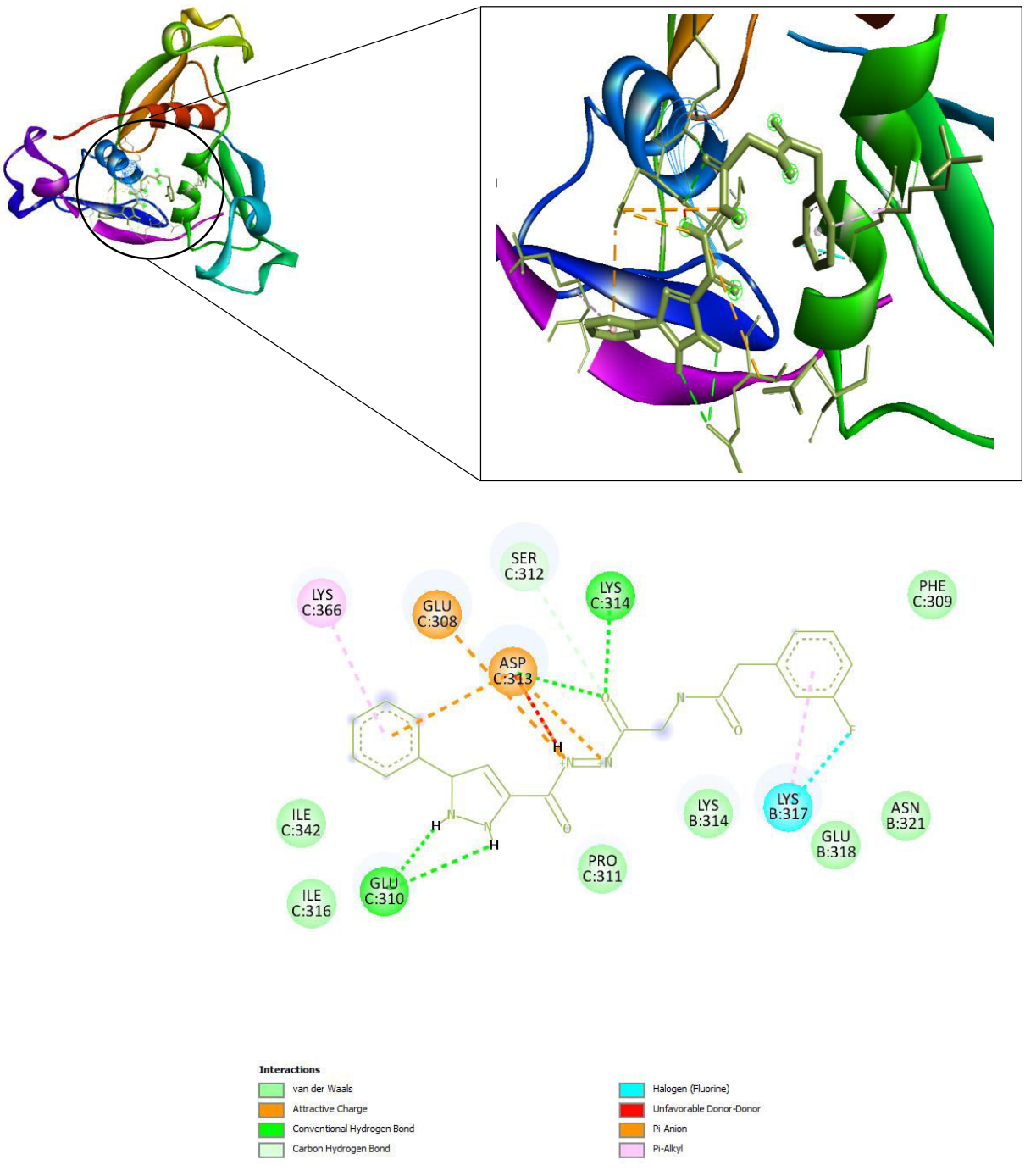

Figure 4.15: 3D and 2D Interactions of PfCSP and ZINC40144754. The 3D interaction of PfHsp90 and ZINC40144754, with binding affinity of -8.3 kcal/mol.

Only ZINC25374360 (**Figure 4.16**) and ZINC71996727 (**Figure 4.17**) were subjected to MDS.

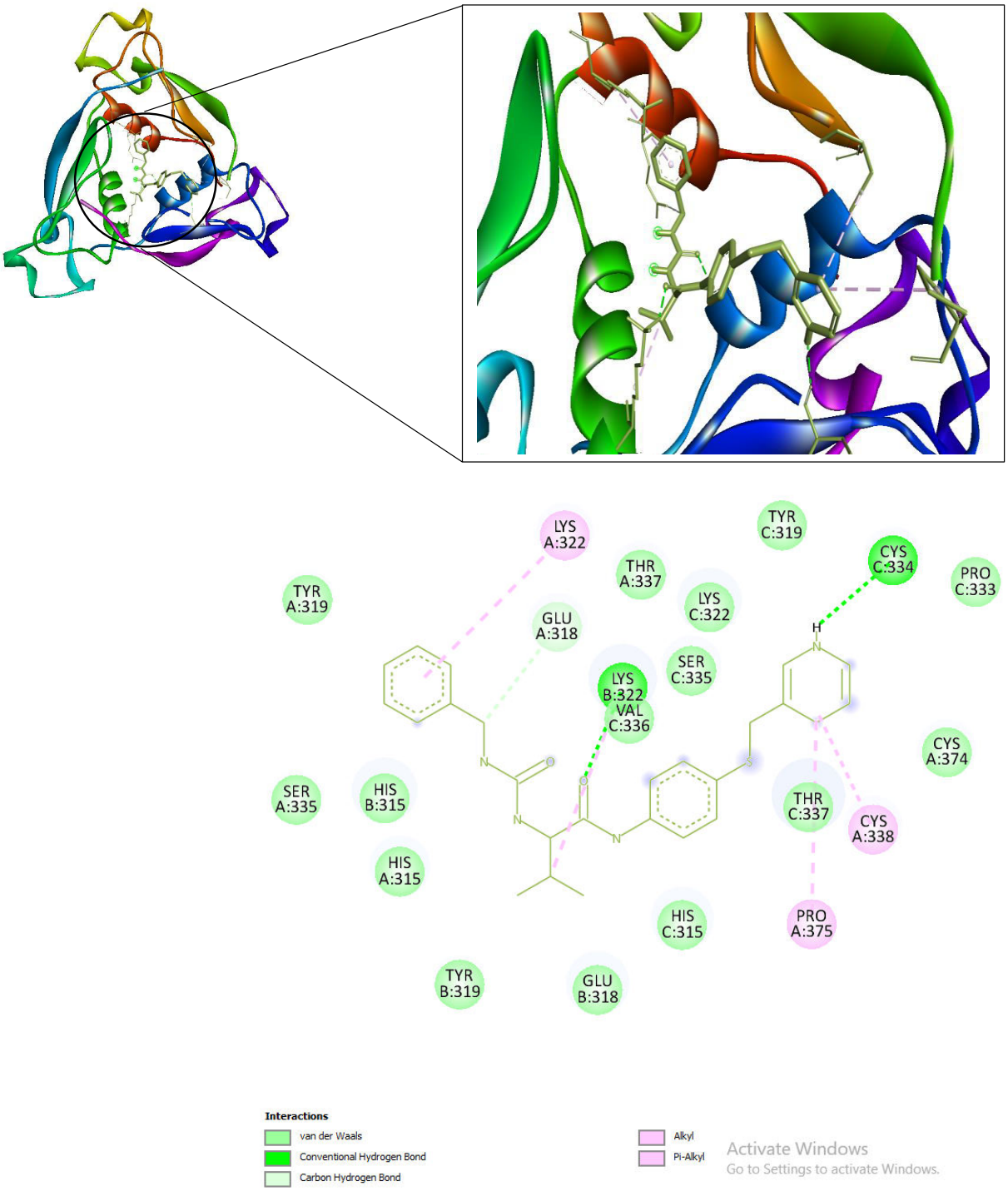

Figure 4.16: 3D and 2D Interactions of PfCSP and ZINC25374360. The 3D interaction of PfHsp90 and ZINC25374360, with binding affinity of -8.1 kcal/mol.

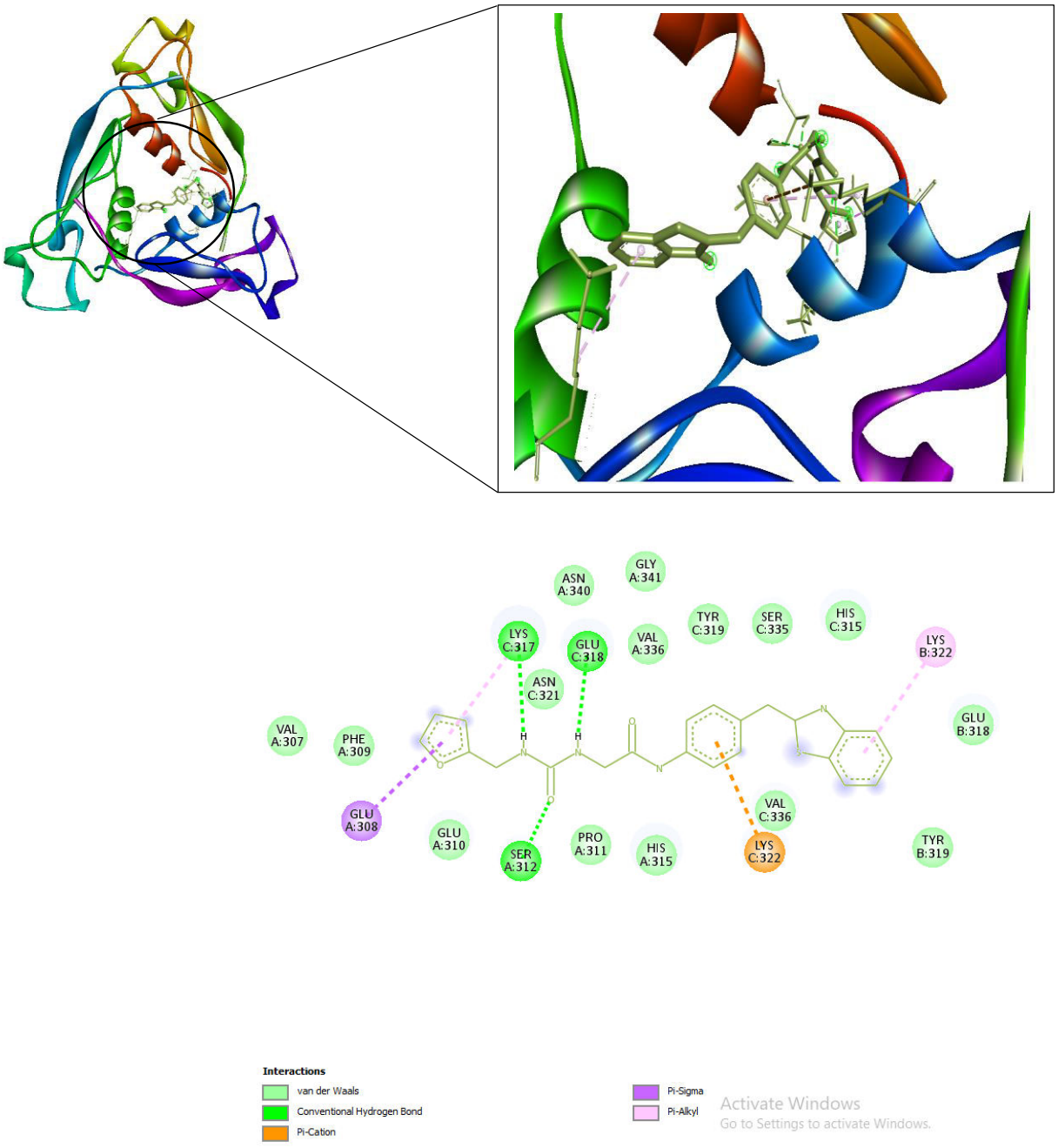

Figure 4.17: 3D and 2D Interactions of PfCSP and ZINC71996727. The 3D interaction of PfHsp90 and ZINC71996727, with binding affinity of -8.9 kcal/mol.

Specific Objective 2

4.11 Molecular Dynamics Simulation (MDS)

As shown in **Figure 4.18**, three (ZINC72163401, ZINC72358537, and ZINC72358557) of the five ZINC database compounds do not experience major deviations. The conformational change of their backbone atoms in complex with PfHsp90 is comparable to the conformations of GDM in complex with the target protein over 100ns MDS. ZINC72163401 and ZINC72358557 have negligible deviation distance of approximately 0.3nm within PfHsp90's binding pocket throughout the 100ns MDS. As for ZINC72358537, before 25ns and after 85ns, its deviation distance is almost 4nm. The deviation distance is below 0.25nm between 25ns and 85ns. ZINC09060002 and ZINC72133064 have high RMSDs throughout the 100ns MDS, indicating increased risk of conformational changes in complex with PfHsp90.

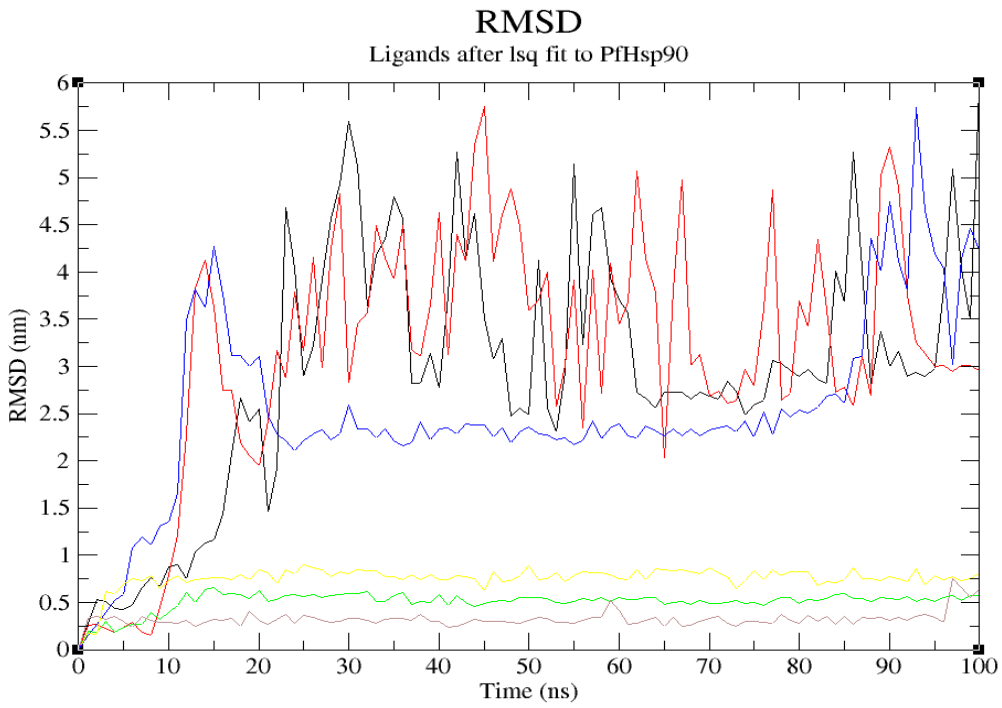

Figure 4.18: RMSD plot of PfHsp90 (PDB ID: 3K60) with GDM as reference ligand and top-five ZINC database compounds as a function of 100ns simulation time. ZINC09060002 (Black), ZINC72133064 (Red), ZINC72163401 (Green), ZINC72358537 (Blue), ZINC72358557 ((Yellow), and GDM (Brown).

On the same note, as shown in **Figure 4.19**, ZINC25374360 and ZINC71996727 do not experience major deviations. For the first 10ns, ZINC25374360 experiences a deviation of approximately 1nm. It then stabilizes for around 25ns before deviating with an approximate distance of 1nm within a 10ns period. From 45ns to 100ns, ZINC25374360 remains relatively stable with minor deviations of an average distance of 0.25nm. ZINC71996727 is more stable than ZINC25374360 because of its negligible deviations. It gains stability within the first 50ns. Even though it deviates a bit for the last 50ns, the deviations are negligible with an average distance of approximately 0.5nm. Therefore, both compounds form complexes with PfCSP that have low risk of conformational changes.

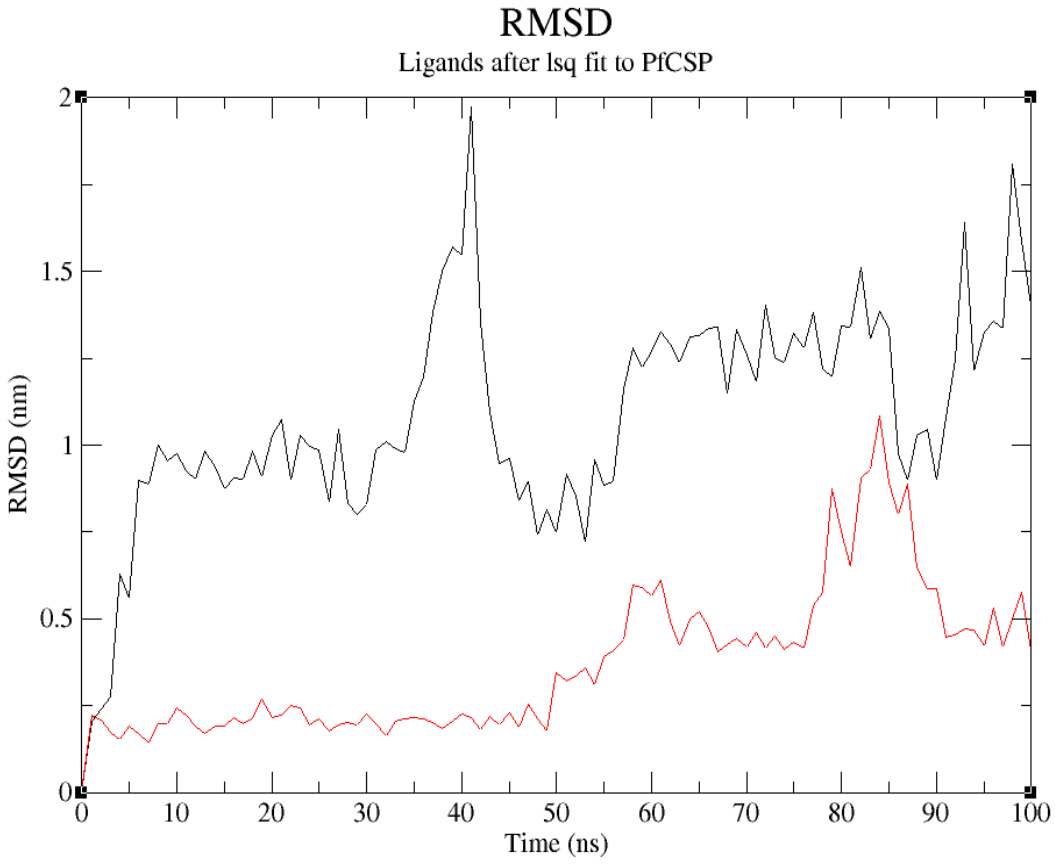

Figure 4.19: RMSD plot of PfCSP (PDB ID: 3VDL) with the two ZINC database compounds as a function of 100ns simulation time. ZINC25374360 (Black) and ZINC71996727 (Red).

The RMSF was calculated to indicate individual residue flexibility, or how much a particular residue moves (fluctuates) during the 100ns simulation. It is a structural indication of which amino acids in a protein or atoms in a chemical compound contribute the most to a molecular motion. In the process, the RMSF measures the displacement of a particular atom, or group of atoms, relative to the reference structure, averaged over the number of atoms (Martínez, 2015). **Figure 4.20** shows the RMSF values of the five ZINC20 database compounds relative to the reference ligand, GDM. GDM fluctuates within a distance of 0.175nm, with the residue at around position 3450 attaining the lowest fluctuation of approximately 0.025nm and the atom at position 3505 reaching a maximum fluctuation of almost 0.2nm.

ZINC72358537 and ZINC72163401 also fluctuates within this range, indicating low divergence from the average position and therefore low structural mobility. Even though ZINC72358557 and ZINC72133064 have atoms that attain a lowest fluctuation of 0.025nm, similar to GDM, some of their atoms surpass the maximum fluctuation threshold of 0.2nm to approximately 0.25nm. Regardless, this 0.05nm difference is low, making them within the desired RMSF levels. As for ZINC09060002, its highest fluctuation surpasses 0.4nm, indicating increased risk of high divergence from the average position and therefore high structural mobility when compared to GDM. These results confirmed that ZINC72163401, ZINC72358537**,** ZINC72133064, and ZINC72358557 do not undergo high divergence from the average positions.

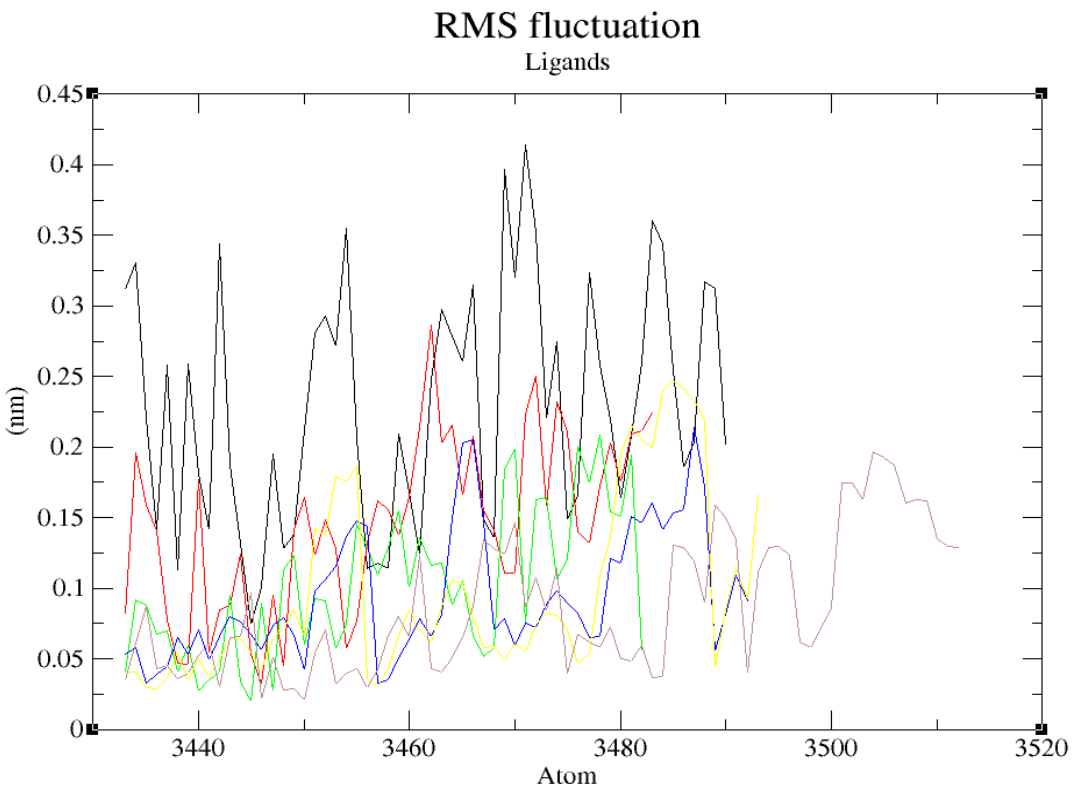

Figure 4.20: RMSF plot of GDM as reference ligand and top-five ZINC database compounds. ZINC09060002 (Black), ZINC72133064 (Red), ZINC72163401 (Green), ZINC72358537 (Blue), ZINC72358557 (Yellow), and GDM (Brown).

Even though ZINC25374360 and ZINC71996727 did not have a reference ligand used for comparison purposes, the movement of their atoms could be assessed based on acceptable fluctuation distances. **Figure 4.21** displays how atoms of the two ZINC compounds fluctuate within an acceptable distance of 0.2nm, proving that they do not undergo high divergence from their average positions.

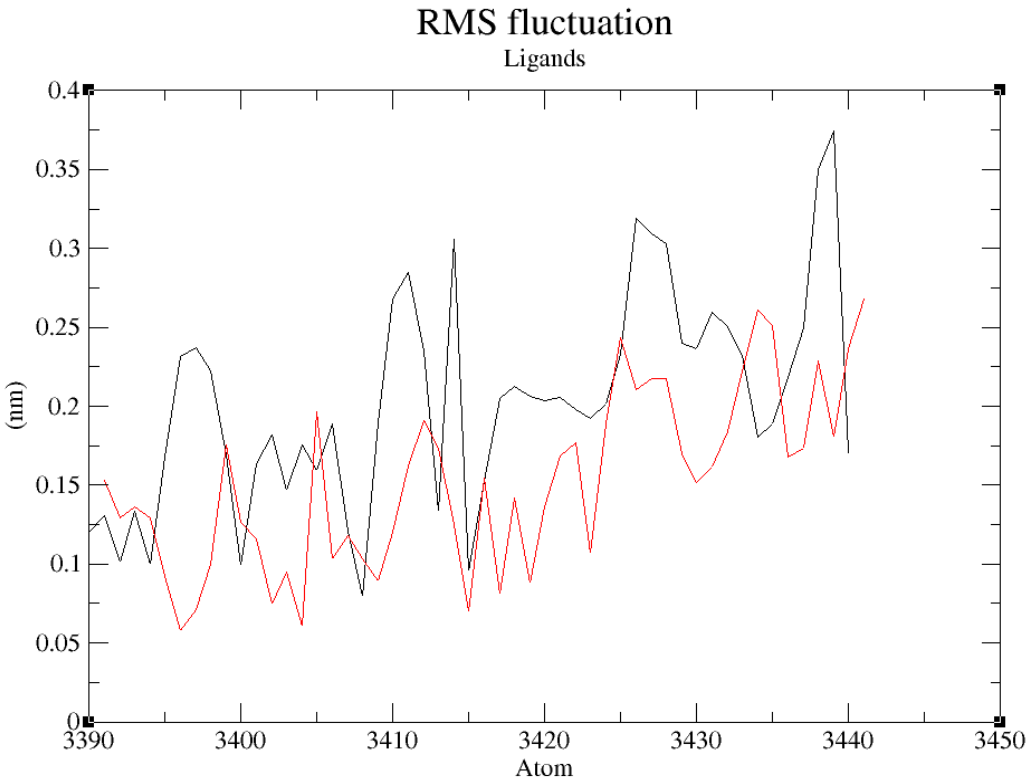

Figure 4.21: RMSF plot of the two ZINC database compounds. ZINC25374360 (Black) and ZINC71996727 (Red).

Hydrogen bonds are essential in protein-ligand complexes because they are considered facilitators of protein-ligand binding. They are believed to increase the binding affinity of a ligand to a protein of interest. **Figure 4.22** shows the number of bonds between PfHsp90 and the six ligands. As the reference, PfHsp90-GDM complex forms 1-3 hydrogen bonds in the course of the 100ns simulation. ZINC09060002 forms a maximum of 4 hydrogen bonds with PfHsp90, ZINC72133064 forms 3, ZINC72163401 forms 4, ZINC72358537 forms 4, and ZINC72358557 forms 6. These results confirmed that all the five ZINC database compounds bind strongly to PfHsp90 when compared with GDM.

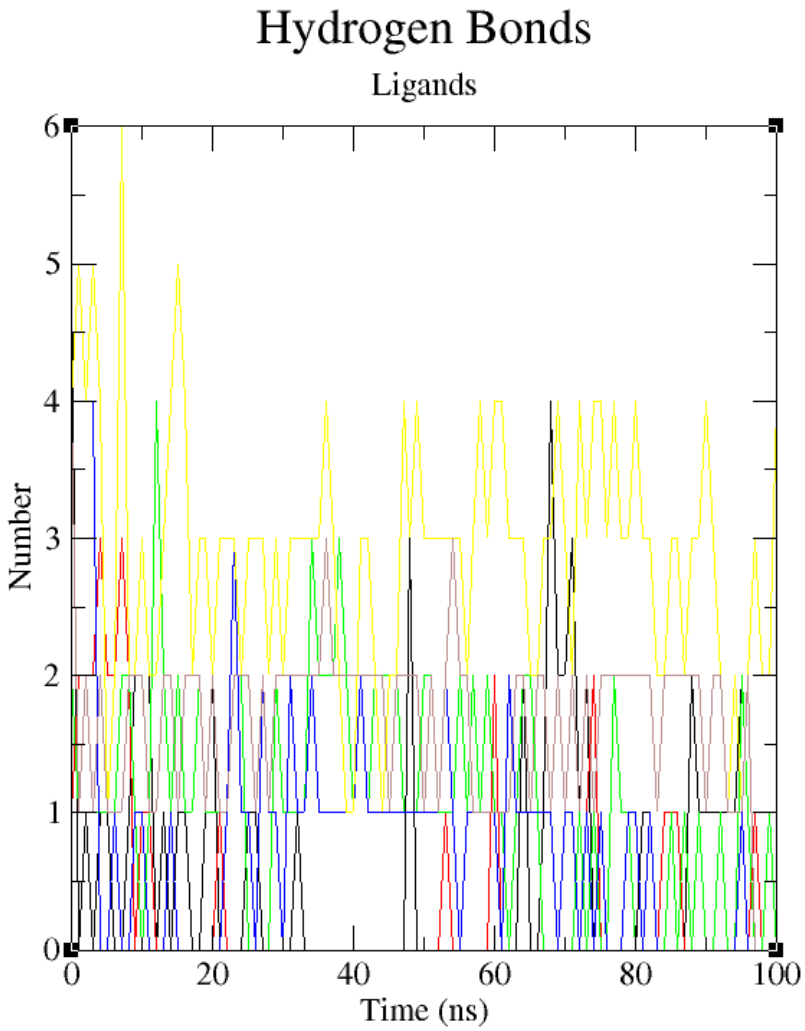

Figure 4.22: Number of Hydrogen Bonds Plot. The number of hydrogen bonds between PfHsp90 (PDB ID: 3K60) with GDM as reference ligand and top-five ZINC database compounds as a function of 100ns simulation time. ZINC09060002 (Black), ZINC72133064 (Red), ZINC72163401 (Green), ZINC72358537 (Blue), ZINC72358557 (Yellow), and GDM (Brown).

In the case of PfCSP, **Figure 4.23** shows the number of bonds between PfCSP and the two ligands, ZINC25374360 and ZINC71996727. Throughout the 100ns simulation, ZINC25374360 forms between 0 to 3 hydrogen bonds with PfCSP while ZINC71996727 forms approximately 1 to 5 hydrogen bonds with the same target protein. Considering the number of hydrogen bonds GDM forms with PfHsp90, these results confirmed that the two ZINC database compounds bind strongly to PfCSP.

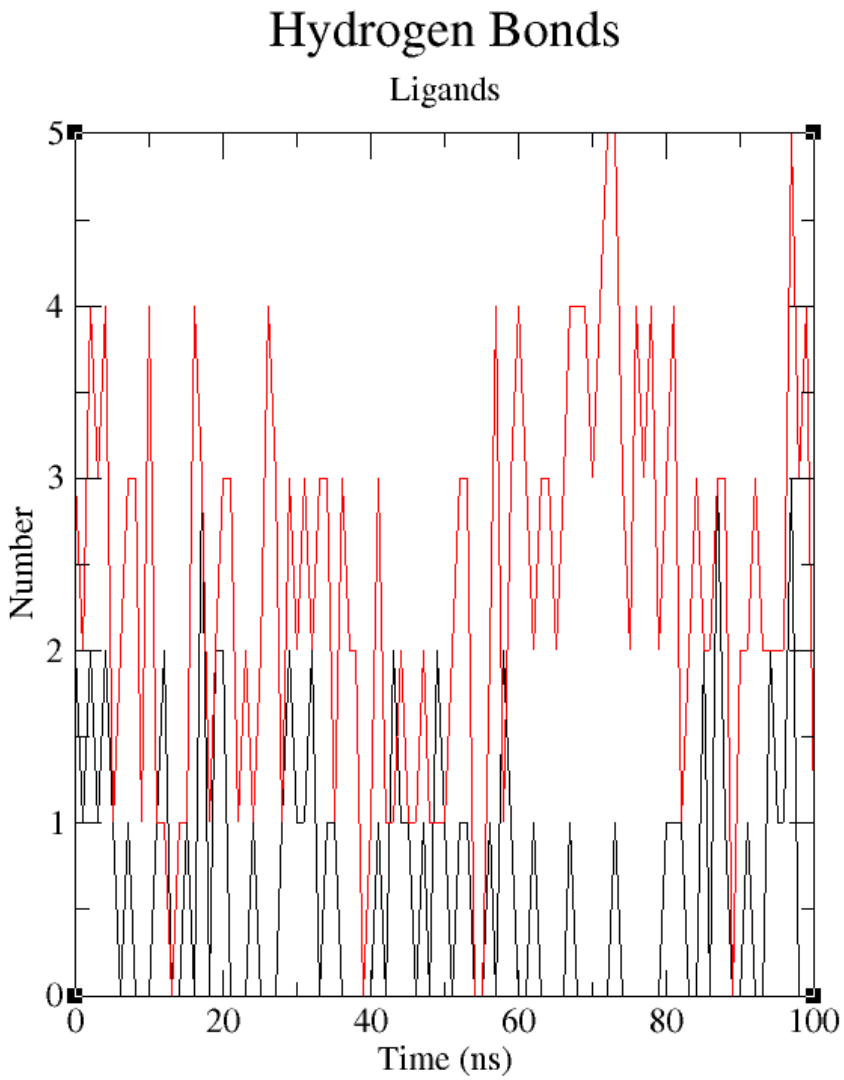

Figure 4.23: Number of Hydrogen Bonds Plot. The number of hydrogen bonds between PfCSP (PDB ID: 3VDL) with the two ZINC database compounds as a function of 100ns simulation time. ZINC25374360 (Black) and ZINC71996727 (Red).

Specific Objective 3

4.12 *In Vitro* Validation of PfHsp90 and PfCSP Inhibitors

The *in vitro* activities of PfHsp90 and PfCSP inhibitors were analyzed against field isolates of the parasite, *P. falciparum* 3D7 laboratory strain. **Figure 4.24** shows promising inhibition of parasite growth, with IC_{50} values of 38.04 ng/mL (ZINC72163401) (**Figure 4.24A**), 25.60 ng/mL

(ZINC72358537) (**Figure 4.24B**), 33.31 ng/mL (ZINC72358557) (**Figure 4.24C**), 105.21 ng/mL (ZINC25374360) (**Figure 4.24D**), and 6.18 ng/mL (ZINC71996727) (**Figure 4.24E**).

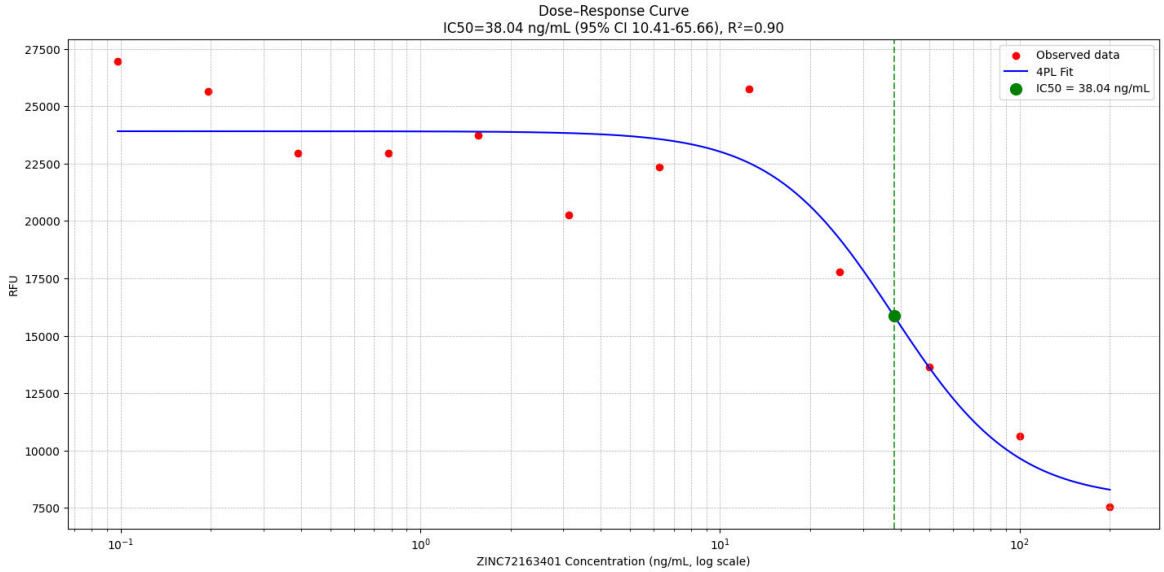

Figure 4.24A: 4PL Curve. IC_{50} value determination of ZINC72163401 using 4PL non-linear regression.

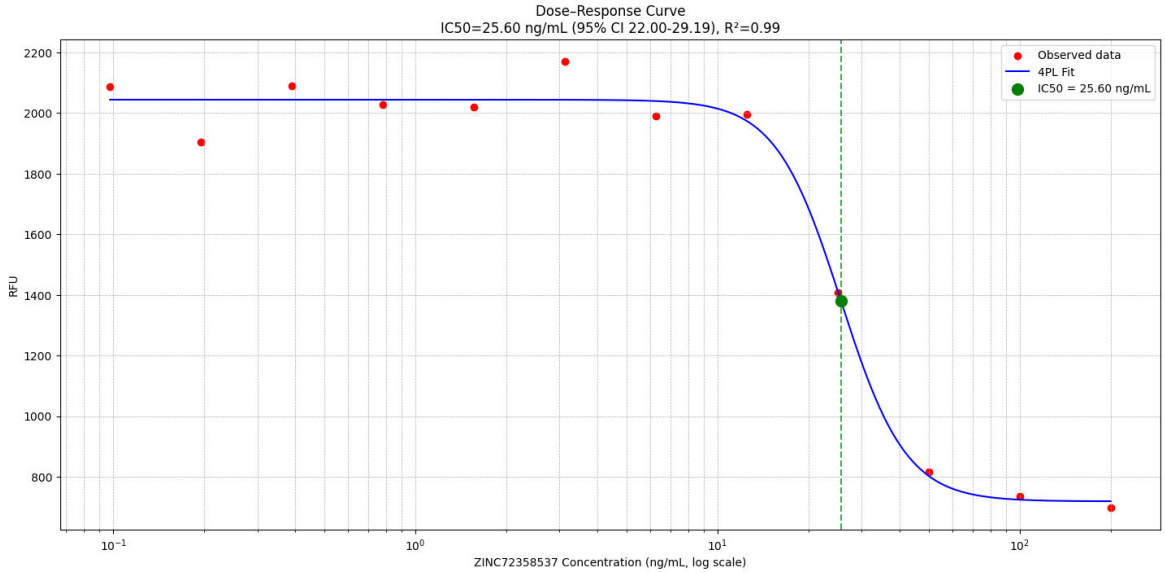

Figure 4.25B: 4PL Curve. IC_{50} value determination of ZINC72358537 using 4PL non-linear regression.

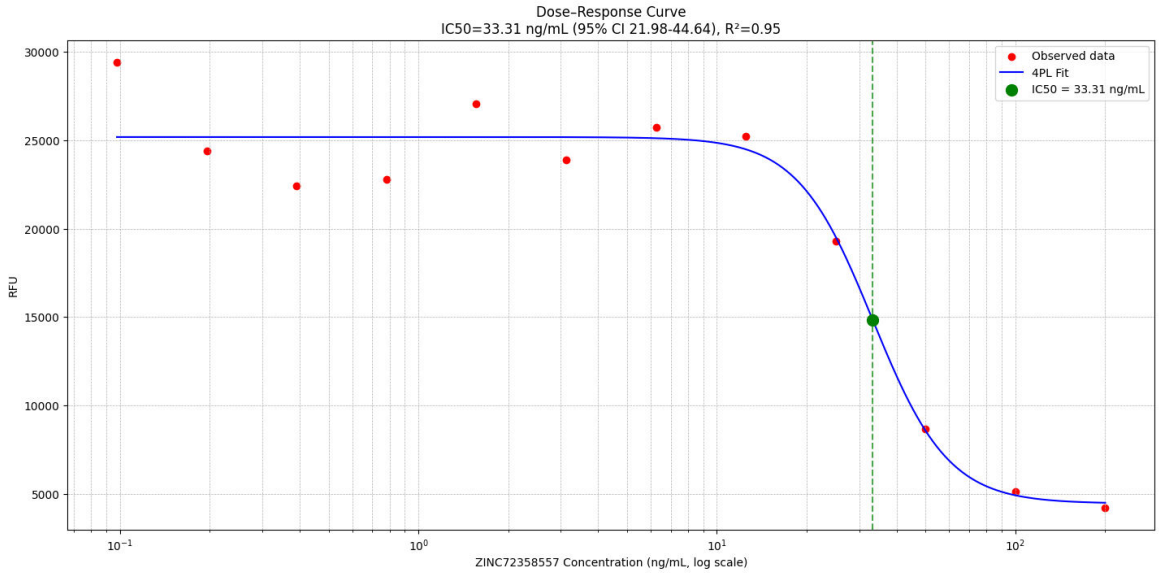

Figure 4.26C: 4PL Curve. IC_{50} value determination of ZINC72358557 using 4PL non-linear regression.

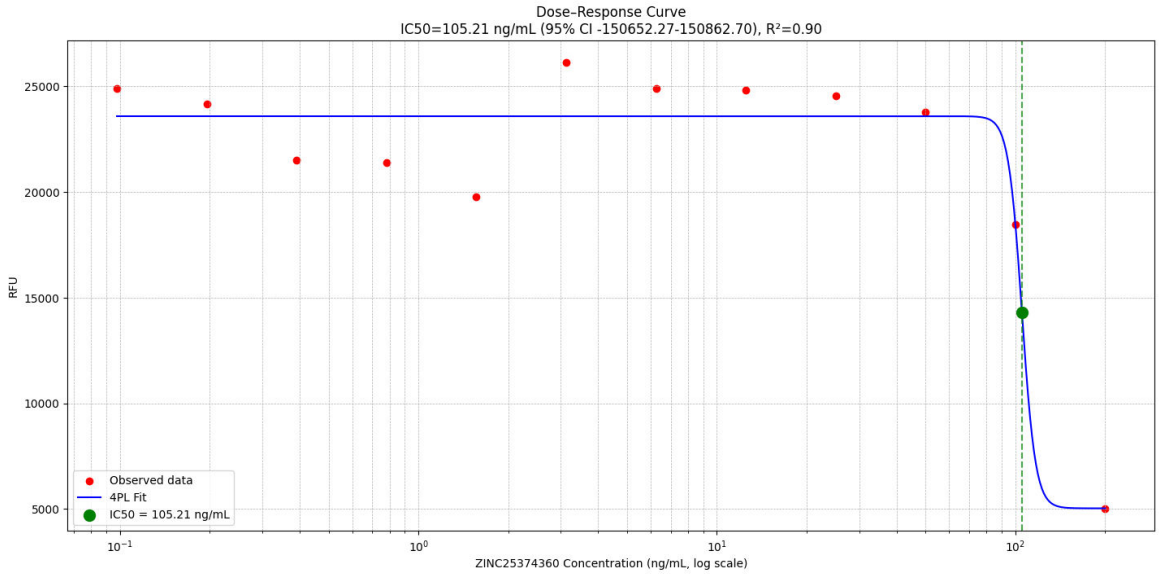

Figure 4.27D: 4PL Curve. IC_{50} value determination of ZINC25374360 using 4PL non-linear regression.

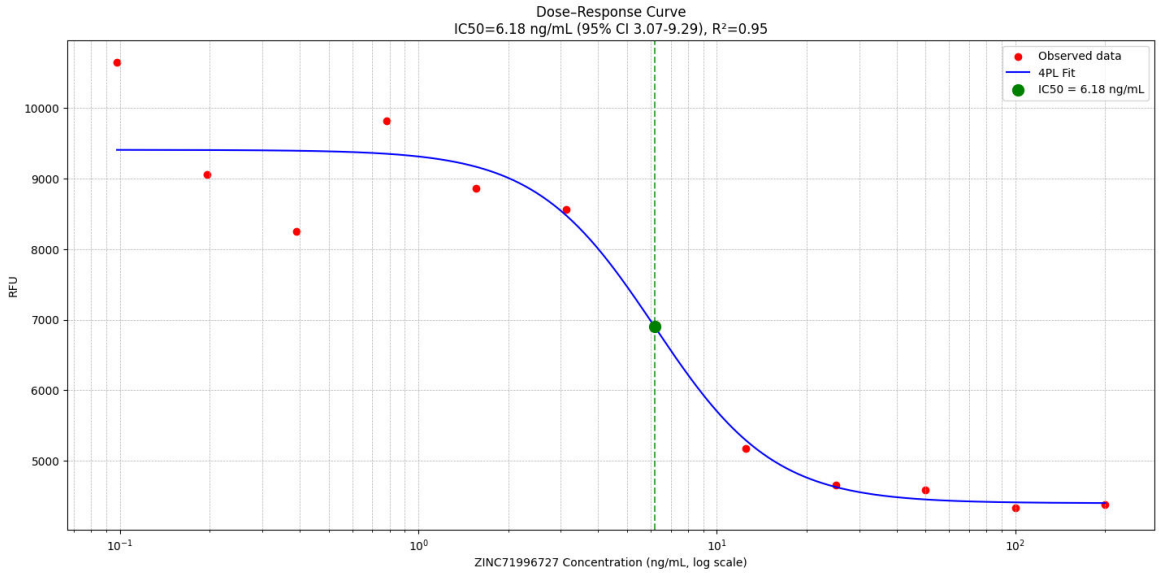

Figure 4.28E: 4PL Curve. IC_{50} value determination of ZINC71996727 using 4PL non-linear regression.

CHAPTER FIVE

DISCUSSION

5.1 Homology Testing

A BLAST query search and multiple sequence alignment revealed homology among the Hsp90 proteins of the five *Plasmodium* species and evolution diversity among the CSP proteins of the parasites. The high identity and similarity scores found during PfHsp90 homologous sequences alignment confirm the strong evolutionary conservation of this protein. Similar conservation patterns have been reported in other proteins across *Plasmodium* species; for instance, histidine-rich proteins and MLH sequences have also been shown to be highly conserved (Fontecha *et al*., 2019; Tarique *et al*., 2017). Consistent with those findings, the present study shows that PfHsp90 retains all three functional domains (NTD, MD, and CTD) across species. This conservation aligns with Hsp90's vital biological functions in all species, particularly its crucial function as a molecular chaperone. Furthermore, the high degree of sequence conservation indicates that PfHsp90 is subject to strong purifying selection, which limits diversity to maintain its function. This high conservation level suggests that PfHsp90 might be a broad-spectrum therapeutic target. Inhibitors targeting it might work against a variety of *Plasmodium* species.

Conversely, the low identity and similarity scores found during alignment of the CSP sequences show evolutionary divergence among the *Plasmodium* species. Unlike Hsp90, CSP did not show sequence conservation, aligning with Patra *et al*. (2021) who discovered that CSPs only share limited homology in region I and the C-terminal region. Thus, the significant immune selection pressures on surface antigens are reflected in the substantial variability seen in this investigation. The *P. falciparum*-specific RTS,S vaccine, which exhibits poor cross-species protection, serves as

an example of how such divergence might facilitate host adaptability and immune evasion while simultaneously making vaccine development more difficult.

Phylogenetic analysis further validated this divergent evolutionary patterns. PfHsp90 remained more distantly linked to Hsp90 from outgroup organisms (distances above 0.25), but it clustered closely with the Hsp90 sequences of the other *Plasmodium* species (distances below 0.10). However, with divergence values more than 1.00, PfCSP displayed distant associations with CSPs from the other *Plasmodium* species. These findings are consistent with a larger evolutionary pattern in which highly variable antigens like CSP indicate parasite adaptation tactics to elude host protection, whereas conserved proteins like Hsp90 disclose species links and possible therapeutic targets (Bonnefoy *et al*., 1994). Collectively, these results highlight the necessity of including both conserved and variable proteins into malaria research to balance the development of species-specific vaccine techniques with the quest for broad-spectrum treatments.

5.2 Hierarchical Virtual Screening

The homology tests and multiple sequence alignment analyses informed the decision to use PfHsp90 and PfCSP as templates and target proteins for downstream *in-silico* processes to achieve objective 1 of this current study. Such conserved and variable targets offer unique opportunities in drug discovery. PfCSP, a divergent antigen, may be more difficult to target but is crucial for species-specific interventions, whereas PfHsp90, a highly conserved target, offers potential for broad-spectrum inhibitors. The pharmacophore-based virtual screening yielded 17 hits with the GDM-derived model and 23 hits with the mAb L9-derieved model. The hits' low RMSD values (below 1 Å) suggest their strong structural similarity to their references ligands, supporting their suitability as starting points for inhibitor development. This finding aligns with earlier pharmacophore-based screening investigations that employed RMSD to confirm the dependability

of possible hits (Alzain *et al*., 2022; Oduselu *et al*., 2023). According to these results, even though additional filtering was still required, the study's low RMSD values increase confidence that the compounds found are structurally relevant candidates for PfHsp90 and PfCSP inhibition.

Molecular docking provided deeper insights into the binding strength of these inhibitors. In the case of PfHsp90, five inhibitors exhibited stronger binding affinities than GDM (-7.5 kcal/mol), with ZINC09060002 (-8.2 kcal/mol) and ZINC72358537 (-8.1 kcal/mol) being particularly promising. The lower the binding energy, the better the binding affinity of an inhibitor to a target protein (Oduselu *et al*., 2023). This suggests that several of the screened compounds may represent superior alternatives to GDM, in agreement with the utility of docking as a predictive tool widely applied in *in-silico* drug discovery (Onyango, 2023).

As for PfCSP, no docking conformation was found between the target protein and mAb L9. Possible factors for the unsuccessful docking between mAb L9 and PfCSP might be low binding affinity of the complex, essential bound-like conformations being away from the complementarity-determining region (CDR) loop conformations, and L9 antibody undergoing large conformational changes between its bound and unbound experimental structure (Fernández-Quintero *et al*., 2023). Regardless, three small-molecule hits (ZINC40144754, ZINC25374360, and ZINC71996727) showed strong affinities below −8.0 kcal/mol, a threshold generally considered indicative of biologically relevant binding. However, ZINC40144754 was excluded after structural analysis showed stability issues because of negative donor-donor interactions and a failure to connect to critical chain A. Their potential as PfCSP inhibitors is highlighted by the retention of ZINC25374360 and ZINC71996727 for MDS, which demonstrates how docking in conjunction with structural visualization may detect binding potential as well as possible stability problems.

5.3 Molecular Dynamics Simulation

Despite the positive results of the molecular docking, which validated our design rationale, additional MDS studies were carried out to confirm and validate the stability of PfHsp90-ligands and PfCSP-ligands complexes to achieve objective 2 of this current study. To identify, analyze, and provide insights for future lead optimization, eight molecular dynamic simulation tests were done. The stability of the ligand when complexed with the protein is shown by the ligands' RMSD analysis. In most cases, the ligand–protein interactions appeared stable across the 100ns simulation window. ZINC72163401, ZINC72358537, and ZINC72358557, with average RMSD value of 0.25nm suggested that their conformations remained well maintained throughout. This kind of low deviation is generally taken as evidence of strong, stable binding (Oduselu *et al*., 2023). In fact, Oduselu *et al*. (2023) argued that complexes with RMSD deviations under 3 Å remain structurally stable, while Alzain *et al*. (2022) also reported similar ranges in their MDS work. Our results fall well within these ranges, reinforcing the conclusion that these three compounds form robust complexes with PfHsp90.

However, not every ligand had the same performance. For example, ZINC09060002 and ZINC72133064 showed significant deviation, with RMSD values as high as 4 nm. Because of this instability, these molecules might not be able to maintain significant interactions in physiological settings, which would restrict their potential as leads. However, ZINC71996727 and ZINC25374360, which both bind PfCSP, were comparatively stable. During the first 10 ns, ZINC25374360 varied by around 1 nm, but it finally settled into a more stable conformation throughout the duration of the simulation. In contrast, ZINC71996727 stabilized earlier and displayed very few variations, indicating that it would form the more dependable PfCSP complex than ZINC25374360.

Further RMSF and hydrogen bonds analysis confirmed the stability of the complexes formed between ZINC25374360 and ZINC71996727 with PfCSP and ZINC72163401, ZINC72358557, and ZINC72358537 with PfHsp90. The fluctuations were within RMSF values of 0.2nm, which is acceptable when compared with the RMSF value of the reference ligand (GDM). There were no major fluctuations to indicate that the inhibitors' atoms shift from their average positions during the 100ns simulation. This finding is consistent with Oduselu *et al*.'s (2023) and Razzaghi-Asl *et al*.'s (2022) studies that ensured RMSF values of their protein-ligand complexes are within acceptable levels to infer their stability.

The hydrogen bond analyses demonstrated that the potential PfHsp90 and PfCSP inhibitors maintained stable conformation in their respective target proteins' active site during the 100ns simulation, suggesting their inhibitory potential and enhanced binding affinity. Hydrogen bond formation between a ligand and target protein is essential in complexes' stability because it increases the binding affinity between the two molecules (Oduselu *et al*., 2023). Compared to the reference ligand GDM, ZINC72163401, ZINC72358537, and ZINC72358557 formed more hydrogen bonds with PfHsp90, indicating stronger binding. The fact that ZINC72358557 was able to form up to six hydrogen bonds is noteworthy and may suggest that it has a strong inhibitory potential. As for PfCSP, ZINC25374360 and ZINC71996727 established up to three and five hydrogen bonds, respectively, indicating relatively tight binding. When combined, these findings suggest that these substances are superior to the reference inhibitors, at least in terms of structural stability.

Overall, the evidence from RMSD, RMSF, and hydrogen bond analyses creates a cohesive picture. While some candidates (ZINC09060002 and ZINC72133064) did not exhibit the necessary stability, others, specifically ZINC72163401, ZINC72358537, ZINC72358557 for PfHsp90, and

ZINC71996727 and ZINC25374360 for PfCSP, stood out as promising scaffolds for additional optimization.

5.4 *In-Vitro* Validation

Since we also intended to perform *in vitro* validation of the inhibitory potential and capability of the lead compounds, ascertaining their stability in complex with their target proteins was not enough. *In vitro* validation has become a popular approach following MDS in recent drug design and discovery processes, as seen in studies by Cheng *et al*. (2023), Kant *et al*. (2022), Onyango (2023), and Ornnork *et al*. (2020). Each of these studies used different assays, but their common objective was to confirm that computationally identified leads can indeed demonstrate biological activity, an objective that this current study shares.

The IC_{50} values of the inhibitors were in the range of 5 – 150 ng/mL. These values can be meaningfully compared with that of chloroquine to place the results into context. Chloroquine was used as a comparator in this study because of its well-established pharmacological characteristics such low toxicity, prolonged duration of action, quick onset, and high tolerance in humans (Zhou *et al*., 2020). Furthermore, it is still one of the most researched antimalarial (Zhou *et al*., 2020). It was used here as a standard by which the effectiveness of novel drugs might be evaluated, not to imply that it is currently clinically useful against resistant forms of malaria. Chloroquine is a simpler reference point due to the complicated pharmacodynamics of other modern treatments, such as artemisinin derivatives (Agarwal *et al*., 2017).

According to Agarwal *et al*. (2017), the highest concentration of chloroquine used for assessment of chemosensitivity against the 3D strain of *P. falciparum* is 50nM. Using the formula below, the IC_{50} value of chloroquine was converted to 25.793 ng/mL, which provides a benchmark for comparing the activity of the five lead compounds.

$$C_{nM} = \frac{C_{ng/mL}}{MW_{kDa}}$$

$$Where\ C_{nM} = concentration\ in\ nanomolar$$
$$C_{ng/mL} = concentration\ in\ nanograms\ per\ milliliter$$
$$MW_{kDa} = molecular\ weight\ in\ kilodaltons$$

ZINC72358537 had an IC_{50} of 25.60 ng/mL, which is strikingly close to that of chloroquine and therefore suggests strong inhibitory potential. ZINC72358557 (33.31 ng/mL) and ZINC72163401 (38.08 ng/mL) also showed promising activity, though at slightly higher concentrations than chloroquine. In contrast, ZINC71996727 recorded the lowest IC_{50} overall at 6.18 ng/mL, indicating a higher potency than chloroquine, whereas ZINC25374360 produced a much higher IC_{50} at 105.21 ng/mL, suggesting weaker inhibition.

These findings indicate that some inhibitors, including ZINC71996727, have strong activity at significantly lower concentrations than chloroquine, whereas others require larger amounts to be effective. This variance emphasizes how crucial it is to evaluate reliability by taking into account both the absolute IC_{50} values and their confidence ranges. In contrast to drugs like ZINC25374360, which have a very broad 95% CI and require more careful interpretation due to variability in their dose–response fits, compounds with narrow confidence intervals, like ZINC72358557 and ZINC72358537, offer stronger evidence of reproducible activity. Prior research has identified wide CIs in antimalarial assays as a weakness that can mask true potency, highlighting the necessity of repeat assays and structural improvement (Biagini *et al*., 2012; Motulsky, 2018).

The dual functional relevance of PfCSP inhibitors is one reason they might be regarded as possible adjuvants in this current study. PfCSP is the main surface protein on sporozoites and is essential for hepatocyte penetration in addition to preventing parasite activity (Kumar *et al*., 2021). Therefore, substances that target PfCSP may improve immune identification of sporozoites by changing antigen presentation in addition to decreasing parasite infectivity. In addition to

Mosquirix, which also targets PfCSP epitopes, this justifies the investigation of PfCSP inhibitors as adjuvants (Laurens, 2020). According to recent attempts to create adjuvants that both limit pathogen function and boost immunity, inhibitors may enhance the quality of the immune response elicited by the vaccine if they can stabilize PfCSP conformations or limit sporozoite invasion (Carter *et al*., 2023; Datoo *et al*., 2021).

Nevertheless, it is important to draw attention to these studies' limitations. The PfCSP inhibitors were not directly tested in conjunction with Mosquirix; therefore, any inferences on increased vaccine efficacy are still theoretical. Immuno-modulation tests and vaccine challenge models are necessary to demonstrate adjuvant action; however, these were outside the purview of this study.

CHAPTER SIX

CONCLUSIONS, RECOMMENDATIONS, AND SUGGETIONS FOR FURTHER RESEARCH

The current study performed virtual screening for small molecules by both molecular docking and pharmacophore analysis approaches after undertaking a thorough assessment of the evolutionary relationship among the different species of the parasite of the genus *Plasmodium*. The Hsp90 protein of the five *Plasmodium* species share a common evolutionary ancestor. Therefore, PfHsp90 could be used as the target protein template for mining novel anti-PfHsp90 compounds with pharmacological activity against *Plasmodium* malaria. However, CSP of the five *Plasmodium* species are not homologous; they do not share a common evolutionary ancestor. Thus, PfCSP was only used to characterize novel PfCSP inhibitors with pharmacological properties on Mosquirix because *P. falciparum* has the highest morbidity and fatality rates.

The first specific objective was to identify novel PfHsp90 and PfCSP inhibitors. The study successfully identified inhibitors with pharmacological activity against *Plasmodium* malaria and potential to enhance Mosquirix efficacy. The IC_{50} values of ZINC72163401, ZINC72358537, and ZINC72358557, three PfHsp90 inhibitors, were near or somewhat higher than those of chloroquine (25.793 ng/mL), suggesting promising inhibitory action. ZINC71996727 showed a very high inhibitory effect (6.18 ng/mL) for PfCSP, whereas ZINC25374360 showed less consistent and weaker inhibition. It is recommended that PfHsp90 inhibitors be given priority for additional optimization as potentially stand-alone antimalarial medications, while PfCSP inhibitors, particularly ZINC71996727, should be investigated further as potential adjuvants to increase the effectiveness of Mosquirix.

The second objective was to assess the stability of the protein-inhibitor complexes using MDS. Three PfHsp90 inhibitors (ZINC72163401, ZINC72358537, and ZINC72358557) formed stable complexes with PfHsp90, indicating their potential as promising therapeutic candidates. Both ZINC25374360 and ZINC71996727 were able to bind to PfCSP in a steady manner, which offers structural support for their possible involvement in regulating immunological responses linked to PfCSP. To improve binding affinity and selectivity, this stability data should be integrated with structural optimization initiatives. Additionally, *in vivo* models should be used to verify biological relevance.

The last objective was to perform *in vitro* validation of the inhibitors' inhibitory potential. The effectiveness of the three PfHsp90 inhibitors (ZINC72163401, ZINC72358537, and ZINC72358557) against *Plasmodium* malaria was validated by *in vitro* tests. Among the PfCSP inhibitors, ZINC71996727 exhibited high potency and ZINC25374360 moderate activity, indicating that PfCSP inhibitors may help boost vaccine-induced immune responses in addition to inhibiting parasites. Because PfCSP is Mosquirix's antigenic target, inhibitors that change its structure or impair its function may enhance immune activation and antigen recognition, which makes their potential as adjuvants more logical. To evaluate synergy, identify ideal formulation ratios, and confirm immunological results *in vivo*, further research should directly analyze PfCSP inhibitors in conjunction with Mosquirix.

Even though this study met its objectives, there are still a number of areas that could use further research. The function of PfCSP inhibitors as adjuvants is one of the primary areas of uncertainty. Although they showed inhibitory activity, they were not tested together with Mosquirix. Therefore, future research should investigate whether these substances actually boost vaccine efficacy by immune-modulatory effects, such as enhanced antigen presentation or more robust antibody

responses. The unpredictability shown in certain dose-response experiments is another drawback. For example, ZINC25374360's potency was less dependable due to its extremely wide confidence ranges. This suggests that in order to more thoroughly confirm its finding, further tests and better curve fitting are required.

Furthermore, structural optimization is an obvious next step. Although certain inhibitors showed efficacy that was comparable to or even better than chloroquine, such as ZINC71996727, further medicinal chemistry work is necessary to lower the effective doses needed and to increase stability and selectivity. Mechanistic research will also be helpful in elucidating how PfCSP inhibitors may alter immune recognition and enhance vaccine efficacy. Lastly, as *in vitro* tests and computer models are unable to accurately mimic pharmacokinetic behavior, bioavailability, or immunological reactions in physiological settings, *in vivo* validation is still crucial. By filling in these gaps, we may better support PfHsp90 inhibitors as possible antimalarial medication candidates and elucidate the potential of PfCSP inhibitors as adjuvants for vaccines.

REFERENCES

Agarwal, P., Anvikar, A. R., Pillai, C. R., & Srivastava, K. (2017). In vitro susceptibility of Indian Plasmodium falciparum isolates to different antimalarial drugs & antibiotics. *Indian Journal of Medical Research, 146*(5), 622–628. https://doi.org/10.4103/ijmr.IJMR_1688_15

Alzain, A. A., Ahmed, Z. A. M., Mahadi, M. A., & Elbadwi, F. A. (2022). Identification of novel *Plasmodium falciparum* dihydroorotate dehydrogenase inhibitors for malaria using in silico studies. *Scientific African, 16*, e01214. https://doi.org/10.1016/j.sciaf.2022.e01214

Araujo, J. S. C., de Souza, B. C., Costa Junior, D. B., Oliveira, L. D. M., Santana, I. B., Duarte, A. A., Do Monte-Neto, R. L., Taranto, A. G., & Leite, F. H. A. (2018). Identification of new promising *Plasmodium falciparum* superoxide dismutase allosteric inhibitors through hierarchical pharmacophore-based virtual screening and molecular dynamics. *Journal of Molecular Modeling, 24*(8), 219. https://doi.org/10.1007/s00894-018-3746-0

Arora, N., Anbalagan, L. C., & Pannu, A. K. (2021). Towards eradication of malaria: Is the WHO's RTS,S/AS01 vaccination effective enough? *Risk Management and Healthcare Policy, 14,* 1033–1039. https://doi.org/10.2147/RMHP.S219294

Atcheson, E., Hill, A. V., & Reyes-Sandoval, A. (2021). A VLP for validation of the *Plasmodium falciparum* circumsporozoite protein junctional epitope for vaccine development. *NPJ Vaccines, 6*(1), 1–9. https://doi.org/10.1038/s41541-021-00302-x

Aurrecoechea, C., Brestelli, J., Brunk, B. P., Fischer, S., Gajria, B., Gao, X., Gingle, A., Grant, G., Harb, O. S., Heiges, M., Innamorato, F., Iodice, J., Kissinger, J. C., Kraemer, E., Li, W., Miller, J. A., Nayak, V., Pennington, C., Pinney, D. F., Roos, D. S., Ross, C., Stoeckert, C. J., Treatman, C., & Wang, H. (2009). PlasmoDB: A functional genomic database for

malaria parasites. *Nucleic Acids Research, 37*(Database issue), D539–D543. https://doi.org/10.1093/nar/gkn814

Ayanful-Torgby, R., Quashie, N. B., Boampong, J. N., Williamson, K. C., & Amoah, L. E. (2018). Seasonal variations in *Plasmodium falciparum* parasite prevalence assessed by varying diagnostic tests in asymptomatic children in southern Ghana. *PLOS ONE, 13*(6), e0199172. https://doi.org/10.1371/journal.pone.0199172

Berman, H. M., Westbrook, J., Feng, Z., Gilliland, G., Bhat, T. N., Weissig, H., ... & Bourne, P. E. (2000). The Protein Data Bank. *Nucleic Acids Research*, 28(1), 235–242. https://doi.org/10.1093/nar/28.1.235

Biagini, G. A., Saliba, K. J., Sykes, M. L., McCarthy, J. S., Charman, S. A., & Avery, V. M. (2012). Repurposing approaches identify existing drugs as potential antimalarials. *Nature Communications*, 3, 1043. https://doi.org/10.1038/ncomms2043

BIOVIA, Dassault Systèmes. (2021). *Discovery Studio Modeling Environment*. San Diego: Dassault Systèmes.

Bonnefoy, S., Attal, G., Langsley, G., Tekaia, F., & Mercereau-Puijalon, O. (1994). Molecular characterization of the heat shock protein 90 gene of the human malaria parasite *Plasmodium falciparum*. *Molecular and Biochemical Parasitology, 67*(1), 157–170. https://doi.org/10.1016/0166-6851(94)90105-8

Bopp, B., Ciglia, E., Ould-Chaib, A., Groth, G., Gohlke, H., & Jose, J. (2016). Design and biological testing of peptidic dimerization inhibitors of human Hsp90 that target the C-terminal domain. *Biochimica et Biophysica Acta (BBA) – General Subjects, 1860*(6), 1043–1055. https://doi.org/10.1016/j.bbagen.2016.01.005

Bratt, N. (2024). Malaria vaccines: Advancements, challenges and the path to eradication. *Malaria Control and Elimination, 13,* 308. https://www.hilarispublisher.com/open-access/malaria-vaccines-advancements-challenges-and-the-path-to-eradication.pdf

Brogi, S., Ramalho, T. C., Kuca, K., Medina-Franco, J. L., & Valko, M. (2020). *In silico* methods for drug design and discovery. *Frontiers in Chemistry, 8,* 612. https://doi.org/10.3389/fchem.2020.00612

Calvo-Calle, J. M., Mitchell, R., Altszuler, R., Othoro, C., & Nardin, E. (2021). Identification of a neutralizing epitope within minor repeat region of *Plasmodium falciparum* CS protein. *NPJ Vaccines, 6*(1), 1–8. https://doi.org/10.1038/s41541-020-00272-6

Carter, D., Coler, R. N., Friede, M., Reed, S. G., & others. (2023). Adjuvant strategies for malaria vaccines: Lessons learned and future directions. *Vaccine*. https://doi.org/10.1016/j.vaccine.2023.05.012

Centers for Disease Control and Prevention. (2018, November 1). *Drug resistance in the malaria-endemic world*. U.S. Department of Health & Human Services. https://www.cdc.gov/malaria/malaria_worldwide/reduction/drug_resistance.html

Centers for Disease Control and Prevention. (2022, November 9). *About malaria*. U.S. Department of Health & Human Services. https://www.cdc.gov/malaria/about/faqs.html

Chakrabarti, A., Singh, V., & Singh, S. (2019). Management and control of antimalarial drug resistance. In S. M. Mandal & D. Paul (Eds.), *Bacterial adaptation to co-resistance* (pp. 297–322). Springer Singapore. https://doi.org/10.1007/978-981-13-8503-2_15

Cheng, Z., Bhave, M., Hwang, S. S., Rahman, T., & Chee, X. W. (2023). Identification of potential p38γ inhibitors via in silico screening, in vitro bioassay and molecular dynamics simulation

studies. *International Journal of Molecular Sciences, 24*(8), 7360. https://doi.org/10.3390/ijms24087360

Cheruiyot, A. C., Auschwitz, J. M., Lee, P. J., Yeda, R. A., Okello, C. O., Leed, S. E., Talwar, M., Murthy, T., Gaona, H. W., Hickman, M. R., Akala, H. M., Kamau, E., & Johnson, J. D. (2016). Assessment of the Worldwide Antimalarial Resistance Network standardized procedure for in vitro malaria drug sensitivity testing using SYBR green assay for field samples with various initial parasitemia levels. *Antimicrobial Agents and Chemotherapy, 60*(4), 2417–2424. https://doi.org/10.1128/AAC.00527-15

Chew, M., Ye, W., Omelianczyk, R. I., Pasaje, C. F., Hoo, R., Chen, Q., Ong, E. Z., Chan, C. X., Haase, A., Duffy, M. F., Mok, B. W., & Preiser, P. (2022). Selective expression of variant surface antigens enables *Plasmodium falciparum* to evade immune clearance *in vivo*. *Nature Communications, 13*(1), 4170. https://doi.org/10.1038/s41467-022-31741-2

Cockburn, I. A., & Seder, R. A. (2018). Malaria prevention: From immunological concepts to effective vaccines and protective antibodies. *Nature Immunology, 19*(11), 1199–1211. https://doi.org/10.1038/s41590-018-0228-6

Daina, A., Michielin, O., & Zoete, V. (2017). SwissADME: a free web tool to evaluate pharmacokinetics, drug-likeness and medicinal chemistry friendliness of small molecules. *Scientific Reports*, 7, 42717. https://doi.org/10.1038/srep42717

Dallakyan, S., & Olson, A. J. (2015). Small-molecule library screening by docking with PyRx. *Methods in Molecular Biology*, 1263, 243–250. https://doi.org/10.1007/978-1-4939-2269-7_19.

Darby, J. F., Vidler, L. R., Simpson, P. J., Al-Lazikani, B., Matthews, S. J., Sharp, S. Y., Aherne, W., & Workman, P. (2020). Solution structure of the Hop TPR2A domain and investigation

of target druggability by NMR, biochemical and *in silico* approaches. *Scientific Reports, 10*(1), 14101. https://doi.org/10.1038/s41598-020-71969-w

Datoo, M. S., Madhavan, M., Bellamy, D., Tinto, H., & the R21/Matrix-M Study Group. (2021). Efficacy of a low-dose candidate malaria vaccine, R21 in adjuvant Matrix-M, with seasonal administration to children in Burkina Faso: A randomised controlled trial. *The Lancet, 397*(10287), 1809–1818. https://doi.org/10.1016/S0140-6736(21)00943-0

Draper, S. J., Sack, B. K., King, C. R., Nielsen, C. M., Rayner, J. C., Higgins, M. K., Long, C. A., & Seder, R. A. (2018). Malaria vaccines: Recent advances and new horizons. *Cell Host & Microbe, 24*(1), 43–56. https://doi.org/10.1016/j.chom.2018.06.008

Duan, M., Bai, Y., Deng, S., Ruan, Y., Zeng, W., Li, X., Wang, M., Wang, Z., & Cui, L. (2022). Different in vitro drug susceptibility profile of *Plasmodium falciparum* isolates from two adjacent areas of northeast Myanmar and molecular markers for drug resistance. *Tropical Medicine and Infectious Disease, 7*(12), 442. https://doi.org/10.3390/tropicalmed7120442

Duay, S. S., Yap, R. C. Y., Gaitano III, A. L., Santos, J. A. A., & Macalino, S. J. Y. (2023). Roles of virtual screening and molecular dynamics simulations in discovering and understanding antimalarial drugs. *International Journal of Molecular Sciences, 24*(11), 9289. https://doi.org/10.3390/ijms24119289

Durrant, J. D., & McCammon, J. A. (2011). Molecular dynamics simulations and drug discovery. *BMC Biology, 9*(1), 71. https://doi.org/10.1186/1741-7007-9-71

Dutta, T., Singh, H., Edkins, A. L., & Blatch, G. L. (2022). Hsp90 and associated co-chaperones of the malaria parasite. *Biomolecules, 12*(8), 1018. https://doi.org/10.3390/biom12081018

Egan, W. J., Merz, K. M., & Baldwin, J. J. (2000). Prediction of drug absorption using multivariate statistics. *Journal of Medicinal Chemistry*, 43(21), 3867–3877. https://doi.org/10.1021/jm000292e

Fernández-Arias, C., Mashoof, S., Huang, J., & Tsuji, M. (2015). Circumsporozoite protein as a potential target for anti-malarials. *Expert Review of Anti-Infective Therapy, 13*(8), 923–926. https://doi.org/10.1586/14787210.2015.1058709

Fernández-Quintero, M. L., Martin, G. M., Lee, W., & Mantis, N. J. (2023). Structural basis of epitope selectivity and potent protection from malaria by PfCSP antibody L9. *Nature Communications, 14*(1), 2815. https://doi.org/10.1038/s41467-023-38509-2

Fontecha, G., Pinto, A., Escobar, D., Matamoros, G., & Ortiz, B. (2019). Genetic variability of *Plasmodium falciparum* histidine-rich proteins 2 and 3 in Central America. *Malaria Journal, 18*(1), 31. https://doi.org/10.1186/s12936-019-2668-3

Francica, J. R., Shi, W., Chuang, G.-Y., Chen, S. J., Da Silva Pereira, L., Farney, S. K., Flynn, B. J., Ou, L., Stephens, T., Tsybovsky, Y., Wang, L. T., Anderson, A., Beck, Z., Dillon, M., Idris, A. H., Hurlburt, N., Liu, T., Zhang, B., Alving, C. R., ... Seder, R. A. (2021). Design of alphavirus virus-like particles presenting circumsporozoite junctional epitopes that elicit protection against malaria. *Vaccines, 9*(3), 272. https://doi.org/10.3390/vaccines9030272

Gao, M., Kang, D., Liu, N., & Liu, Y. (2023). In silico discovery of small-molecule inhibitors targeting SARS-CoV-2 main protease. *Molecules, 28*(14), 5320. https://doi.org/10.3390/molecules28145320

Ghose, A. K., Viswanadhan, V. N., & Wendoloski, J. J. (1999). A knowledge-based approach in designing combinatorial or medicinal chemistry libraries for drug discovery. *Journal of Combinatorial Chemistry*, 1(1), 55–68. https://doi.org/10.1021/cc9800071

Gross, M. (2019). Fresh efforts needed against malaria. *Current Biology, 29*(9), R301–R303. https://doi.org/10.1016/j.cub.2019.04.041

Hall, T. A. (1999). BioEdit: A user-friendly biological sequence alignment editor and analysis program for Windows 95/98/NT. *Nucleic Acids Symposium Series*, 41, 95–98.

Han, J., Goldstein, L. A., Hou, W., Chatterjee, S., Burns, T. F., & Rabinowich, H. (2018). HSP90 inhibition targets autophagy and induces a CASP9-dependent resistance mechanism in NSCLC. *Autophagy, 14*(6), 958–971. https://doi.org/10.1080/15548627.2018.1434471

Hatherley, R., Clitheroe, C. L., Faya, N., & Bishop, Ö. T. (2015). *Plasmodium falciparum* Hop: Detailed analysis on complex formation with Hsp70 and Hsp90. *Biochemical and Biophysical Research Communications, 456*(1), 440–445. https://doi.org/10.1016/j.bbrc.2014.11.103

Honoré, F. A., Méjean, V., & Genest, O. (2017). Hsp90 is essential under heat stress in the bacterium *Shewanella oneidensis*. *Cell Reports, 19*(4), 680–687. https://doi.org/10.1016/j.celrep.2017.03.082

Hoter, A., El-Sabban, M. E., & Naim, H. Y. (2018). The HSP90 family: Structure, regulation, function, and implications in health and disease. *International Journal of Molecular Sciences, 19*(9), Article 2560. https://doi.org/10.3390/ijms19092560

Huck, J. D., Que, N. L., Immormino, R. M., Shrestha, L., Taldone, T., Chiosis, G., & Gewirth, D. T. (2019). NECA derivatives exploit the paralog-specific properties of the site 3 side pocket of Grp94, the endoplasmic reticulum Hsp90. *Journal of Biological Chemistry, 294*(44), 16010–16019. https://doi.org/10.1074/jbc.RA119.009960

Ibrahim, Z. Y. U., Uzairu, A., Shallangwa, G. A., Abechi, S. E., & Isyaku, S. (2022). Virtual screening and molecular dynamic simulations of the antimalarial derivatives of 2-anilino

4-amino substituted quinazolines docked against a Pf-DHODH protein target. *Egyptian Journal of Medical Human Genetics, 23*(1), 119. https://doi.org/10.1186/s43042-022-00329-2

Irwin, J. J., Tang, K. G., Young, J., Dandarchuluun, C., Wong, B. R., Khurelbaatar, M., Moroz, Y. S., Mayfield, J., & Sayle, R. A. (2020). ZINC20—A Free Ultralarge-Scale Chemical Database for Ligand Discovery. *Journal of Chemical Information and Modeling*, 60(12), 6065–6073. https://doi.org/10.1021/acs.jcim.0c00675

Islam, S. U., Shehzad, A., Sonn, J. K., & Lee, Y. S. (2017). PRPF overexpression induces drug resistance through actin cytoskeleton rearrangement and epithelial-mesenchymal transition. *Oncotarget, 8*(34), 56659–56671. https://doi.org/10.18632/oncotarget.17855

Julien, J. P., & Wardemann, H. (2019). Antibodies against *Plasmodium falciparum* malaria at the molecular level. *Nature Reviews Immunology, 19*(12), 761–775. https://doi.org/10.1038/s41577-019-0209-5

Jo, S., Kim, T., Iyer, V. G., & Im, W. (2008). CHARMM-GUI: A web-based graphical user interface for CHARMM. *Journal of Chemical Theory and Computation*, 4(2), 350–354. https://doi.org/10.1021/ct7003014

Kant, V., Kumar, P., Ranjan, R., Kumar, P., Mandal, D., & Vijayakumar, S. (2022). In silico screening, molecular dynamic simulations, and in vitro activity of selected natural compounds as an inhibitor of Leishmania donovani 3-mercaptopyruvate sulfurtransferase. *Parasitology Research, 121*(7), 2093–2109. https://doi.org/10.1007/s00436-022-07532-5

Khalid, K., Irum, S., Ullah, S. R., & Andleeb, S. (2022). *In silico* vaccine design based on a novel vaccine candidate against infections caused by *Acinetobacter baumannii*. *International*

Journal of Peptide Research and Therapeutics, 28(1), 1–17. https://doi.org/10.1007/s10989-021-10316-7

Kim, S., Chen, J., Cheng, T., Gindulyte, A., He, J., He, S., ... & Bolton, E. E. (2021). PubChem in 2021: New data content and improved web interfaces. *Nucleic Acids Research*, 49(D1), D1388–D1395. https://doi.org/10.1093/nar/gkaa971

Kisalu, N. K., Idris, A. H., Weidle, C., Flores-Garcia, Y., Flynn, B. J., Sack, B. K., Murphy, S., Schön, A., Freire, E., Francica, J. R., Miller, A. B., Gregory, J., March, S., Liao, H. X., Haynes, B. F., Wiehe, K., Trama, A. M., Saunders, K. O., Gladden, M. A., Monroe, A., ... Seder, R. A. (2018). A human monoclonal antibody prevents malaria infection by targeting a new site of vulnerability on the parasite. *Nature Medicine, 24*(4), 408–416. https://doi.org/10.1038/nm.4512

Koes, D. R., & Camacho, C. J. (2012). ZINCPharmer: pharmacophore search of the ZINC database. *Nucleic Acids Research*, 40(W1), W409–W414. https://doi.org/10.1093/nar/gks378

Koren, J., & Blagg, B. S. (2020). The right tool for the job: An overview of Hsp90 inhibitors. In *HSF1 and molecular chaperones in biology and cancer* (pp. 135–146). https://doi.org/10.1007/978-3-030-40204-4_9

Krysztofinska, E. M., Evans, N. J., Thapaliya, A., Murray, J. W., Morgan, R. M., Martinez-Lumbreras, S., & Isaacson, R. L. (2017). Structure and interactions of the TPR domain of Sgt2 with yeast chaperones and Ybr137wp. *Frontiers in Molecular Biosciences, 4,* 68. https://doi.org/10.3389/fmolb.2017.00068

Kumar, K., Sharma, P., Gupta, R., Singh, S., Kumar, S., Yadav, A., & Sharma, S. (2021). Plasmodium falciparum circumsporozoite protein: structure, function, and vaccine design. *Trends in Parasitology, 37*(6), 457–470. https://doi.org/10.1016/j.pt.2021.02.005

Kurup, S. P., Butler, N. S., & Harty, J. T. (2019). T cell-mediated immunity to malaria. *Nature Reviews Immunology*, 19(7), 457–471. https://doi.org/10.1038/s41577-019-0158-z

Langlois, A. C., Manzoni, G., Vincensini, L., Coppée, R., Marinach, C., Guérin, M., … Silvie, O. (2020). Molecular determinants of SR-B1-dependent *Plasmodium* sporozoite entry into hepatocytes. *Scientific Reports, 10*(1), 12117. https://doi.org/10.1038/s41598-020-70468-2

Laurens, M. B. (2020). RTS,S/AS01 vaccine (Mosquirix™): An overview. *Human Vaccines & Immunotherapeutics, 16*(3), 480–489. https://doi.org/10.1080/21645515.2019.1669415

Lee, W. C., Russell, B., & Rénia, L. (2019). Sticking for a cause: The falciparum malaria parasite's cytoadherence paradigm. *Frontiers in Immunology, 10,* 1444. https://doi.org/10.3389/fimmu.2019.01444

Li, L., Wang, L., You, Q. D., & Xu, X. L. (2020). Heat shock protein 90 inhibitors: An update on achievements, challenges, and future directions. *Journal of Medicinal Chemistry, 63*(5), 1798–1822. https://doi.org/10.1021/acs.jmedchem.9b00940

Lipinski, C. A., Lombardo, F., Dominy, B. W., & Feeney, P. J. (2001). Experimental and computational approaches to estimate solubility and permeability in drug discovery and development settings. *Advanced Drug Delivery Reviews*, 46(1–3), 3–26. https://doi.org/10.1016/S0169-409X(00)00129-0

Loubens, M., Vincensini, L., Fernandes, P., Briquet, S., Marinach, C., & Silvie, O. (2021). Plasmodium sporozoites on the move: Switching from cell traversal to productive invasion

of hepatocytes. *Molecular Microbiology, 115*(5), 870–881. https://doi.org/10.1111/mmi.14645

Mader, S. L., Lopez, A., Lawatscheck, J., Luo, Q., Rutz, D. A., Gamiz-Hernandez, A. P., Sattler, M., Buchner, J., & Kaila, V. R. I. (2020). Conformational dynamics modulate the catalytic activity of the molecular chaperone Hsp90. *Nature Communications, 11*(1), Article 1410. https://doi.org/10.1038/s41467-020-15050-0

Maiga, F. O., Wele, M., Toure, S. M., Keita, M., Tangara, C. O., Refeld, R. R., Thiero, O., Kayentao, K., Diakite, M., Dara, A., Li, J., Toure, M., Sagara, I., Djimdé, A., Mather, F. J., Doumbia, S. O., & Shaffer, J. G. (2021). Artemisinin-based combination therapy for uncomplicated *Plasmodium falciparum* malaria in Mali: A systematic review and meta-analysis. *Malaria Journal, 20*(1), 356. https://doi.org/10.1186/s12936-021-03890-0

Mak, O. W., Sharma, N., Reynisson, J., & Leung, I. K. M. (2021). Discovery of novel Hsp90 C-terminal domain inhibitors that disrupt co-chaperone binding. *Bioorganic & Medicinal Chemistry Letters, 38,* 127857. https://doi.org/10.1016/j.bmcl.2021.127857

Marques-da-Silva, C., Peissig, K., & Kurup, S. P. (2020). Pre-Erythrocytic Vaccines against Malaria. *Vaccines*, 8(3), 400. https://doi.org/10.3390/vaccines8030400

Martínez, L. (2015). Automatic identification of mobile and rigid substructures in molecular dynamics simulations and fractional structural fluctuation analysis. *PLOS ONE, 10*(3), e0119264. https://doi.org/10.1371/journal.pone.0119264

Mengist, H. M., Dilnessa, T., & Jin, T. (2021). Structural basis of potential inhibitors targeting SARS-CoV-2 main protease. *Frontiers in Chemistry, 9,* 622898. https://doi.org/10.3389/fchem.2021.622898

Meyer, K. J., Caton, E., & Shapiro, T. A. (2018). Model system identifies kinetic driver of Hsp90 inhibitor activity against African trypanosomes and *Plasmodium falciparum*. *Antimicrobial Agents and Chemotherapy, 62*(8), e00056-18. https://doi.org/10.1128/AAC.00056-18

Mishra, D., Shekhar, S., Chakraborty, S., & Chakraborty, N. (2018). Carboxylate clamp tetratricopeptide repeat (TPR) domain containing Hsp90 co-chaperones in Triticeae: An insight into structural and functional diversification. *Environmental and Experimental Botany, 155,* 31–44. https://doi.org/10.1016/j.envexpbot.2018.06.020

Motulsky, H. (2018). *Intuitive biostatistics* (4th ed.). Oxford University Press.

Muegge, I., Heald, S. L., & Brittelli, D. (2001). Simple selection criteria for drug-like chemical matter. *Journal of Medicinal Chemistry*, 44(12), 1841–1846. https://doi.org/10.1021/jm010125v

Murillo-Solano, C., Dong, C., Sanchez, C. G., & Pizarro, J. C. (2017). Identification and characterization of the antiplasmodial activity of Hsp90 inhibitors. *Malaria Journal, 16*, 292. https://doi.org/10.1186/s12936-017-1940-7

Nadeem, A. Y., Shehzad, A., Islam, S. U., Al-Suhaimi, E. A., & Lee, Y. S. (2022). Mosquirix™ RTS,S/AS01 vaccine development, immunogenicity, and efficacy. *Vaccines, 10*(5), 713. https://doi.org/10.3390/vaccines10050713

NCBI Resource Coordinators. (2023). Database resources of the National Center for Biotechnology Information. *Nucleic Acids Research*, 51(D1), D20–D26. https://doi.org/10.1093/nar/gkac118

Oduselu, G. O., Afolabi, R., Ademuwagun, I., Vaughan, A., & Adebiyi, E. (2022). Structure-based pharmacophore modeling, virtual screening, and molecular dynamics simulation studies

for identification of *Plasmodium falciparum* 5-aminolevulinate synthase inhibitors. *Frontiers in Medicine, 9*, 1022429. https://doi.org/10.3389/fmed.2022.1022429

Oladipo, H. J., Tajudeen, Y. A., Oladunjoye, I. O., Yusuff, S. I., Yusuf, R. O., Oluwaseyi, E. M., AbdulBasit, M. O., Adebisi, Y. A., & El-Sherbini, M. S. (2022). Increasing challenges of malaria control in sub-Saharan Africa: Priorities for public health research and policymakers. *Annals of Medicine and Surgery, 81*, 104366. https://doi.org/10.1016/j.amsu.2022.104366

Onyango, H., Odhiambo, P., Angwenyi, D., & Okoth, P. (2022). *In silico* identification of new anti-SARS-CoV-2 main protease (Mpro) molecules with pharmacokinetic properties from natural sources using molecular dynamics simulations and hierarchical virtual screening. *Journal of Tropical Medicine, 2022,* 3697498. https://doi.org/10.1155/2022/3697498

Onyango, O. H. (2023). *In silico* models for anti-COVID-19 drug discovery: A systematic review. *Advances in Pharmacological and Pharmaceutical Sciences, 2023,* 4562974. https://doi.org/10.1155/2023/4562974

Ornnork, N., Kiriwan, D., Lirdprapamongkol, K., Choowongkomon, K., Svasti, J., & Eurtivong, C. (2020). Molecular dynamics, MM/PBSA and in vitro validation of a novel quinazoline-based EGFR tyrosine kinase inhibitor identified using structure-based in silico screening. *Journal of Molecular Graphics and Modelling, 99*, 107639. https://doi.org/10.1016/j.jmgm.2020.107639

Oyen, D., Torres, J. L., Cottrell, C. A., Richter King, C., Wilson, I. A., & Ward, A. B. (2018). Cryo-EM structure of *P. falciparum* circumsporozoite protein with a vaccine-elicited antibody is stabilized by somatically mutated inter-Fab contacts. *Science Advances, 4*(10), eaau8529. https://doi.org/10.1126/sciadv.aau8529

Park, H. K., Yoon, N. G., Lee, J. E., Hu, S., Yoon, S., Kim, S. Y., Hong, J. H., Nam, D., Chae, Y. C., Park, J. B., & Kang, B. H. (2020). Unleashing the full potential of Hsp90 inhibitors as cancer therapeutics through simultaneous inactivation of Hsp90, Grp94, and TRAP1. *Experimental & Molecular Medicine, 52*(1), 79–91. https://doi.org/10.1038/s12276-019-0360-x

Patra, A. P., Pathak, V., Rameswara Reddy, S., Chhatre, A., Dmello, C., Narayan, S., Singh, D., Kumar, K. A., Ainavarapu, S. R. K., & Sharma, S. (2021). Surface expressed *Plasmodium* circumsporozoite protein (CSP) modulates cellular flexibility and motility. *BioRxiv*. https://doi.org/10.1101/2021.08.04.455043

Pousibet-Puerto, J., Salas-Coronas, J., Sánchez-Crespo, A., Molina-Arrebola, M. A., Soriano-Pérez, M. J., Giménez-López, M. J., Vázquez-Villegas, J., & Cabezas-Fernández, M. T. (2016). Impact of using artemisinin-based combination therapy (ACT) in the treatment of uncomplicated *Plasmodium falciparum* malaria in a non-endemic zone. *Malaria Journal, 15*(1), 339. https://doi.org/10.1186/s12936-016-1408-1

Posfai, D., Eubanks, A. L., Keim, A. I., Lu, K.-Y., Wang, G. Z., Hughes, P. F., Kato, N., Haystead, T. A., & Derbyshire, E. R. (2018). Identification of Hsp90 inhibitors with anti-Plasmodium activity. *Antimicrobial Agents and Chemotherapy, 62*(4), e01799-17. https://doi.org/10.1128/AAC.01799-17

Que, N. L., Crowley, V. M., Duerfeldt, A. S., Zhao, J., Kent, C. N., Blagg, B. S., & Gewirth, D. T. (2018). Structure based design of a Grp94-selective inhibitor: Exploiting a key residue in Grp94 to optimize paralog-selective binding. *Journal of Medicinal Chemistry, 61*(7), 2793–2805. https://doi.org/10.1021/acs.jmedchem.7b01608

Radli, M., & Rüdiger, S. G. D. (2018). Dancing with the diva: Hsp90–client interactions. *Journal of Molecular Biology, 430*(18), 3029–3040. https://doi.org/10.1016/j.jmb.2018.05.026

Ramos, S., Ademolue, T. W., Jentho, E., Wu, Q., Guerra, J., Martins, R., Pires, G., Weis, S., Carlos, A. R., Mahú, I., Seixas, E., Duarte, D., Rajas, F., Cardoso, S., Sousa, A. G. G., Lilue, J., Paixão, T., Mithieux, G., Nogueira, F., & Soares, M. P. (2021). A hypometabolic defense strategy against *Plasmodium* infection. *bioRxiv.* https://doi.org/10.1101/2021.09.08.459402

Rashid, S., Lee, B. L., Wajda, B., & Spyracopoulos, L. (2020). Nucleotide binding and active site gate dynamics for the Hsp90 chaperone ATPase domain from benchtop and high field 19F NMR spectroscopy. *The Journal of Physical Chemistry B, 124*(15), 2984–2993. https://doi.org/10.1021/acs.jpcb.0c00626

Razzaghi-Asl, N., Mirzayi, S., Mahnam, K., Adhami, V., & Sepehri, S. (2022). In silico screening and molecular dynamics simulations toward new human papillomavirus 16 type inhibitors. *Research in Pharmaceutical Sciences, 17*(2), 189–208. https://doi.org/10.4103/1735-5362.335177

Rodrigues-da-Silva, R. N., Martins da Silva, J. H., Singh, B., Jiang, J., Meyer, E. V. S., Santos, F., Banic, D. M., Moreno, A., Galinski, M. R., Oliveira-Ferreira, J., & Lima-Junior, J. D. C. (2016). In silico identification and validation of a linear and naturally immunogenic B-cell epitope of the Plasmodium vivax malaria vaccine candidate merozoite surface protein-9. *PLOS ONE, 11*(1), e0146951. https://doi.org/10.1371/journal.pone.0146951

Sá, M., Costa, D. M., & Tavares, J. (2022). Imaging infection by vector-borne protozoan parasites using whole-mouse bioluminescence. In S. M. Marques & F. F. Esteves da Silva (Eds.),

Bioluminescence: Methods and protocols (Vol. 1, pp. 353–366). Springer. https://doi.org/10.1007/978-1-0716-2453-1_29

Sachdeva, C., Wadhwa, A., Kumari, A., Hussain, F., Jha, P., & Kaushik, N. K. (2020). In silico potential of approved antimalarial drugs for repurposing against COVID-19. *Omics: A Journal of Integrative Biology, 24*(10), 568–580. https://doi.org/10.1089/omi.2020.0154

Sarfo, J. O., Amoadu, M., Kordorwu, P. Y., Adams, A. K., Gyan, T. B., Osman, A. G., Agordzo, S. A., Torto, M., Mbeve, G., & Ansah, E. W. (2023). Malaria amongst children under five in sub-Saharan Africa: A scoping review of prevalence, risk factors and preventive interventions. *European Journal of Medical Research, 28*(1), 80. https://doi.org/10.1186/s40001-023-01046-1

Schopf, F. H., Biebl, M. M., & Buchner, J. (2017). The HSP90 chaperone machinery. *Nature Reviews Molecular Cell Biology, 18*(6), 345–360. https://doi.org/10.1038/nrm.2017.20

Shehzad, A., Ravinayagam, V., AlRumaih, H., Aljafary, M., Almohazey, D., Almofty, S., Al-Rashid, N. A., & Al-Suhaimi, E. A. (2019). Application of three-dimensional (3D) tumor cell culture systems and mechanism of drug resistance. *Current Pharmaceutical Design, 25*(34), 3599–3607. https://doi.org/10.2174/1381612825666191014163923

Shiragannavar, S., & Madagi, S. (2021). *In silico* vaccine design tools. In S. K. Singh (Ed.), *Vaccine development*. IntechOpen. https://doi.org/10.5772/intechopen.100180

Silva, N. S. M. da, Torricillas, M. da S., Minari, K., Barbosa, L. R. S., Seraphim, T. V., & Borges, J. C. (2020). Solution structure of *Plasmodium falciparum* Hsp90 indicates a high flexible dimer. *Archives of Biochemistry and Biophysics, 690*, 108468. https://doi.org/10.1016/j.abb.2020.108468

Sinha, S., Sarma, P., Sehgal, R., & Medhi, B. (2017). Development in assay methods for in vitro antimalarial drug efficacy testing: A systematic review. *Frontiers in Pharmacology, 8,* 754. https://doi.org/10.3389/fphar.2017.00754

Spiegelberg, D., Abramenkovs, A., Mortensen, A. C. L., Lundsten, S., Nestor, M., & Stenerlöw, B. (2020). The HSP90 inhibitor Onalespib exerts synergistic anti-cancer effects when combined with radiotherapy: An *in vitro* and *in vivo* approach. *Scientific Reports, 10*(1), 5923. https://doi.org/10.1038/s41598-020-62293-4

Stofberg, M. L., Caillet, C., de Villiers, M., & Zininga, T. (2021). Inhibitors of the *Plasmodium falciparum* Hsp90 towards selective antimalarial drug design: The past, present and future. *Cells, 10*(11), 2849. https://doi.org/10.3390/cells10112849

Storti-Melo, L. M., Cassiano, G. C., de Souza Baptista, A. R., & Machado, R. L. D. (2022). Circumsporozoite protein from *Plasmodium vivax* and its relationship to human malaria. In *New advances in neglected tropical diseases* (Working title). IntechOpen. https://doi.org/10.5772/intechopen.102529

Swearingen, K. E., Lindner, S. E., Shi, L., Shears, M. J., Harupa, A., Hopp, C. S., Vaughan, A. M., Springer, T. A., Moritz, R. L., Kappe, S. H. I., & Sinnis, P. (2016). Interrogating the Plasmodium sporozoite surface: Identification of surface-exposed proteins and demonstration of glycosylation on CSP and TRAP by mass spectrometry-based proteomics. *PLoS Pathogens, 12*(4), e1005606. https://doi.org/10.1371/journal.ppat.1005606

Tahghighi, A., Mohamadi-Zarch, S. M., Rahimi, H., Marashiyan, M., Maleki-Ravasan, N., & Eslamifar, A. (2020). In silico and in vivo anti-malarial investigation on 1-(heteroaryl)-2-

((5-nitroheteroaryl)methylene) hydrazine derivatives. *Malaria Journal, 19*(1), 1–12. https://doi.org/10.1186/s12936-020-03467-0

Takashima, E., Tachibana, M., Morita, M., Nagaoka, H., Kanoi, B. N., & Tsuboi, T. (2021). Identification of novel malaria transmission-blocking vaccine candidates. *Frontiers in Cellular and Infection Microbiology, 11,* 1224. https://doi.org/10.3389/fcimb.2021.805482

Tamura, K., Stecher, G., & Kumar, S. (2021). MEGA11: Molecular Evolutionary Genetics Analysis version 11. *Molecular Biology and Evolution*, 38(7), 3022–3027. https://doi.org/10.1093/molbev/msab120

Tan, J., Sack, B. K., Oyen, D., Zenklusen, I., Piccoli, L., Barbieri, S., Foglierini, M., Silacci Fregni, C., Marcandalli, J., Jongo, S., Abdulla, S., Perez, L., & Corradin, G. (2018). A public antibody lineage that potently inhibits malaria infection through dual binding to the circumsporozoite protein. *Nature Medicine, 24*(4), 401–407. https://doi.org/10.1038/nm.4513

Tarique, M., Ahmad, M., Chauhan, M., & Tuteja, R. (2017). Genome wide in silico analysis of the mismatch repair components of *Plasmodium falciparum* and their comparison with human host. *Frontiers in Microbiology, 8*, 130. https://doi.org/10.3389/fmicb.2017.00130

The UniProt Consortium. (2023). UniProt: The universal protein knowledgebase in 2023. *Nucleic Acids Research*, 51(D1), D523–D531. https://doi.org/10.1093/nar/gkac105

Tintó-Font, E., Michel-Todó, L., Russell, T. J., Casas-Vila, N., Conway, D. J., Bozdech, Z., Llinás, M., & Cortés, A. (2021). A heat-shock response regulated by the PfAP2-HS transcription factor protects human malaria parasites from febrile temperatures. *Nature Microbiology, 6*(9), 1163–1174. https://doi.org/10.1038/s41564-021-00940-w

Traoré, K., Diakité, S. A., Bah, S., Konaté, D. S., Dabitao, D., Sanogo, I., Sangaré, M., Dama, S., Keita, B., Doumbouya, M., Guindo, M. A., Doumbia, S., & Diakité, M. (2019). Susceptibility of *Plasmodium falciparum* isolates to antimalarial drugs in a highly seasonal malaria endemic village in Mali. *Research Square*. https://doi.org/10.21203/rs.2.17605/v1

Trott, O., & Olson, A. J. (2010). AutoDock Vina: Improving the speed and accuracy of docking with a new scoring function, efficient optimization, and multithreading. *Journal of Computational Chemistry*, 31(2), 455–461. https://doi.org/10.1002/jcc.21334

Uwimana, A., Legrand, E., Stokes, B. H., Ndikumana, J. M., Warsame, M., Umulisa, N., Ngamije, D., Munyaneza, T., Mazarati, J., Munguti, K., & Fidock, D. A. (2020). Emergence and clonal expansion of in vitro artemisinin-resistant *Plasmodium falciparum* kelch13 R561H mutant parasites in Rwanda. *Nature Medicine, 26,* 1602–1608. https://doi.org/10.1038/s41591-020-1005-2

Valéa, I., Adjei, S., Usuf, E., Traore, O., Ansong, D., Tinto, H., Owusu Boateng, H., Some, A. M., Buabeng, P., Vekemans, J., Kotey, A., Vandoolaeghe, P., Cullinane, M., Traskine, M., Ouedraogo, F., Sambian, D., Lievens, M., Tahita, M. C., Jongert, E., … Agbenyega, T. (2020). Long-term immunogenicity and immune memory response to the hepatitis B antigen in the RTS,S/AS01E malaria vaccine in African children: A randomized trial. *Human Vaccines & Immunotherapeutics, 16*(6), 1464–1470. https://doi.org/10.1080/21645515.2019.1695457

Van Der Spoel, D., Lindahl, E., Hess, B., Groenhof, G., Mark, A. E., & Berendsen, H. J. C. (2005). GROMACS: Fast, flexible, and free. *Journal of Computational Chemistry*, 26(16), 1701–1718. https://doi.org/10.1002/jcc.20291

Veber, D. F., Johnson, S. R., Cheng, H. Y., Smith, B. R., Ward, K. W., & Kopple, K. D. (2002). Molecular properties that influence the oral bioavailability of drug candidates. *Journal of Medicinal Chemistry*, 45(12), 2615–2623. https://doi.org/10.1021/jm020017n

Wang, L. T., Hurlburt, N. K., Schön, A., Flynn, B. J., Flores-Garcia, Y., Pereira, L. S., Kiyuka, P. K., Dillon, M., Bonilla, B., Zavala, F., Idris, A. H., Francica, J. R., Pancera, M., & Seder, R. A. (2022). The light chain of the L9 antibody is critical for binding circumsporozoite protein minor repeats and preventing malaria. *Cell Reports, 38*(7), Article 110367. https://doi.org/10.1016/j.celrep.2022.110367

Wang, L. T., Pereira, L. S., Flores-Garcia, Y., O'Connor, J., Flynn, B. J., Schön, A., Yap, C., Yang, A. S. P., Ward, A. B., Gaudinski, M. R., Darko, S., Tan, J., Shi, W., Tani, K., Andrews, S., Wei, H., McDermott, A. B., Nason, M. C., Zhang, B., … Seder, R. A. (2020). A potent anti-malarial human monoclonal antibody targets circumsporozoite protein minor repeats and neutralizes sporozoites in the liver. *Immunity, 53*(4), 733–744.e8. https://doi.org/10.1016/j.immuni.2020.08.014

Wang, T., Mäser, P., & Picard, D. (2016). Inhibition of *Plasmodium falciparum* Hsp90 contributes to the anti-malarial activities of aminoalcohol-carbazoles. *Journal of Medicinal Chemistry, 59*(13), 6344–6352. https://doi.org/10.1021/acs.jmedchem.6b00591

Wankhede, Y. S., Khairnar, V. V., Patil, A. R., & Darekar, A. B. (2024). Drug discovery tools and in silico techniques: A review. *International Journal of Pharmaceutical Sciences Review and Research, 84*(7), 63–72. https://doi.org/10.47583/ijpsrr.2024.v84i07.009

Whitesell, L., Robbins, N., Huang, D. S., McLellan, C. A., Shekhar-Guturja, T., LeBlanc, E. V., & Cowen, L. E. (2019). Structural basis for species-selective targeting of Hsp90 in a

pathogenic fungus. *Nature Communications, 10*(1), 1–17. https://doi.org/10.1038/s41467-018-08248-w

World Health Organization. (2022, March 30). *Malaria*. https://www.who.int/news-room/fact-sheets/detail/malaria

WWARN In Vitro Module. (2011). *P. falciparum drug sensitivity assay using SYBR® Green I (Procedure INV02)*. Worldwide Antimalarial Resistance Network. Retrieved from WWARN official SOP document.

Yuno, A., Lee, M.-J., Lee, S., Tomita, Y., Rekhtman, D., Moore, B., & Trepel, J. B. (2018). Clinical evaluation and biomarker profiling of Hsp90 inhibitors. In *Chaperones: Methods and Protocols* (pp. 423–441). Springer. https://doi.org/10.1007/978-1-4939-7477-1_29

Zhang, F. Z., Ho, D. H. H., & Wong, R. H. F. (2018). Triptolide, a HSP90 middle domain inhibitor, induces apoptosis in triple manner. *Oncotarget, 9*(32), 22301–22315. https://doi.org/10.18632/oncotarget.24737

Zhou, W., Wang, H., Yang, Y., Chen, Z. S., Zou, C., & Zhang, J. (2020). Chloroquine against malaria, cancers and viral diseases. *Drug Discovery Today, 25*(11), 2012–2022. https://doi.org/10.1016/j.drudis.2020.09.010

Zininga, T., & Shonhai, A. (2019). Small molecule inhibitors targeting the heat shock protein system of human obligate protozoan parasites. *International Journal of Molecular Sciences, 20*(23), 5930. https://doi.org/10.3390/ijms20235930

Zininga, T., Makumire, S., Gitau, G. W., Njunge, J. M., Pooe, O. J., Klimek, H., Ramatsui, L., Prinsloo, E., Hawanawa, G., Dirr, H. W., & Shonhai, A. (2015). *Plasmodium falciparum* Hop (PfHop) interacts with the Hsp70 chaperone in a nucleotide-dependent fashion and

exhibits ligand selectivity. *PLOS ONE, 10*(8), e0135326. https://doi.org/10.1371/journal.pone.0135326

APPENDICES

Appendix 1: WWARN INV02 Procedure

Procedure

1. **Aseptic procedures**

    - All procedures (except centrifugation) are performed in a level II biosafety cabinet.
    - The Biosafety cabinet surface is wiped down with aseptic solution at the beginning and the end of every day.
    - Close the valves on gas cylinders at the end of each day.
    - The incubator and the storage surfaces are cleaned at least every 3 months.

2. **Preparation of lysis buffer (1 L)**

    - Dissolve 15.76 g Tris-HCl completely in about 700 mL cell culture water using a magnetic stirrer.
    - Adjust pH to 7.5 using concentrated hydrochloric acid.
    - Add 20 mL 0.5 M EDTA to give a final concentration of 10mM (2% w/v).
    - Add 160 mg saponin (0.016 % w/v final).
    - Add 16.0 mL Triton X-100 (1.6 % v/v final).
    - Add cell culture water to bring the final volume to 1 Litre.
    - Mix the solution thoroughly, avoiding the creation of bubbles.
    - Vacuum filter the solution using 0.2µ pore to remove any particulate matter and store indefinitely at RT.

3. **SYBR Green I stock solution**

    - Thaw 10000x SYBR Green I concentrate (invitrogen) at RT in laminar flow hood in a darkened room.
    - Aliquot 30 µL into amber-colored Eppendorf tubes, label with the day's date and store at -20oC for up to 6 months.

4. **Lysis buffer containing SYBR Green I (15 mL)**

    - This solution should be made fresh in a darkened room.
    - Thaw one 30 µL aliquot of SYBR Green I (Section 6.5).
    - Add 30 µL SYBR Green I to 15 mL lysis buffer (20x final SYBR Green concentration). 15 mL lysis buffer is adequate for one 96 plate.
    - Pipette to mix, avoiding the creation of bubbles.

5. **Preparation of malaria cultures and sensitivity assay**

- Determine % parasitaemia of malarial culture.
- For fresh field isolates ≤ 0.3%, run the assay at 2% hematocrit in complete medium (preparation of medium is described in WWARN procedure INV02) without reducing the parasitaemia.
- If parasitaemia of culture-adapted samples or fresh field isolates are > 0.3, dilute to 0.3% or 0.15% parasitaemia using complete culture medium for 72 or 96hr incubations respectively at 2% hematocrit in complete medium. A 72h assay is adequate for most drugs; 96h incubation can be used for slow acting drugs like antibiotics.
- Fresh field isolate are not washed prior to the assay.
- Using automated liquid handler or manually, add 100 µL malaria-infected erythrocytes to each well on a pre-dosed drug plate (for preparation see WWARN procedure INV03).
- Incubate cultures for 72hrs or 96hrs at 37oC in a humidified chamber, under a gas mixture of 90% N2, 5% O2, and 5% CO2, or in a candle jar.
- After the 72hr or 96 hr incubation, add 100 µL lysis buffer containing 20x SYBR Green I (see section 6.6) to each well, in a dark room.
- Incubate the plates at RT in the dark for 24 hrs.
- Read fluorescence on a fluorescence plate reader with excitation and emission wavelength bands centered at 485 and 530 nm, respectively.
- Determine the IC50 using an appropriate analysis programme.

Appendix 2: Hsp90 Sequences of the Five *Plasmodium* Species and the Five Outgroups

P. falciparum Hsp90

>tr|Q8IC05|Q8IC05_PLAF7 Heat shock protein 90 OS=*Plasmodium falciparum* (isolate 3D7) OX=36329 GN=PF3D7_0708400 PE=1 SV=1
MSTETFAFNADIRQLMSLIINTFYSNKEIFLRELISNASDALDKIRYESITDTQKLSAEPEFFIRIIPDKTNNTLTIEDSGIGMT
KNDLINNLGTIARSGTKAFMEAIQASGDISMIGQFGVGFYSAYLVADHVVVISKNNDDEQYVWESAAGGSFTVTKDET
NEKLGRGTKIILHLKEDQLEYLEEKRIKDLVKKHSEFISFPIKLYCERQNEKEITASEEEEGEGEGEREGEEEEEKKKKTGE
DKNADESKEENEDEEKKEDNEEDDNKTDHPKVEDVTEELENAEKKKKEKRKKKIHTVEHEWEELNKQKPLWMRKPE
EVTNEEYASFYKSLTNDWEDHLAVKHFSVEGQLEFKALLFIPKRAPFDMFENRKKRNNIKLYVRRVFIMDDCEEIIPEW
LNFVKGVVDSEDLPLNISRESLQQNKILKVIKKNLIKKCLDMFSELAENKENYKKFYEQFSKNLKLGIHEDNANRTKITE
LLRFQTSKSGDEMIGLKEYVDRMKENQKDIYYITGESINAVSNSPFLEALTKKGFEVIYMVDPIDEYAVQQLKDFDGKK
LKCCTKEGLDIDDSEEAKKDFETLKAEYEGLCKVIKDVLHEKVEKVVVGQRITDSPCVLVTSEFGWSANMERIMKAQA
LRDNSMTSYMLSKKIMEINARHPIISALKQKADADKSDKTVKDLIWLLFDTSLLTSGFALEEPTTFSKRIHRMIKLGLSID
EEENNDIDLPPLEETVDATDSKMEEVD

P. knowlesi Hsp90

>XP_038969368.1 heat shock protein 90, putative [*Plasmodium knowlesi* strain H]
MSKETFAFNADIRQLMSLIINTFYSNKEIFLRELISNASDALDKIRYESITDTQKLSAEPEFYIRIIPDK
TNNTLTIEDSGIGMTKNDLINNLGTIARSGTKAFMEAIQASGDISMIGQFGVGFYSAYLVADHVVVVSKN
NDDEQYVWESAAGGSFTVTKDESNEKIGRGTKIILHLKDDQLEYLEEKRIKDLVKKHSEFISFPIKLYCE
RQNEKEITASEDEAEEEDADGEKKKEGKDELEEGEDADKEKKEDNEEEEDKEKGDDHPKVEDVTEELENA
EKKKKKEKRKKKIHTVEHEWEELNKQKPLWMRKPEEVTNEEYASFYKSLTNDWEDHLAVKHFSVEGQLEF
KALLFIPKRAPFDMFENRKKRNNIKLYVRRVFIMDDCEEIIPEWLNFVKGVVDSEDLPLNISRESLQQNK
ILKVIKKNLIKKCLDMFSELAENKDNYKKFYEQFSKNLKLGIHEDNANRAKITELLRFQTSKSGDEMIGL
KEYVDRMKENQKDIYYITGESINAVSNSPFLEALTKKGFEVIYMVDPIDEYAVQQLKDFEGKKLKCCTKE
GLDIDDSEEAKKTFETMKAEYEGLCKVIKDVLHEKVEKVVVGQRITDSPCVLVTSEFGWSANMERIMKAQ
ALRDNSMTSYMLSKKIMEINARHPIITALKQKADADKSDKTVKDLIWLLFDTSLLTSGFALEEPTTFSKR
IHRMIKLGLSIDEDENNDIELPPLEETIDATDSKMEEVD

P. ovale Hsp90

>SBT30398.1 heat shock protein 90, putative [*Plasmodium ovale* wallikeri]
MSKETFAFNADIRQLMSLIINTFYSNKEIFLRELISNASDALDKIRYEAITDTEKLSAEPEFFIRIIPDK
TNNTLTIEDSGIGMTKNDLINNLGTIARSGTKAFMEAMQASGDISMIGQFGVGFYSAYLVADHVVVISKN
NDDEQYVWESAAGGSFTVTKDETNEKMGRGTKIILHLKEDQLEYLEEKRIKDLVKKHSEFISFPIKLYCE
RQNEKEITASEDEDDEEGKKKKDDVDEEKGEEKEDGEENKEKKEDNEEEKGDHPKVEDVTEELENVEKKK
KDKKKKKIHTVEHEWEELNKQKPLWMRKPEEVTNEEYASFYKSLTNDWEDHLAVKHFSVEGQLEFKALLF
IPKRAPFDMFENRKKRNNIKLYVRRVFIMDDCEEIIPEWLNFVKGVVDSEDLPLNISRESLQQNKILKVI
KKNLIKKCLDMFSELAENKDNYKKFYEQFSKNLKLGIHEDNANRAKITELLRFQTSKSGDEMIGLKEYVD
RMKENQKDIYYITGESINAVSNSPFLEALTKKGFEVIYMVDPIDEYAVQQLKDFDGKKLKCCTKEGLDID
DSEEAKKNFETLKAEYEGLCKVIKDVLHEKVEKVVVGQRITDSPCVLVTSEFGWSANMERIMKAQALRDN
SMTSYMLSKKIMEINARHPIISALKQKADADKSDKTVKDLIWLLFDTSLLTSGFALEEPTTFSKRIHRMI
KLGLSIDEEENNDIELPPLEETIEGADSKMEEVD

P. malariae Hsp90

>XP_028859990.1 heat shock protein 90, putative [*Plasmodium malariae*]
MSKETFAFNADIRQLMSLIINTFYSNKEIFLRELISNASDALDKIRYEAITDTQKLSAEPEFFIRIIPDK
TNNTLTIEDSGIGMTKNDLINNLGTIARSGTKAFMEAIQASGDISMIGQFGVGFYSAYLVADHVVVISKN
NDDEQYVWESAAGGSFTVTKDETNEKIGRGTKIILHLKEDQLEYLEEKRIKDLVKKHSEFISFPIKLYCE
RQNEKEITASEEEEEEGEREGEGEQDTDKKKGENEEDKDEEVEDGDEEGDKEKKEDNEEDKVDHPKVEDV
TEELEKVEKKKKKKIHTVEHEWEELNKQKPLWMRKPEEVTNEEYASFYKSLTNDWEDHLAVKHFSVEGQL
EFKALLFIPKRAPFDMFENRKKRNNIKLYVRRVFIMDDCEEIIPEWLNFVKGVVDSEDLPLNISRESLQQ
NKILKVIKKNLIKKCLDMFSELAENKDNYKKFYEQFSKNLKLGIHEDNANRAKITELLRFQTSKSGDEMI
GLKEYVDRMKENQKDIYYITGESINAVSNSPFLEALTKKGFEVIYMVDPIDEYAVQQLKDFDGKKLKCCT

KEGLDIDDSEEAKKNFETLKAEYEGLCKVIKDVLHEKVEKVVVGQRITDSPCVLVTSEFGWSANMERIMK
AQALRDNSMTSYMLSKKIMEINARHPIITALKHKADADKSDKTVKDLIWLLFDTSLLTSGFALEEPTTFS
KRIHRMIKLGLSIDEEDNNDIELPPLEETVEGTDSKMEEVD

P. vivax Hsp90

>SCO64938.1 heat shock protein 90, putative [*Plasmodium vivax*]
MSKETFAFNADIRQLMSLIINTFYSNKEIFLRELISNASDALDKIRYEAITDTQKLSAEPEFFIRIIPDK
TNNTLTIEDSGIGMTKNDLINNLGTIARSGTKAFMEAIQASGDISMIGQFGVGFYSAYLVADHVVVVSKN
NDDEQYVWESAAGGSFTVTKDETNEKMGRGTKIILHLKDDQLEYLEEKRIKDLVKKHSEFISFPIKLYCE
RQNEKEITASEDEAEEEDAEGEKKKKEGKDQLDDGDKQAQEGEGADNKEKKEHNEEDEDKDKGEDHPKVE
DVTEELENAEKKKKKEKKKKKIHTVEHEWEELNKQKPLWMRKPEEVTNEEYASFYKSLTNDWEDHLAVKH
FSVEGQLEFKALLFIPKRAPFDMFENRKKRNNIKLYVRRVFIMDDCEEIIPEWLNFVKGVVDSEDLPLNI
SRESLQQNKILKVIKKNLIKKCLDMFSELAENKDNYKKFYEQFSKNLKLGIHEDNANRAKITELLRFQTS
KSGDEMIGLKEYVDRMKENQKDIYYITGESINAVSNSPFLEALTKKGFEVIYMVDPIDEYAVQQLKDFEG
KKLKCCTKEGLDIDDSEEAKKTFETMKAEYEGLCKVIKDVLHEKVEKVVVGQRITDSPCVLVTSEFGWSA
NMERIMKAQALRDNSMTSYMLSKKIMEINARHPIITALKQKADADKSDKTVKDLIWLLFDTSLLTSGFAL
EEPTTFSKRIHRMIKLGLSIDEEENNDIELPPLEETIDATDSKMEEVD

H. sapiens Hsp90

>NP_005339.3 heat shock protein HSP 90-alpha isoform 2 [Homo sapiens]
MPEETQTQDQPMEEEEVETFAFQAEIAQLMSLIINTFYSNKEIFLRELISNSSDALDKIRYESLTDPSKL
DSGKELHINLIPNKQDRTLTIVDTGIGMTKADLINNLGTIAKSGTKAFMEALQAGADISMIGQFGVGFYS
AYLVAEKVTVITKHNDDEQYAWESSAGGSFTVRTDTGEPMGRGTKVILHLKEDQTEYLEERRIKEIVKKH
SQFIGYPITLFVEKERDKEVSDDEAEEKEDKEEEKEKEEKESEDKPEIEDVGSDEEEEKKDGDKKKKKKI
KEKYIDQEELNKTKPIWTRNPDDITNEEYGEFYKSLTNDWEDHLAVKHFSVEGQLEFRALLFVPRRAPFD
LFENRKKKNNIKLYVRRVFIMDNCEELIPEYLNFIRGVVDSEDLPLNISREMLQQSKILKVIRKNLVKKC
LELFTELAEDKENYKKFYEQFSKNIKLGIHEDSQNRKKLSELLRYYTSASGDEMVSLKDYCTRMKENQKH
IYYITGETKDQVANSAFVERLRKHGLEVIYMIEPIDEYCVQQLKEFEGKTLVSVTKEGLELPEDEEEKKK
QEEKKTKFENLCKIMKDILEKKVEKVVVSNRLVTSPCCIVTSTYGWTANMERIMKAQALRDNSTMGYMAA
KKHLEINPDHSIIETLRQKAEADKNDKSVKDLVILLYETALLSSGFSLEDPQTHANRIYRMIKLGLGIDE
DDPTADDTSAAVTEEMPPLEGDDDTSRMEEVD

T. gondii Hsp90

>XP_002368278.1 heat shock protein HSP90 [Toxoplasma gondii ME49]
MADTETFAFNADIQQLMSLIINTFYSNKEIFLRELISNASDALDKIRYEAITDPEKLKGAERLFIRIVPN
KQNNTLTIEDDGIGMTKAELVNNLGTIARSGTKAFMEALQAGGDISMIGQFGVGFYSAYLVADKVTVVSR
HNDDEMYVWESSAGGSFTVSKAEGQFENIVRGTRIILHMKEDQTEYLEDRRLKDLVKKHSEFISFPIELA
VEKSVDKEITESEDEEKPAEDAEEKKEEGEEEKKEEGAEKKKKTKKVKEVVVEYEQLNKQKPLWMRKPED
VTWEEYCAFYKSLTNDWEDPLAVKHFSVEGQLEFKALLFLPKRAPFDLFETRKKRNNVRLYVRRVFIMDD
CEDLIPEWLNFVRGVVDSEDLPLNISRESLQQNKILKVIKKNLVKKCLEMFQELEEKKEDYTKFYEQFSK
NLKLGIHEDTSNRNKIAELLRFHTSKSGDDVVSLKEYVDRMKESQKDIYYITGESRQSVASSPFLEALRK
KGYEVIYMTDPIDEYAVQQLKEFDGKKLRCCTKKGLELEDDEEEKKKFEELKAEFEPLCKLMKEVLHDKV
EQVVVSNRITDSPCVLVTSEYGWSANMERIMKAQALRDNSMTTYMVSKKTMEINPTNPIMEELKKKSNAD
KSDKTVKDLIWLLFDTALLTSGFSLDEPTQFAARIHRMIKLGLSIDEDDEELRAEEDLPPLEEVEGAVEE
TSKMEEVD

C. parvum Hsp90

>XP_626924.1 Hsp90, partial [Cryptosporidium parvum Iowa II]
RFFISIKQITIKMVETFAFNADIQQLMSLIINTFYSNKEIFLRELISNASDALDKIRYESLTDPEQLKSN
EEMHIRIIPDKVNNTLTIEDSGIGMTKNELINNLGTIARSGTKAFMEAIQAGGDVSMIGQFGVGFYSAYL
VADKVTVITKHNGDEQYIWESSAGGSFTITNDTSDNKLQRGTRIILHLKEDQLDYLEERTLRDLVKKHSE
FISFPIELSVEKTTEKEITDSDVDEEEEKKEGEDGEDAPKIEEVKEKEPKKKKITEVTQSWDLLNKNKPI
WMRKPEEVTFEEYSSFYKSISNDWEDPLAVKHFSVEGQLEFKAILFIPRRAPFDLFETRKKRNNIKLYVR
RVFIMDDCEELIPEFLGFVRGVVDSEDLPLNISRESLQQNKILKVIKKNIVKKCLELITEITEKPDDYKK
FYEQFSKNLKLGIHEDTTNRNKISELLRYQTSKSGEELISLREYVDRMKENQKEIYYITGESIQAVQNSP

FLEKLRKLDYEVIYMVDPIDEYCVQQMKEFDGKKLRCCTKEGLTLEETAEEKEAFEALQKEYEPLCQLIK
EVLHDKVDKVITSQRISDSPCVLVTSEFGWSANMERIMKAQALRDTSMTSYMMSKKTMEINPYNSIITEL
KTKIANDKSDKTVKDLIWLLYDTSLLTSGFSLEDPTQFSSRINRMIKLGLSIDEEDIVDDLPPLEPVNDA
ELQASKMEEVD

B. bovis Hsp90

>XP_001611554.1 putative Heat shock protein 90-3 [Babesia bovis T2Bo]
MATAQQETYAFNADISQLLSLIINAFYSNKEIFLRELISNASDALEKIRYEAIKDPKQVEDFPEYQISLS
ADKTNKTLTIEDTGIGMTKTDLINNLGTIAKSGTKAFMEAIQAGADMSMIGQFGVGFYSAYLVADKVTVV
SKNNNDDQYVWESNASGHFTVTKDESEDQLKRGTRLILHLKDDQSEYLEERRLKELVKKHSEFISFPIRL
SVEKTTETEVTDDEAEPTEAESKPEEKITDVTEEEEEKEKEAEKDGEEKTEKKKRKVTNVTREWEMLNKQ
KPIWMRLPTEVTNEEYASFYKNLSNDWEDHLAVKHFSVEGQLEFKAILFVPKRAPFDMFENRKKKNNIKL
YVRRVFIMDDCDELIPEWLGFVKGVVDSEDLPLNISREVLQQNKILKVIRKNLVKKCLELFSELTEKKED
FKKFYEQFSKNLKLGIHEDNTNRNKISELLRYETSKSGDEAISLKEYVDRMKPEQKYIYYITGESKQSVA
NSPFLECLRSRGIEVIYMTDPIDEYAVQQIKEFEGKKLKCCTKENLELEDTEEERKNFETLEKEMEPLCR
LIKEILHDKVEKVVCGKRFTESPCALVTSEFGWSANMERIMKAQALRDSSFGSFMISKKTMELNPHHSIM
KELRQRAETDKSDKTLKDLVWLLYDTAMLTSGFNLDDPTQFGGRIYRMIKLGLSLDDEPTGEDVDLPPLD
EVVVDPKMEEVD

T. annulate Hsp90

>XP_952473.1 heat shock protein 90, putative [Theileria annulata]
MASKEETPDQEVYAFNADISQLLSLIINAFYSNKEIFLRELISNASDALEKIRYEAIKDPKQIEDQPDYY
IRLYADKNNNTLTIEDSGIGMTKADLVNNLGTIAKSGTRAFMEALQAGSDMSMIGQFGVGFYSAYLVADK
VTVVSKNNADDQYVWESSASGHFTVKRDDSHEPLKRGTRLILHLKEDQTEYLEERRLKELVKKHSEFISF
PISLSVEKTQETEVTDDEAEPEEEKKLEEEDKDKEEKVEDVTDEKVTDVTEEEEKKEEKKKKKRKVTNVT
REWEMLNKQKPIWMRLPTEVTNEEYASFYKNLTNDWEDHLAVKHFSVEGQLEFKALLFVPRRAPFDMFES
RKKKNNIKLYVRRVFIMDDCEELIPEWLSFVKGVVDSEDLPLNISRETLQQNKILKVIRKNLVKKCLELF
NELTEKKEDFKKFYEQFSKNLKLGIHEDNANRSKIAELLRFETTKSGDELVSLKEYVDRMKSDQKFVYYI
TGESKQSVASSPFLETLKARDYEVLYMTDPIDEYAVQQIKEFEGKKLKCCTKEGLELDEGEDEKKSFEAL
KEEMEPLCKHIKEVLHDKVEKVVCGTRFTDSPCALVTSEFGWSANMERIMKAQALRDSSITSYMLSKKIM
EINPRHSIMKELKARAANDKTDKTVKDLVWLLYDTALLTSGFNLDEPTQFGNRIYRMIKLGLSLDDEEHV
EDDSSMPPLDEPVVDSKMEEVD

Appendix 3: CSP Sequences of the Five *Plasmodium* Species

P. falciparum CSP

>sp|Q7K740|CSP_PLAF7 Circumsporozoite protein OS=*Plasmodium falciparum* (isolate 3D7) OX=36329 GN=CSP PE=1 SV=1
MMRKLAILSVSSFLFVEALFQEYQCYGSSSNTRVLNELNYDNAGTNLYNELEMNYYGKQENWYSLKKNSRSLGENDD
GNNEDNEKLRKPKHKKLKQPADGNPDPNANPNVDPNANPNVDPNANPNVDPNANPNANPNANPNANPNANPNANPN
ANPNANPNANPNANPNANPNANPNANPNANPNANPNANPNANPNVDPNANPNANPNANPNANPNANPNANPNANPN
ANPNANPNANPNANPNANPNANPNANPNANPNANPNANPNANPNKNNQGNGQGHNMPNDPNRNVDENANANSAVK
NNNNEEPSDKHIKEYLNKIQNSLSTEWSPCSVTCGNGIQVRIKPGSANKPKDELDYANDIEKKICKMEKCSSVFNVVNSS
IGLIMVLSFLFLN

P. knowlesi CSP

>AEJ33939.1 circumsporozoite protein, partial [*Plasmodium knowlesi*]
NVNGVSFNNVDTSSLGAAQVRQSASRGRGLGEKPKEGDDKEKKEEKKEEKEKEKEKEKEEEPKKLNENKL
KQPEQAGPGGEQPAPRPGGEQAGPGGEQPAPRPGGEQPAPRPGGEQPAPRPGGEQPAPRPGGEQAGPGGE
QPAPRPGGEQPAPRPGGEQAGPGGEQPAPRPGGEQAGPGGEQPAPRPGGEQPAPGPGGEQPAPAPRREQP
APGGEQPAPGAGAGDGARGGNAGAGKGQGQNNQGANVPNEKVVNDYLHKIRSSVTTEWTPCSVTCGNGVR
IRRRAHADKKKAEDLTM

P. ovale CSP

>QCZ35286.1 circumsporozoite protein, partial [*Plasmodium ovale* wallikeri]
VYAHNGNSMEGRKLNELCYNNVDLYNTLFDGLDVESSTNQAFFLNSKKTLRLLNENPKENKKKKKNDKIP
VENKLKQGNKENDPPAPVPQGDPPAPVPQGNPPAPVPQGNPPAPVPQGDPPAPVPQGDPPAPQGDPPAPV
PQGDPPAPVPQGDPPAPVPQGNPPAPVPQGDPPAPVPQGDPPAPVPQGDPPAPVPQGDPPAPAPQGDPPAPAPQGDGKP
PAPAPAPQGDGNQPAPGKGKSENQKEKDEKNAANNPPSEDDIKKYLDKIRRDITENWSPCSVTCGLGVRV
RKKAGASAKKANELTINDVETEICKIENCSSIFNVVSNSIGLVIFLFL

P. malariae CSP

>QWO71690.1 circumsporozoite protein, partial [*Plasmodium malariae*]
GNDAGNDAGNDAGNAAGNAAGNAAGNAAGNAAGNAAGNAAGNAAGNAAGNAAGNAAGNAAGNAAGNAAGN
AAGNAAGYAAGNDAGNAAGNXAGNAAGNXAGNAAGNAAGNAAGNAAGNAAGNAAGNDAGNAAGNAAGNAA
GNAAGNAAGNAAGNAAGNAAGNAAGNAAGNAAGNAAGNAAGNAAGNAAGNAAGNAAGNAAGNAAGNAAGN
EKAKNKDNKVDANTNKKDNQEENNDSXNGPSEEHIKNYLESIRNSITEEWSPCSVTCGSGIRXRRKVGAK
NKKPAELVLSDLETEICSLDKCSSIFNVXS

P. vivax CSP

>AAG43992.1 circumsporozoite protein, partial [*Plasmodium vivax*]
PDDEEGDAKKKKDGKKAEPKNPRENKLKQPGDRADGQPAGDRAAGQPAGDGAAGQPAGDGAAGQPAGDGA
AGQPAGDRAAGQPAGDGAAGQPAGDGAAGQPAGDRAAGQPAGDRAAGQPAGDRAAGQPAGDRAAGQPAGD
RAAGQPAGDRAAGQPAGDRADGQPAGDRAAGQPAGDRAAGQPAGNGAGGQAAGGNAANKKAEDAGGNAGG
NAGGNAGGQGQNNEGANAPNEKSVKEYLDKVRATVGTEWTPCSVTCGVGVRVR

Appendix 4: NACOSTI Approval

REPUBLIC OF KENYA

NATIONAL COMMISSION FOR SCIENCE,TECHNOLOGY & INNOVATION

Ref No: 231299

Date of Issue: 10/September/2025

RESEARCH LICENSE

This is to Certify that Mr.. Harrison Onyango Okello of Masinde Muliro University of Science and Technology, has been licensed to conduct research as per the provision of the Science, Technology and Innovation Act, 2013 (Rev.2014) in Kisumu on the topic: IN-SILICO DISCOVERY OF PROTEIN INHIBITORS WITH PHARMACOLOGICAL PROPERTIES AGAINST PLASMODIUM MALARIA for the period ending : 10/September/2026.

License No: NACOSTI/P/25/4179161

231299

Applicant Identification Number

Ag. Director General
NATIONAL COMMISSION FOR SCIENCE,TECHNOLOGY & INNOVATION

Verification QR Code

NOTE: This is a computer generated License. To verify the authenticity of this document, Scan the QR Code using QR scanner application.

See overleaf for conditions